Colibr-e Sapphire

2022 AIAA Graduate Team Aircraft Design Competiton

An Agile Hybrid STOL Aircraft

Submitted on May 14, 2022

POLITECNICO
MILANO 1863

COLIBR-E

Team Members

Luca Bottà
AIAA Number 1343325

Alessandro Garatti
AIAA Number 1343327

Andrea Romani
AIAA Number 1343375

Carlo Spitale
AIAA Number 1344535

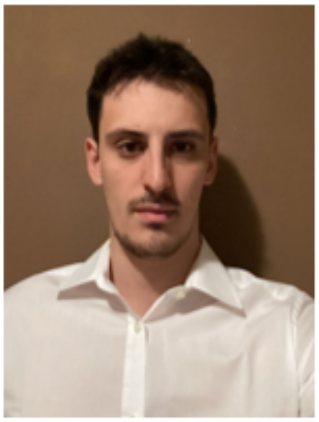

Marco Tomasoni
AIAA Number 1343326

Team Advisors

Lorenzo Trainelli

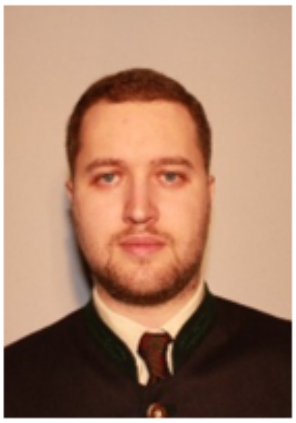

Carlo E. D. Riboldi

Executive summary

Nowadays great effort in the development of electric mobility is being made. The world is shifting toward sustainable energy sources and aviation is following the trend as well, despite a number of difficulties.

In response to the Request For Proposal of the 2021-2022 American Institute of Aeronautics and Astronautics (AIAA) Graduate Team Aircraft Design Competition, the Colibr-e Team is proud to present ***Colibr-e Sapphire***: an innovative green alternative to the current state of general aviation.

Starting with a market analysis and scouting the current competition, the Team aims to propose an airplane capable of performing various missions that competitors are not able to offer with a single non expensive and cheap to maintain/operate aircraft.

Following with performance analysis and structural layout, new concepts were introduced such as battery swapping to have an extremely low turn around time with a positive impact on safety and maintenance.

Subsequently a cost analysis will consolidate the previous price assumptions, different business cases are presented along with certification and safety considerations.

Colibr-e Sapphire will be able to perform a 300 nmi mission with a full electric take-off and landing from any airfield or airport switching on it's fuel engine only during cruise to cut down emissions of toxic pollutants up to 80% and with the remaining pollutants being emitted at high altitudes far from human beings. Finally, being able to perform aerotaxi, flight school, cargo and medical missions with close to none modification to the aircraft, ***Colibr-e Sapphire*** represents a green agile hybrid-electric aircraft.

Contents

List of Symbols and Acronyms

AC	Aerodynamic Center
AEO	All Engines Operative
AOA	Angle of Attack
AR	Aspect Ratio
AFT	Afterwards
BP	Battery Pack
BSFC	Break Specific Fuel Consumption
CAPEX	Capital Expenditures
CAS	Calibrated Air Speed
CG	Center of Gravity
CGR	Climb gradient
CO	Carbon Monoxide
CO2	Carbon Dioxide
CPI	Consumer Price Index
CPL	Commercial Pilot Licence
DAPCA	Development and Procurement Costs of Aircraft
DEP	Distributed Electric Propulsion
DOC	Direct Operating Cost
EAS	Equivalent Air Speed
EM	Electric Motor
EPMS	Energy and Power Management System
ESC	Electronic Speed Controller
FAA	Federal Aviation Administration
FAR	Federal Aviation Regulation
FDOC	Fixed Direct Operating Cost
FE	Full Electric
FOD	Foreign Object Debris
FOV	Field Of View
FQ	Flying Qualities
FWD	Forward
GA	General Aviation
GEN	Generator
GMHO	Ground Max Height
G/OMFWD	Ground/Operational Max Forward
GMAFT	Ground Max Afterwards
GPS	Global Positioning System
HC	Hydrocarbons
HE	Hybrid Electric
HT	Horizontal Tail
ICAO	International Civil Aviation Organization
ICE	Internal Combustion Engine
IOC	Indirect Operating Cost
IFR	Instrument Flight Rules
ISA	International Standard Atmosphere
KEAS	Knots of Equivalent Airspeed
KIAS	Knots of Indicated Airspeed
KTAS	Knots of True Airspeed
LE	Leading Edge
LIB	Lithium-Ion Battery
LLT	Lifting Line Theory
LND	Landing
MAC	Mean Aerodynamic Chord
MCP	Maximum Continuous Power
MLG	Main Landing Gear
MTOM	Maximum Take-Off Mass
MTOW	Maximum Take-Off Weight
NLG	Nose Landing Gear
NMC	Nickel Manganese Cobalt
NOx	Nitrogen Oxide
OMAFT	Operational Max Afterwards
OMH	Operational Max Height
PGS	Power Generation System
PGS	Power Generation System
PHE	Parallel Hybrid Electric
PPL	Private Pilot Licence
RFP	Request for Proposal
ROC	Rate of climb
SAR	Search And Rescue
SAS	Stability Augmentation System
SHE	Serial Hybrid Electric
SG&A	Selling, General and Administration
SM	Static Margin
SMP	Sizing Matrix Plot
SOC	State of Charge
STOL	Short Take-Off and Landing
TAS	True Air Speed
TBO	Time Between Overhauls
TCAS	Traffic Alert and Collision Avoidance System
TE	Trailing Edge
TO	Take-off
TRL	Technology Readiness Level
VDOC	Variable Direct Operating Cost
VFR	Visual Flight Rules
VLA	Very Large Aircraft
VT	Vertical Tail
VTOL	Vertical Take-Off and Landing
WAAC	Weighted Average Cost of Capital
WB	Weight and Balance

Symbol	Description	Unit of measurement
α	Angle of attack	deg
α_t	Twist angle	deg
β	Sideslip angle	deg
ΔY	fraction of wingspan blown by the DEP array	
Δy	propeller tips distance over propeller radius	
δ	Control surface deflection	deg
η	Efficiency	-
γ	Flight path angle	deg
Λ	Sweep angle	deg
λ	Taper ratio	-
ρ	Density	kg/m^3
σ	Throttle	-
Φ	Bank angle	deg
ξ	Non-dimensional position	-
Ω	Turn rate	deg/s
b	Wing span	m
C_l, C_d, C_m	Airfoil lift, drag, moment coefficient	-
C_L, C_D, C_M	3D lift, drag, moment coefficient	-
$C_{\mathcal{L}}$,$C_{\mathcal{M}}$,$C_{\mathcal{N}}$	Rolling, pitching, yawing moment coefficients	-
C_X	Longitudinal force coefficient	-
c	Chord	m
D_P	Propeller diameter	m
e	Oswald parameter	-
g	Gravity acceleration	m/s^2
h	Altitude	m, ft
i	Incidence	deg
k	Induced drag coefficient	-
L	Distance between quarter chords	m
M	Mach number	-
m	Mass	kg
N	Number of EM	-
n	Load factor	-
P	Power	W
P_b	Shaft brake power	W
p, q, r	Roll, pitch, yaw rates	rad/s
q	Dynamic pressure	Pa
Re	Reynolds number	-
S	Surface	m^2
$\mathcal{S}$	Field length	m, ft
T	Temperature	$^\circ C$
V_{HT}	Tail volume	-
V	Airspeed	kts
V_{S0}	Stall speed in landing configuration	kts
V_{S1}	Stall speed in take-off configuration	kts
V_{NE}	Never exceed speed	kts
V_V	Vertical speed	fpm
V_X	Steepest climb speed	kts
V_Y	Fastest climb speed	kts

$V_{max\mathcal{E}}$	Best endurance speed	kts
$V_{max\mathcal{R}}$	Best range speed	kts
x	distance from LE	m
x_c	propeller distance from LE over MAC	
$\overline{y}$	postion of MAC along semi-span	m
W	Weight	N, lbs

Sub/Superscripts

Subscripts	Definition
APP	Approach
BR	Brake/Braking
FL	Flare
HT	Horizontal tail
LND	Landing
REF	Reference
TO	Take-off
VT	Vertical tail
a	aileron
e	elevator
P	Propeller
r	rudder
w	wing

Conversions

SI system	Imperial units
1 m	3.2808 ft
1 kg	2.2046 lbs
1 Pa	0.0209 psf
1 W	$1.341 \cdot 10^{-}3$ HP
1 L	0.2641 US gal
1852 m	1 nm
0.51 m/s	1 kt

1 Market Analysis

1.1 Introduction

Global pollution reduction, greenhouse gasses emission control and environmental sustainability are nowadays central pillars to all companies and startups. As a result the products of the technology industry are more and more shifted to green improvement and reduction of fossil fuels consumption. In a world where the automotive field is leader in hybrid-electric and full electric motors development, the aviation one is falling behind. Nevertheless, recent researches and tests have shown the potential applicability of hybrid-electric and full electric propulsion for aircraft. NASA X-57 Maxwell, for example, has proven how the recent batteries capacity and energy density improvement can be a gateway for a greener and sustainable aviation. Such progress is mandatory: the EEA (European Environmental Agency) states that emissions due to air and sea transport will make up to 40% of the global amount by 2050 if counter-measures are not taken [1]. AIAA's RFP for GA "Hybrid-Electric STOL Air Taxi Design" proposes an alternative to this negative trend with the development of a lower emission aircraft for civil transport. ***Colibr-e Sapphire*** not only represent a concrete solution to all this problem with it's extremely lower pollution but also opens the possibility of a new air transport market thanks to it's STOL capabilities and agile configuration.

1.2 Potential Market, STOL and Hybrid-electric Advantages

Taking the airplane to reach a destination is one of the fastest and safest way to travel, unfortunately whenever we want to fly to our destinations we face the same problems: pollution caused by airplanes is extremely high, airports are hard to reach, check-in takes a lot of time and, if we don't live close to a big city, reaching our destination can take several hours more after the plane ride. Because of this many people prefer land traveling using cars, trains and busses. What if there was a solution to combine the benefits of both worlds? The following report illustrates the conceptual design of an aircraft able to fly quickly anyone as close as possible to their destination with low emissions, high comfort and with all the benefits of air travel. This new vision of Aerotaxi service will allow the aviation field to finally be a viable competitor to land transport for short/medium range travels. Moreover, due to its extremely low take-off and landing distances, this aircraft might be used in the future for trans-urban and interurban traffic using small airways just outside cities and places of interest.

In order to cut down emissions, an hybrid-electric propulsive system is the best option due to the fact that a full electric configuration will not be able to grant an acceptable MTOW and range. Even state-of-the-art lithium-ion rechargeable batteries have hard times reaching specific energies of 0.9 MJ/kg while aviation gas can easily reach 43.5 MJ/kg. The use of an hybrid-electric propulsion lets us to have the best of the two worlds, with the

possibility to grant better performances by the year of release (2031). Using electric motor will also allow to reduce noise pollution around cities, presenting another advantage with respect to current transportation.

1.3 Competitors

The first step to perform a detailed market analysis is to review the strong points and weak points of the current competition. The main goal of the Team is to design an ”agile” aircraft, able to be used in many roles such as aerotaxi, flight school, utility and medical (with aerotaxi role being the main drive to the design). Because of this, the competitors are scouted between airplanes and helicopters able to transport the same amount of passengers, or used for similar objective of the one under project.

	C172S	PA-28 TX	SR-20	DA40	Robinson R44	Beechcraft Bonanza G36	P2006T	AS 350	AW109	UH-1	HH-65	AS365	King Air 90	King Air 200
Empty Weight	736 kg	766 kg	964 kg	795 kg	658 kg	1142 kg	819 kg	1220 kg	1576 kg	2300 kg	2673 kg	2239 kg	3150 kg	3419 kg
MTOW	1113 kg	1157 kg	1383 kg	1198 kg	1089 kg	1656 kg	1230 kg	2250 kg	3000 kg	4309 kg	4032 kg	4250 kg	4580 kg	5669 kg
Range	696 nmi	522 nmi	709 nmi	724 nmi	300 nmi	716 nmi	650 nmi	257 nmi	464 nmi	207 nmi	388 nmi	464 nmi	1321 nmi	1490 nmi
Take-off distance	1630 ft	1608 ft	1685 ft	1000 ft	(helicopter)	2180 ft	1293 ft	(helicopter)	(helicopter)	(helicopter)	(helicopter)	(helicopter)	1984 ft	3300 ft
Cost	370'000 $	369'000 $	550'000 $	420'000 $	425'000 $	777'000 $	625'000 $	2'400'00 $	400'000 $ up to 6'000'000 $	960'000 $	9'000'000 $	2'400'000 $ up to 4'800'00 $	1'600'000 $	760'000 $
operating cost per hr (without pilot)	180 $/hr	200 $/hr	187 $/hr	193 $/hr	420 $/hr	275 $/hr	144 $/hr	923 $/hr	1125 $/hr	644 $/hr	8000 $/hr	2053 $/hr	1100 $/hr	1500 $/hr
Number produced in 1 year	785	841	106	95	125	226	58	85	32	516	20	23	54	88
														Airschool
														Aerotaxi
														SAR
														Medical

Figure 1: Competitors

Flight school aircraft

The strong points of airplanes used for flight school are the low acquisition cost and long range. On the other hand all of these airplanes are single engine, using Lycoming O-360, O-320 and IO-390. All of these are piston engines with the first two being designed in the ’50s and the latter in the early 2000s. Moreover the Cessna 172 was designed in the ’50s, the Diamond DA-40 and the Cirrus SR-20 in the ’90s and the Piper PA-28 in the ’60s. This brings the need for new cutting-edge technologies offering better reliability and better flying experience.

Aerotaxi aircraft

The best aspects of aertoaxi aircraft is the range and, for helicopters, the ability to perform a vertical take-off. On the flip side the acquisition cost is greater than the last category with the price of a new helicopter and it’s operating cost being extremely high as well as the hours of maintenance. Moreover airplanes, like the DA-40 and G-36, suffer from the same problems explained on the previous paragraph.

SAR / Medical Aircraft

SAR and medical aircraft are characterised by a good range and large useful payload. This is mainly dictated by two aspects: these aircraft are a modification of GA or military aircraft able to transport more than 4 people and the need to transport a patient or a wounded person to the nearest hospital which can be far from his position and also (in the case of SAR) search for him. The biggest drawback of this aircraft category is the extremely high acquisition cost and operating cost. Moreover only the helicopters are able to land and take-off from any location, while airplanes used for medical transport need to operate from runways which can not be available.

1.4 Surveys

In order to have a better understanding of the market, data coming from potential clients, potential buyers, airfields and airports have to be collected. To do so, different surveys were released and sent to European and American citizens, aerotaxi companies (with a distinction between those operating mainly with airplanes and with helicopters), airfields and airports.

Citizens

This survey was completed by 50+ people. One of the first data collected was the one regarding pollution: does the general public care about noise and greenhouse gasses reduction? Is there an interest from the general public in the hybrid-electric future? As can be seen from Figure 2, noise reduction has the majority of people divided between a high and an average interest in the topic. Talking about emissions reduction, the vast majority of the subjects expressed a very high interest in a greener future. This consideration is further reinforced by data shown in Figure 3, where people expressed a will to give up some comfort during their flight in favour of less pollution for both long and short travels.

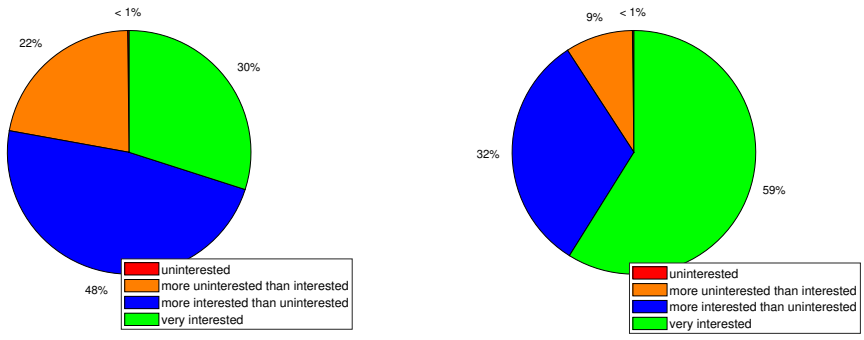

(a) Noise **(b)** Pollution

Figure 2: Noise and Pollution reduction interest from general public

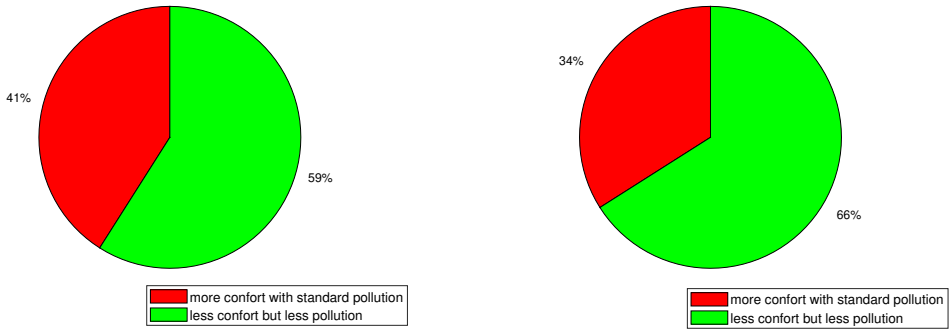

(a) For routes of 250 nm **(b)** For routes of 50 nm

Figure 3: Comfort vs pollution

The second data to be collected regarded the usefulness of the aircraft in question: does it make sense to have a STOL just to be able to take off from any airfield? Is the 300 nm range enough? Is it too much? Looking at Figure 4 it can be seen how only a small percentage of travellers would use an aerotaxi transport for routes above 300 nm. The rest is spread all over all the spectrum. Moreover, it's evident how the travellers live in all kinds of cities, from very small rural towns to metropolis, with only a small percentage having easy access to principal airports. In addition to this, from Figure 5 it is noticeable how customers are willing to pay more to be able to take-off closer to their home and land closer to their destination.

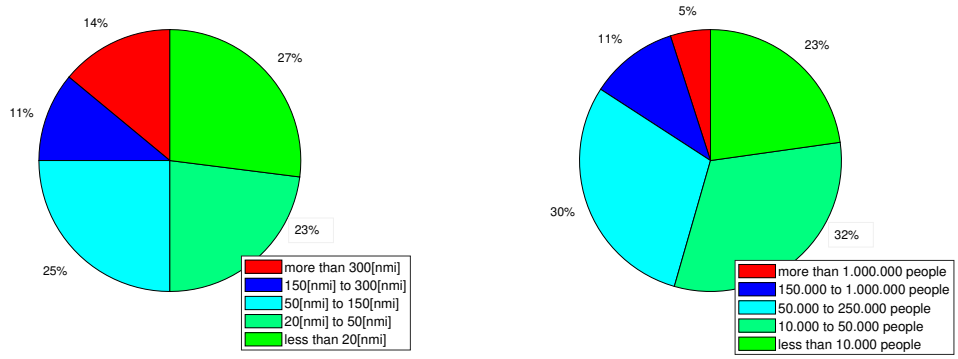

(a) Desired routes **(b)** City of provenience

Figure 4: Usefulness of the airplane

Aerotaxi operators

This survey was completed by 12 major companies with a distinction between those operating with airplanes and those operating with helicopters.

The first needed data was the one regarding their operation: can the airplane under project compete with

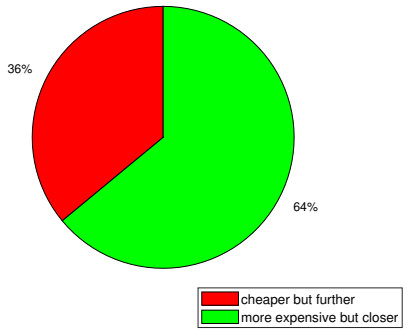

Figure 5: Cost vs proximity

the aircraft used by those companies? Are their operations compatible with the capability of our aircraft? As it is visible from Figure 6, the capabilities of the airplane under study are not enough to compete with those of the aircraft used for aerotaxi transport by companies operating with airplanes. On the other hand it is perfectly capable of not only competing but surpassing the range of the helicopters used in the public and utility transport.

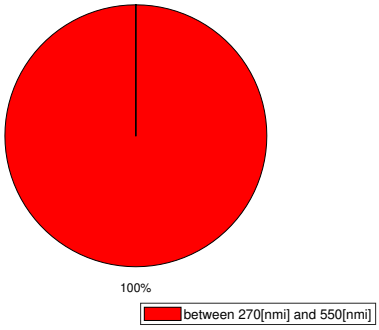

(a) Airplanes operating companies

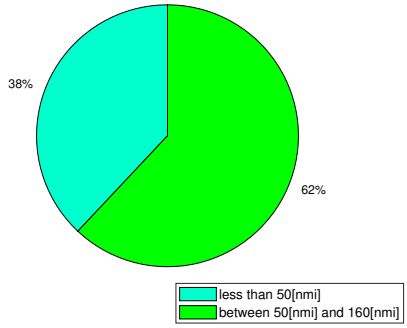

(b) Helicopters operating companies

Figure 6: Aerotaxi companies routes

The second information needed regarded airplane constructive aspects: what material to use? What configuration to install? Looking at Figure 7 is possible to see how airplane-operating companies largely prefer a metal construction while helicopter-operating ones mostly prefer a composite construction, this is due to the fact that in helicopters the lightness of the fuselage is way more crucial than it is in a fixed wing aircraft. Regarding cockpit configuration the Team wanted to know if companies preferred to have a redundancy of commands or could accept to have a single pilot aircraft with only one pilot station. This would change the seating configuration of the airplane as well as the fuselage shape itself. From Figure 8 it can be clearly seen how for both samples the two-pilot configuration was vastly preferred.

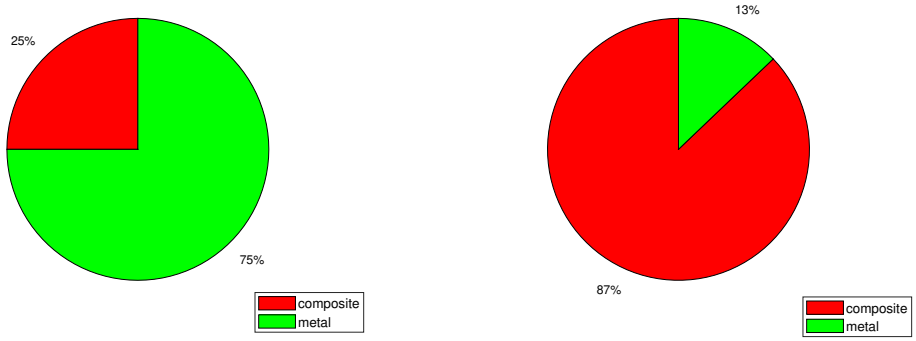

(a) Airplanes operating companies **(b)** Helicopters operating companies

Figure 7: Preferred materials

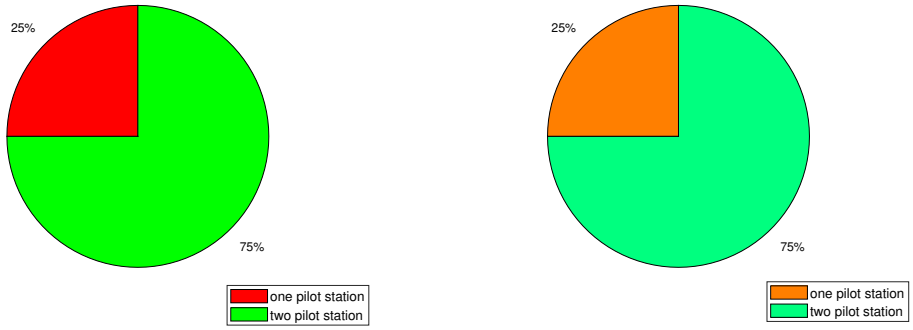

(a) Airplanes operating companies **(b)** Helicopters operating companies

Figure 8: Preferred configuration

Airfields and Airports

This survey was completed by 50 airports and airfields. Data collected in this study were absolutely pivotal to determine whether the airplane could even operate and what ground structures it could rely on, before take-off and after landing. First of all, information about availability of fuel and electric energy sources had to be collected, in Figure 9 the fuels available in both airports and airfield are shown.

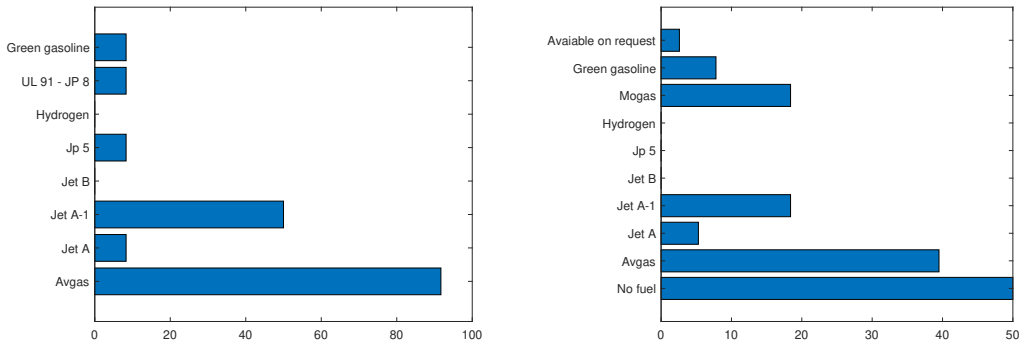

(a) Airports **(b)** Airfields

Figure 9: Fuel availability

Not just fuel, but also electric energy is needed. In order to find out if there might be a charging station available at turn around place, two main questions were asked: how likely do you think you will have electric charging stations by 2031? How much having an operating hybrid electric aerotaxi aircraft from your airport/airfield would be an incentive in installing those charging stations? From Figure 10 it's noticeable divided are airports and airfields owner in the prospective of installing electric charging station.

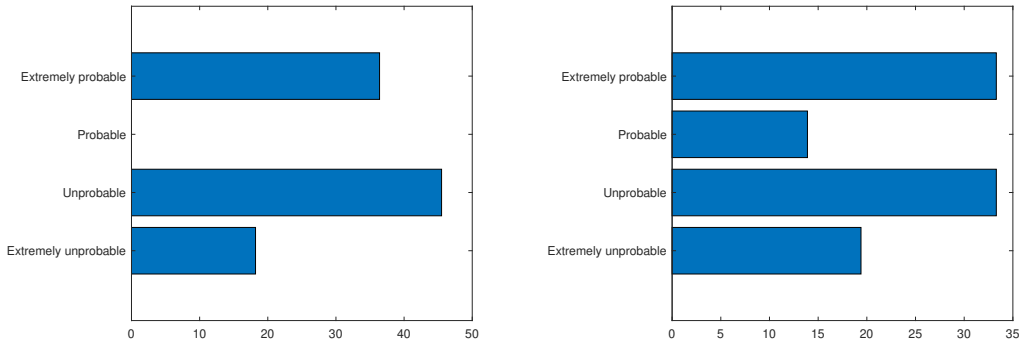

(a) Airports **(b)** Airfields

Figure 10: Probability of having electric charging stations by 2031

At first glance, this result seems very limiting for the operation of the airplane under project, which relies mainly on electric energy to achieve the required power. However, this data coupled with results shown in Figure 11, gives an extraordinarily optimistic prospective in electric energy availability.

The second set of data collected was used to help designing the airplane. To do so, the Team asked some questions regarding runway type and length, as well as hangar availability and sizes. Talking about runway length, 100% of the subjects stated to have runways longer than 650 ft. On top of that, in Figure 12 their wideness are shown.

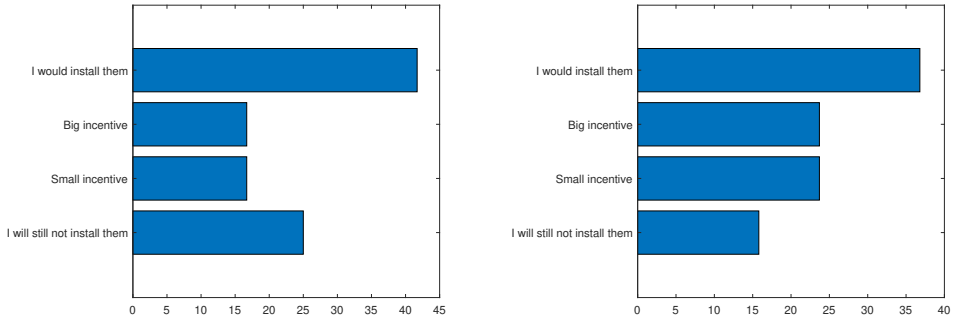

(a) Airports **(b)** Airfields

Figure 11: How much having an operating hybrid electric aircraft by 2031 would represent an incentive in installing the previous structures

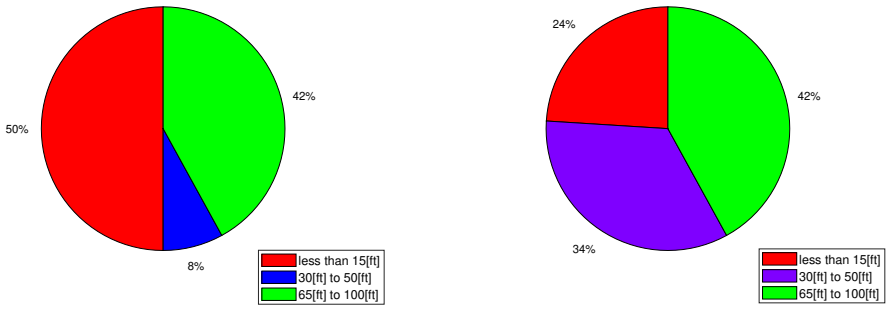

(a) Airports **(b)** Airfields

Figure 12: Runway wideness

After that, runway types had to be investigated, since this information would be critical in choosing an appropriate take-off power, wing design and landing gear structure. This information is shown in Figure 13.

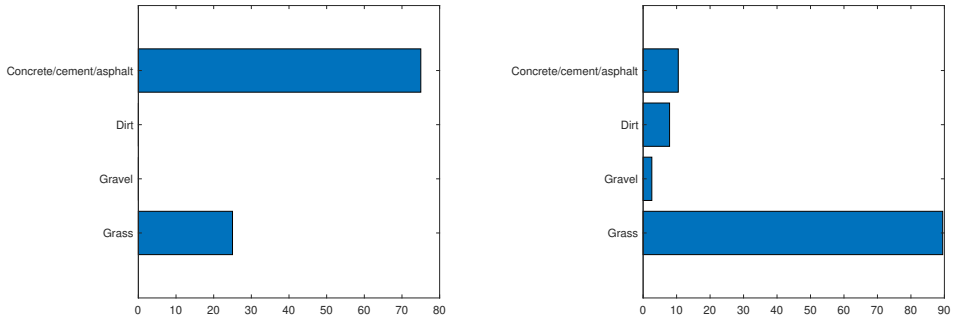

(a) Airports **(b)** Airfields

Figure 13: Runway type

The last information needed regarded hangar sizes. This is crucial to estimate the maximum vertical, longitudinal and span-wise dimensions. From collected data, the average size is 100x80x15 ft for airports and 65x55x15 ft for airfields.

1.5 Results and Project Guidelines

To sum up, what emerges from market analysis is that the need for a greener future is visible from both the general public and the global governments. This kind of push will not only help from an image point of view, but also from an economic one: US and EU started to take action against global warming with the US wanting to cut in half their greenhouse gasses production by 2030 and the EU targeting net-zero emissions by 2050. In order to reach this goal both governments started to give out incentives towards the develop and purchase of everything that is ”low-emissions” like cars, household items, bikes ecc... The aircraft under exam will not only gain advantage from these incentives but also avoid extra taxation due to pollution. From a structural point of view, the aircraft will be made of metal alloys (preferably aluminum) to increase maintainability and reduce the acquisition and operating cost making the airplane competitive in the market. Despite being a single pilot airplane, it will have two piloting stations: this will not be an impediment when choosing to fly in single pilot configuration, since the second station can be easily detached, allowing to load up to three passengers. Anyway, the option to use the aircraft as a trainer for flight schools will be granted.

The aircraft must be able to lift off in a short distance (less than 300 ft) and from any terrain of narrow runways, allowing it to operate from any airport or airfield and to open a new market of air transport ”close to your home, close to your destination”. This aspect will make it standing out from the airplane world, making it competitive with helicopters as well. Said aircraft are able to take-off vertically but are characterised by extremely high acquisition and operating cost and a lot of maintenance hours. Choosing to buy the airplane under project will require buyers to give up the ability to use heliports in favour of an aircraft that costs less than half to buy, less than one fifth to operate, less than one tenth of the maintenance time and still able to operate from any airport and airfields as well as most flying fields. This will impact the design of the landing gear. The batteries will be able to be charged on ground. To allow the airplane to be refueled in the biggest amount of airports and airfields, the fuel to be used must be one between Avgas, Jet A-1 and Mogas, with Avgas being the most available. Moreover to go one step beyond the RFP, the Team decided to implement a swappable battery system to grant a turn around time of 15 minutes even after the maximum range operation.

Talking about the maximum dimensions of the airplane, the height must not exceed 15 ft, the airplane must not be longer than 55 ft from nose to tail and the wing span must not be more than 65 ft to allow it to park in any hangar.

2 Sizing Mission

In order to carry out an effective preliminary data collection, it is of capital importance to clarify what kind of mission profile the aircraft will have to perform. Even though the most likely mission type will be a short-medium range flight, a sizing mission cue is already given by RFP, which requires to size the aircraft to a more demanding mission type.

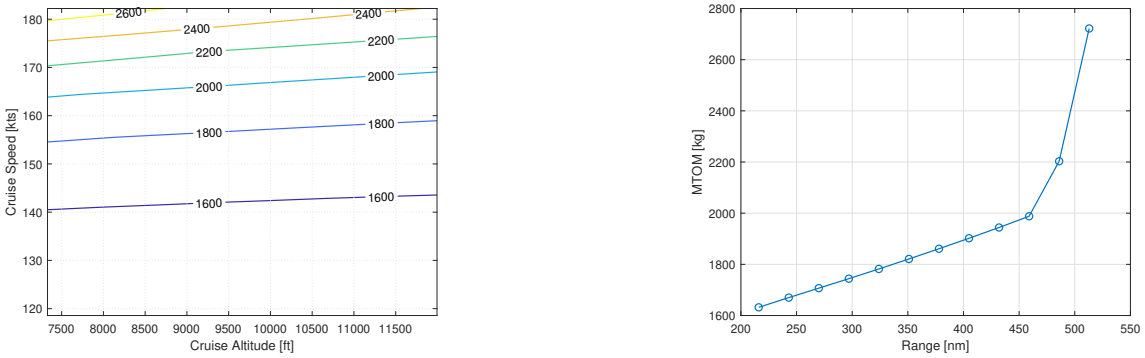

(a) MTOM vs cruise altitude and speed

(b) MTOM vs range

Figure 14: Sensitivity studies

After the analysis of survey results, and sensitivity studies 14, some mission profiles have been compared. Then the Team, considering mandatory and tradable requirements, imposed by AIAA request for proposal, defined the following sizing mission:

- Take-Off within 300 ft (full electric) with max payload.
- Initial climb (full electric) until the transition altitude is reached
- A 300 nm cruise leg performed at 150 kts at an altitude of 9000 ft. This altitude is feasible for a non-pressurized aircraft with good comfort for passengers. Batteries are charged during this phase (if needed).
- Descent until zero altitude with a rate of descent equal to the third part of rate of climb.
- 45 minute of loiter at sea level as imposed by IFR reserve.
- A diversion capability of 27 nm has been considered by the Team, as a result of a study conducted about distribution of airfields in European and North American territory. The diversion is composed by:
  - Climb at 5000 ft with a rate of climb of 1500 ft/min.
  - Cruise at 5000 ft at max range speed.
  - Descent until zero altitude.
- Landing within 300 ft (full electric)

3 Preliminary Studies

3.1 Existing prototypes of hybrid-electric Aircraft

Despite many concept and prototypes of full-electric and hybrid-electric aircraft are into development, few of them are operative nowadays. At present days, Pipistrel Velis Electro is the only type certified electric aircraft in the world, while the vast majority of FE aircraft in production are motor glider or very light aircraft (VLA). A number of HE aircraft concept is now into study, but existing ones are prototypes or technology demonstrators. Among today's flying models we can cite Siemens Diamond e-star (SHE), Airbus e-fan1.2 (SHE), Embry-Riddle eco eagle (PHE), Cambridge SOUL (PHE). All of them are 2 seaters with a maximum takeoff weight not greater than 1000 kg. At the same time there is a great innovation push in the field of urban air mobility. Startups of this type are Joby Aviaiton, Lilium, Volocopter, Wisk, Archer Aviation, Kitty Hawk, Bell Nexus. None of mentioned aircraft share similar characteristics with ***Colibr-e Sapphire***. Due to the fact that reference models for preliminary data estimation are not adequate or even unavailable, the Team decided to consider conventional aircraft as baseline for preliminary studies and data collection.

3.2 Configuration

Preliminary configuration choices concern topics like wing mounting, powertrain mounting and layout, landing gear configuration, fuselage shape and cross section.

Wing mounting

The Team decided upon high wing mounting. Advantages of this choice are various: higher clearance from ground, improved lateral stability, easier ground operations (i.e. loading and unloading), possibility to mount engines on wing with higher clearance for propellers, better ground visibility for pilot, more space available inside fuselage.

Powertrain mounting and layout

Evaluations about propellers' location conducted to the decision of wing-mounted engines. This choice was driven by some considerations about wing-mounted engine options: higher clearance from ground preventing FOD impact, possibility to exploit propellers jet to blow the wing 3.4 and possibility to increase disk diameter. There are different possible design layout for distributed propulsion. The first one divide total power installed into 'conventional powertrain', demanded to generate thrust, (usually consisting in few powerful motors with big propeller disks) and DEP powertrain, which is demanded only to generate extra lift by blowing the wing (usually

consisting in an array of small motors coupled with small propellers). This is the propulsive configuration of X-57. An alternative methodology is to design a single powertrain to accomplish both tasks. This solution is characterized by a large number of small electric motors that ensure at the same time thrust required and extra lift needed for each flight phase. This is the layout of conceptual aircraft like ELECTRA AERO. Depending on propulsion system layout there are different ways to proceed in the design, as explained in section 3.4.

Landing gear

Landing gear had to be tricycle to ease ground movements and operations. Moreover, the Team decided to go for a retractable landing gear to increment cruise performance and lower fuel consumption.

Fuselage

Since the aircraft is not pressurized, the Team decided for a square cross section: a circular cross section would simply increment the manufacturing cost and maintenance time, with negligible advantages for the airplane.

3.3 Preliminary data collection

Given the lack of reference models, as stated above, data collection was focused on existing aircraft which share some common aspect with ***Colibr-e Sapphire***. In particular Cessna 172, Tecnam P2006T and Nasa X-57 Maxwell have been considered at first. Cessna 172 is widely considered as a benchmark for nearly every general aviation aircraft. It has been taken into account as a reference for the category of 4 seat light plane. Tecnam P2006T was chosen because of similarity on technology, layout, configuration, furthermore NASA chose this very model as a baseline for the development of its own electric aircraft, the X-57 Maxwell. The latter was taken into account too, as a suitable reference in electric aviation field, and even as a possible competitor. Mission and performance common aspects have been taken into consideration. To have a wider view on parameters, Team consulted different categories of aircraft on Jane's All the World Aircraft: 4-seat utility twin propeller, 4-seat light plane, light utility twin prop transport and STOL. None of them present neither full electric nor hybrid-electric propulsion configuration, nevertheless they had been studied because of some common aspect with the mission case (i.e. payload, dimensions, takeoff weight, performance, configuration).

3.3.1 Airframe mass estimation

Another point of reference for regression data used is given by Roskam. The original regression data was then modified to accommodate the peculiarities of an hybrid electric configuration. Typically for conventional aircraft the empty mass is composed by structure, fixed equipment, powerplant and engine. Regression used accounts

only for structure, fixed equipment and powerplant mass. The historical data used for airframe mass regression (from Roskam data [2]) are presented in the following table. Graphical result is presented in figure 15.

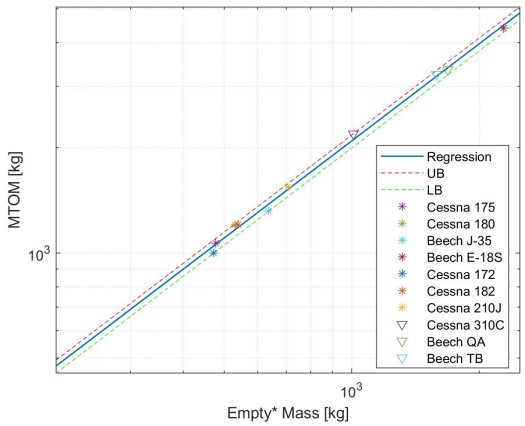

Figure 15: Empty mass vs MTOM

	MTOM [kg]	**Empty mass** [kg]	**ratio**
Cessna 175	1066.9	477.6	0.45
Cessna 180	1203	530.3	0.44
Beech J-35	1316.6	635.6	0.48
Beech E-18S	4403.8	2286.3	0.52
Cessna 172	998.8	471.7	0.47
Cessna 182	1203.1	538.4	0.45
Cessna 210J	1543.6	707.3	0.46
Cessna 310C	2192.8	1009.2	0.46
Beech QA	3345	1688	0.50
Beech TB	3246	1584.9	0.49

Table 3: Airframe mass regression data

3.3.2 Batteries

State-of-the-Art technology and future perspectives of batteries had been analyzed. Electric aviation future development is strictly connected to batteries performance, especially in terms of specific energy [Wh/kg]. Evaluation of battery performance and future expectations has been carried out carefully because of its strong impact on design process.

Present day technology

Today's market for rechargeable batteries is dominated by Lithium-Ion batteries. Since LIBs came on the market in the 1990s, their energy density has more than doubled while the cost has dropped by a factor of 15. Li-ion batteries have a number of advantageous over other chemistries: they are low maintenance, easy to store with a much smaller self discharge rate, fast charge, long lifetime, and cycling performances. Most important thing, they can store over four times as much energy as lead acid batteries and twice as much energy as nickel based. Typical lithium-ion designs can hold from 100 to 265 Wh/kg, while the highest specific energy of modern prototypes is around 400 Wh/kg. Today's price for state-of-the-art LIB packs is roughly 150-120 $/kWh. The expected cost will decline to well below 100 $/kWh by 2024, a cost level that all future batteries must reach to be competitive [3]. Actual electric aircraft such as Pipistrel Velis Electro and Nasa X-57 Maxwell prototype, use Li-ion battery packs. Pipistrel Velis Electro is the only certified electric aircraft at present day. Its battery pack is constructed of cylindrical Li-Ion type cells which use the NMC chemistry (Nickel Manganese Cobalt). The entire BP is capable of 11.0 kWh energy storage and weights 60 kg, with a specific energy around 183 Wh/kg. It takes 2 hours to recharge from 30% to 100% and allows a 60 minutes endurance.

NASA X-57 prototype uses Li-ion battery as well. BP's mass is about 390 kg, capable of 69.1 kWh energy of which 47 kWh usable. Specific energy is less than 177 Wh/kg. Anyway, regardless their excellent performance, LIBs still don't meet aviation's needs.

10-years forecast

Nowadays, great expectation exists about actual chemistry improvement and new technology developments. Li-ion technology is expected to reach an energy limit within few years. Nevertheless, recent discoveries may overcome present limits [4].

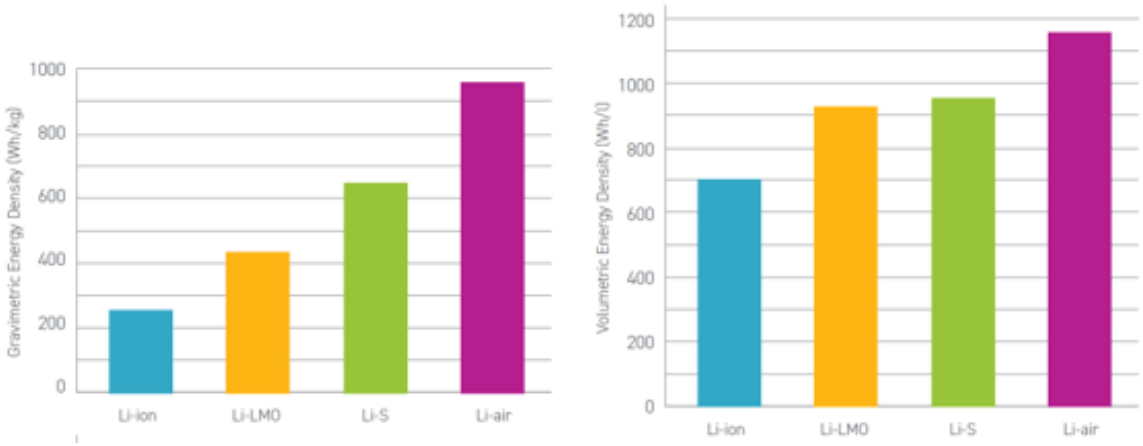

(a) Gravimetric energy density **(b)** Volumetric energy density

Figure 16: Future development for batteries technology

New generation of **advanced Li-ion batteries** is expected to be deployed before the first generation of solid state batteries. They are expected to keep all the advantages of lithium technology along with increased performance.

Among the most promising chemistries there is **lithium-sulfur** technology. Theoretical specific energy of this batteries is extraordinarily high: four times greater than that of lithium-ion. That makes it a perfect fit for the aviation industry. Recent prototypes proved to be able to reach 470 Wh/kg. Battery developers estimate not unreasonable to anticipate 600 Wh/kg by 2025. For applications requiring long battery life, this technology is expected to reach the market just after solid state lithium-ion.

Solid state batteries represent a paradigm shift in terms of technology with respect to modern Li-ion batteries. In the latter, ions move from one electrode to another across the liquid electrolyte, in the former the liquid is replaced by a solid compound. This technology presents some important advantages: first a huge improvement in safety, since solid electrolytes are non-flammable when heated, unlike their liquid counterparts. Second, it permits the use of innovative, high-voltage high-capacity materials, enabling denser, lighter batteries with better

shelf-life as a result of reduced self-discharge. Moreover, at system level, it will bring additional advantages such as simplified mechanics as well as thermal and safety management.

Another promising solution is represented by **lithium-metal** batteries. Despite performance seem to be not so high as lithium-sulfur, laboratory tests conducted by Sion Power have shown as this technology could have a relevant role in the future of battery both for eV batteries and for high energy batteries. Test results, carried out in 2018 at cell level, are shown in Figure 17.

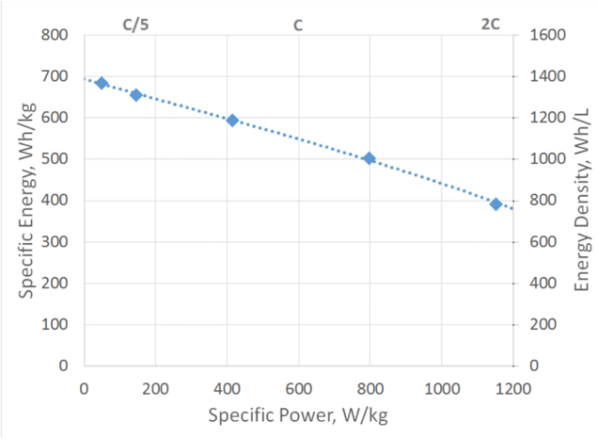

Figure 17: Sion Power Licerion-HE battery

Also **lithium-Air** technology have a great potential, but studies about this technology are still at initial stage. For this reason, it is unlikely that this technology will be available in few years. **Structural batteries** technology has been considered too but, at this stage, seems to be too expensive and not mature enough for aviation application and therefore not reliable.

In the aviation field, in fact, not only specific energy has to be taken into account. Any battery intended for use as a power source or routinely carried on aircraft, must be safe, reliable, require minimal maintenance, and be able to operate efficiently over a wide environmental envelope. This implies that only a part among all new technologies mentioned so far, can be considered to be likely ready in the next decade. A fundamental parameter to be taken into account is represented by Technology Readiness Level (TRL), which indicates the 'maturity level' of a new technology. In the following figure are shown TRLs of some technologies mentioned in this paragraph.

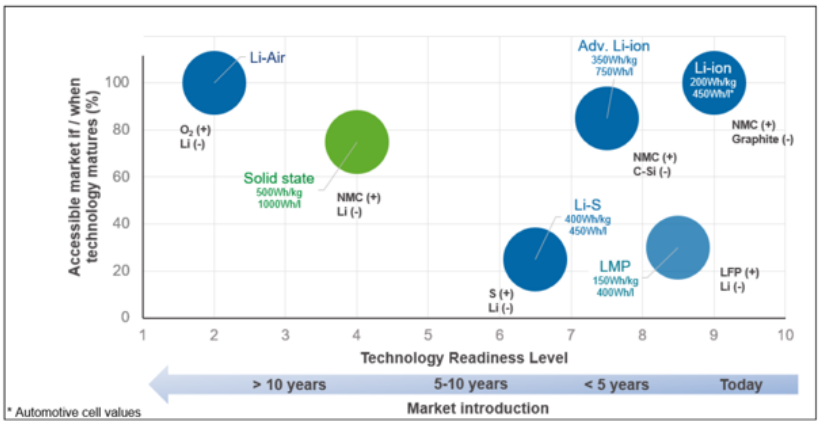

Figure 18: TRL battery technology

We are now at a stage where prediction is difficult. The Team considered lithium-sulfur the most promising technology. A reasonable specific energy value assumption for the near future is 400 Wh/kg. Battery developers generally estimate the availability of batteries with specific energy greater than 750 Wh/kg by around 2035 [5]. The Team decided to choose carefully, preferring to be conservative in estimation of batteries' performance. $\mathbb{E}$ = 420 [Wh/kg] and $\mathbb{P}$ = 980 [W/kg] have been hypothesized.

3.3.3 Electric Motors

Aviation's electric motors development is now at the beginning so few models exist. Electric motors are characterized by very high operating efficiency, typically 92% ÷ 98%, while thermal efficiency of combustion engines ranges between 24% and 50%. EMs present also higher power-to-weight ratio with respect to internal combustion engines, reaching values between 4 and 7, while common internal combustion engines barely reach 1. This means also that they are smaller than internal combustion engine. This characteristics make electric motor the perfect (and only) solution to implement a distributed propulsion on an aircraft.

Electric motors present also operative advantages with respect to common ICEs. They are low maintenance, easier to replace, generate lower noise and no emissions. A linear regression has been worked out on present technology motors, accounting for power output versus dry weight. Data used for regressions were obtained directly from manufacturer's datasheets 4 and regarded only electric motors up to a power threshold, in accordance with the technology adopted for distributed propulsion system. The linear regression obtained is shown in the following Figure 19.

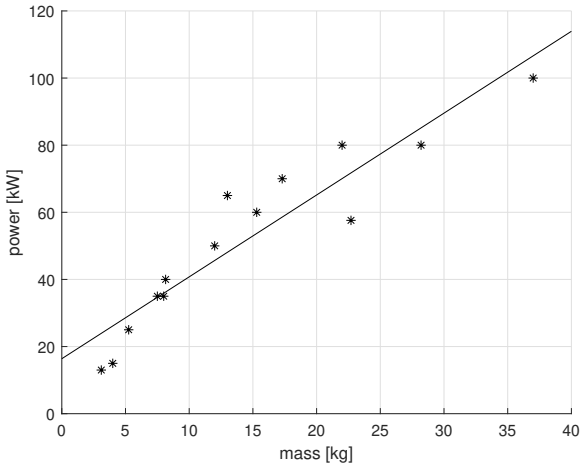

Figure 19: EM regression

Electric Motor	**peak power** [kW]	**mass** [kg]
Pipistrel E-811	57.6	22.7
Siemens SP70D	92	26
Siemens SP90G	65	13
MGM COMPRO RET20	13	3.1
MGM COMPRO RET30	15	4
MGM COMPRO RET60	35	7.5
MGM COMPRO REB30	40	8.15
MGM COMPRO REB50	50	12
MGM COMPRO REB60	60	15.3
MGM COMPRO REB90	80	22
MGM COMPRO REX30	25	5.25
MGM COMPRO REX50	35	8
MGM COMPRO REX90	70	17.3

Table 4: EMs regression data

3.3.4 Power generation System

The power generation system considered for ***Colibr-e Sapphire***, is composed by a single internal combustion engine (ICE) and a directly-driven generator, which transforms mechanical power into electrical power. A single regression has been constructed, combining ICE regression with generators' one. Concerning the first, a wide range of general aviation ICEs has been considered. A list of Continental, Rotax, Lycoming (and others) engines has been analyzed 5; then, a linear regression on performance of interest has been carried out. Figure 20 presents the relation between maximum continuous output power and dry mass.

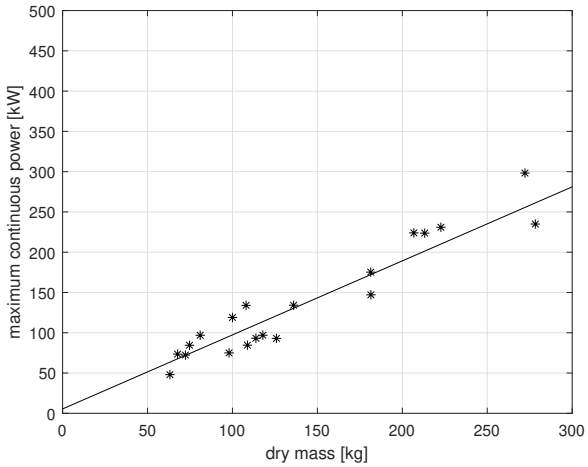

Figure 20: ICE regression

ICE	**Power** [kW]	**Dry mass** [kg]
Rotax 582	48	63.2
Rotax 912	73.5	67.7
Rotax 914	84.5	74.7
Lycoming O-235-C	84.6	108.8
Lycoming O-235-F2B	93.21	113.8
Lycoming O-290-D	96.94	117.9
Lycoming O-360-A	134.2	136
Lycoming TIO-360-A	147.1	181.5
Lycoming O-540-F1B5	175.24	181.4
Lycoming IO-540-K1E5	223.71	213.2
Lycoming IO-720	298.28	272.2
Continental O-200-A	75	98
Continental IO-240-B	93	125.9
Continental IO-550-A	224	206.8
Continental IO-550-N	231	222.7
Continental TSIO-550-B	261	317
Continental TSIO-550-N	235	278.3
UL-Tech 260i	72.3	72.3
UL-Tech 350iSA	96.9	81
UL-Tech 390iS	119	100
UL-Tech 520i	134	108

Table 5: ICE regression data

Generators regression was constructed by taking into account electric motor/generators delivering a relatively large amount of continuous power (Table 6 and Figure 21).

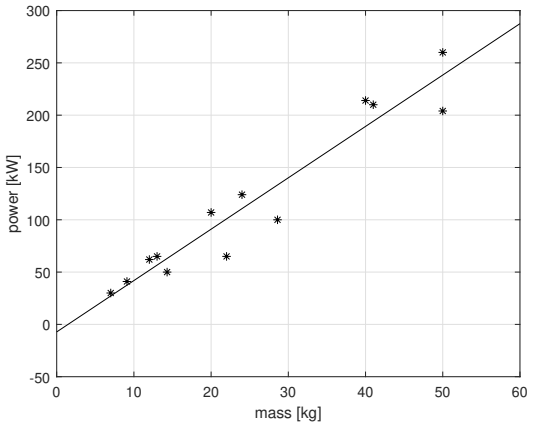

Figure 21: Generator Regression

Generators	**Power** [kW]	**Mass** [kg]
Emrax 188	30	7
Emrax 208	41	9.1
Emrax 228	62	12
Emrax 228 (x2 stacked)	124	24
Emrax268	107	20
Emrax 268 (x2 stacked)	214	40
Emrax348	210	41
Safran GENEUS 50	50	14.3
Safran GENEUS US 100	100	28.6
Siemens sp90g	65	13
Siemens sp200d	204	50
Siemens sp260d	260	50
MGM COMPRO REB90	65	22

Table 6: Generator Regression Data

Summing up, Figure 22 presents the final relation consfor the PGS.

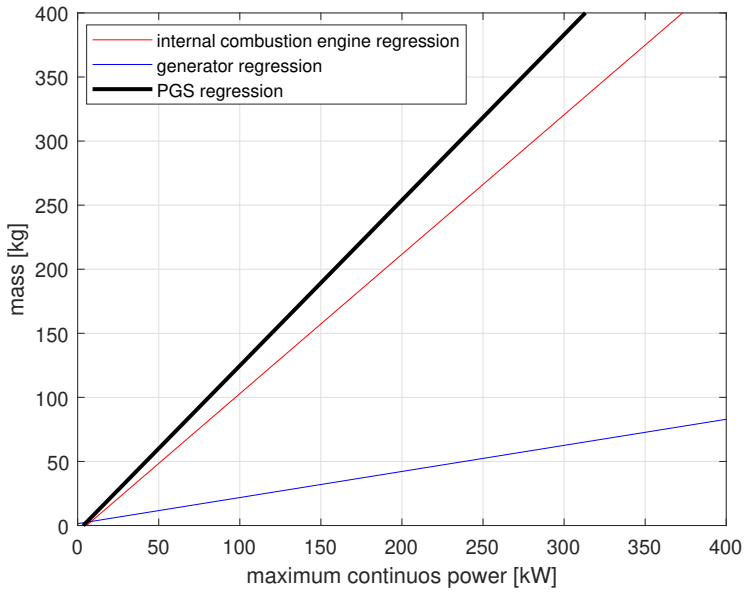

Figure 22: Power generation system regression

3.3.5 Preliminary aerodynamic data

First approximation of aircraft drag polar is based on a **parabolic drag polar** model, which rely on few initial parameters.

$$C_D = C_{D_0} + kC_L^2$$

Referring to this model, estimations had to be done for zero-lift drag coefficient, aspect ratio and Oswald parameter. Parameter k is expressed as:

$$k = \frac{1}{\pi AR\, e}$$

In order to get an initial value for k, preliminary guess for wing aspect ratio AR and Oswald parameter e have been made. Typically e ranges between $0.75 \div 0.85$. General aviation aircraft usually present AR values between 7 and 8. Anyway, DEP allows to increase AR with respect to conventional aircraft [6], as explained later in section 5.1. As initial values $\boldsymbol{e = 0.85}$ and $\boldsymbol{AR = 10}$ have been chosen.

Drag coefficient build up

Zero-lift drag coefficient is one of the most difficult parameter to estimate at initial stage. As a first rough value, Tecnam P2006T coefficient was considered, $C_{D_0} = 0.024$. This approximation is based on consideration about general arrangement of aircraft external layout (i.e. high wing, retractable gear, lack of wing strut and dimensions) Later on, a more detailed estimation was made and the value was updated considering wet surfaces.

Maximum-lift coefficient

Short takeoff and landing performance requirements imply to achieve values of maximum-lift coefficient as high as possible during take-off and landing phases in order to decrease terminal speeds. An initial guess for maximum C_L was made for different aircraft configurations, namely clean, takeoff and landing. Hypothesized values are $C_{L_{MAX}} = 2$ in clean configuration, $C^{TO}_{L_{MAX}} = 4$ for take-off and $C^{LND}_{L_{MAX}} = 6$ for landing. It must be noted that these values will have to be achieved by the entire aircraft, hence with the use of high lift devices and distributed propulsion. Technical papers [7], [6] claim it is possible to reach such high values (even $C_{L_{MAX}}$ in excess of 6) with proper use of distributed propulsion coupled with adequate airfoil.

3.4 Sizing Matrix Plot and propulsive configuration

Sizing matrix plot is a useful design tool which allows to define a preliminary wing loading and power loading.In the case of a 'conventional' aircraft, SMP accounts for total power available (or installed) which is demanded to produce thrust and fly the constraints, at a given wing loading. A 'conventional' SMP has been developed at first.

Constraints definition

The most strict constraints concern STOL capability of the aircraft. RFP specifies a maximum field length of 300 ft (91 m) for take-off and landing over a 50 ft obstacle distances, with dry pavement (sea level ISA+18°F day). Initial climb rate at sea level is required to be at least 1500 ft/min. Service ceiling of at least 14000 ft for terrain clearance in mountainous areas, and minimum cruise speed is 150 kts.

Another set of constraints comes from application of FAR requirements. The airplane belongs to CFR Part 23 ('Normal Category Airplanes') and is defined as a level 2 (configuration of 2 to 6 passengers) low speed airplane. The aircraft is required to meet 14 CFR §23.67 for climb in one engine inoperative condition (if treated as a twin engine airplane). Aircraft must also meet 14 CFR §23.49 regarding maximum stalling speed which cannot exceed 61 kts at maximum weight. Constraints that have been considered are shown in Table 7

Constraint	Imposed by	Parameters	Condition
Take-Off distance	RFP	300 ft over a 50' obstacle	@ 0 ft ISA+ 18°F
Landing distance	RFP	300 ft over a 50' obstacle	@ 0 ft ISA+ 18°F
Rate of climb	RFP	1500 ft/min	@ 0 ft ISA+ 18°F
Stall speed	Team	59 kts	@ 0 ft ISA STD (Clean configuration)
Cruise speed	Team	180 kts	@ 9000 ft ISA STD
Service ceiling	Team	15000 ft	with +100 ft/min
Climb gradient (AEO)	FAR §23.67	at least 8.3%	@ 0 ft MCP, LG up, flaps TO
Climb gradient (OEI)	FAR §23.67	Show steady climb rate	@ 5000 ft
Climb grad (balked landing)	FAR §23.67	at least 3.3%	@ TOGA, LG down, flaps LND

Table 7: SMP constraints

As Figure 23 shows, design space turned out to be extremely restricted due to some constraints, in particular TO distance and LND distance requirements. It is clear that a **DEP** model had to be included in constraints formulation, to take into account effect of blown lift (as a function of power). When dealing with distributed propulsion, power is used not only to produce thrust but also to generate lift, in fact, airflow produced by propellers blows the airfoil to generate extra lift. As a consequence constraints curves are modified.

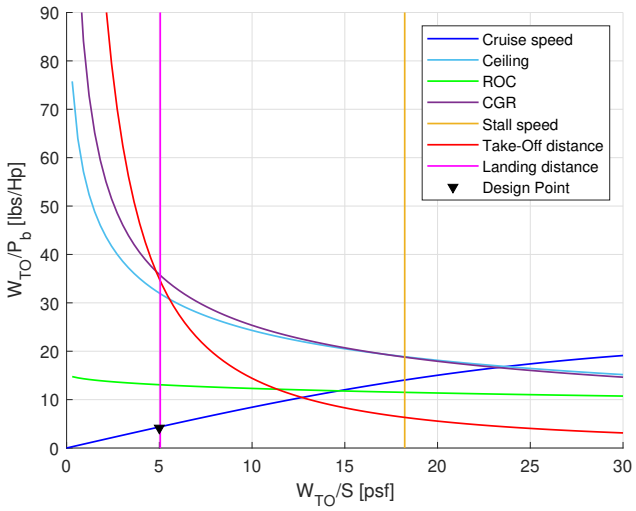

Figure 23: 'Conventional' SMP

Propulsive configuration - Patterson Model

The aerodynamic interaction between powertrain and lifting devices is strong and could not be neglected. Patterson model has been used to estimate increase in lift coefficient due to blown lift. To account for modifications on constraints, a MATLAB script was developed based on Matrone's work [8]. At this point a propulsive configuration had to be defined. Two main possible ways to design powertrain and blown lift integration were considered.

Configuration A - SPLITTED propulsive system It consists of two separate systems: one system is dedicated to produce thrust ('propulsive system'), while the other is dedicated to generate augmented lift ('high-lift system'). During high-power and high-lift demanding phases (i.e. takeoff), both systems are working. During cruise phase, only 'propulsive system' is working.

Configuration B - SINGLE propulsive system Consists of only one system: an array of motors which operate simultaneously. It must be sized so that meets thrust and lift needs for every flight phase.

To take into account these different solutions during initial sizing phase, SMP had to be modified accordingly:

- For Configuration A, it is useful to develop two distinct SMP, one accounting for 'power-to-thrust', and the other accounting for 'power-to-lift'. The output is a couple of design point each one of which satisfies constraints. This method allows to size the two systems separately.

- For Configuration B, it is mandatory to develop a single SMP which takes into account both constraints regarding 'power-to-thrust' required and power linked to 'lift increase requirement'. The output is a single design point that fulfill all constraints, considering that power installed is modifying lift coefficient.

The Team decided to investigate both design possibilities. Results are shown in figure 24

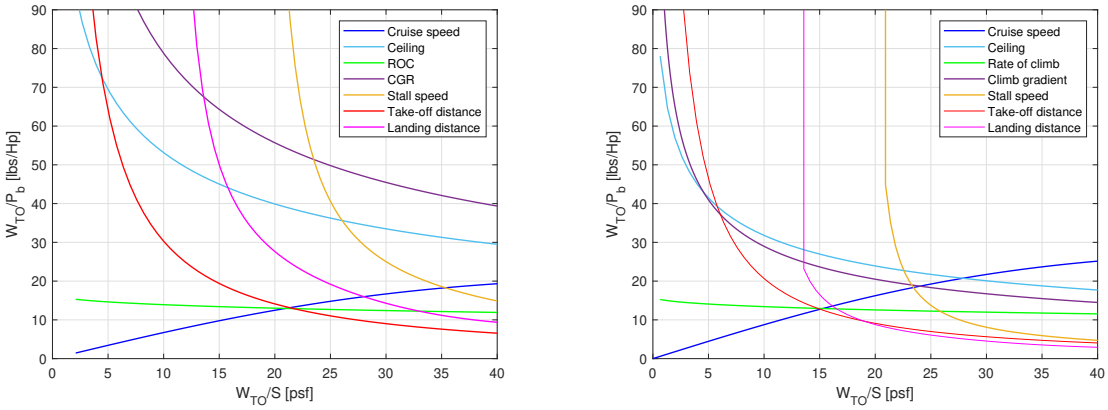

(a) SMP with SINGLE propulsive system

(b) SMP with SPLITTED propulsive system

Figure 24: Modified SMPs

The Team decided to proceed considering **configuration B**, whose associated design space is depicted in 24a. As shown by figures above, design space resulting from single propulsive system option is larger. Patterson model allows furthermore to make preliminary considerations about engine number. Various configuration with different EM numbers have been considered, in particular with 6 EMs, 8 EMs and 10 EMs. DEP sizing, which is necessary to be estimated at this stage, is treated in detail in section 5.4.

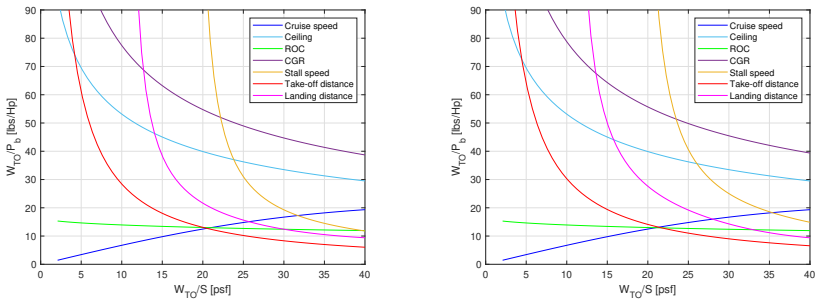

(a) 6 electric motors

(b) 8 electric motors

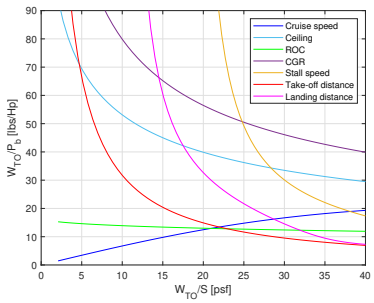

(c) 10 electric motors

Figure 25: SMP with SINGLE propulsive system

Final SMP accounts for a **SINGLE** propulsive system with **8 EMs**. Design space and design point are reported in Figure 26.

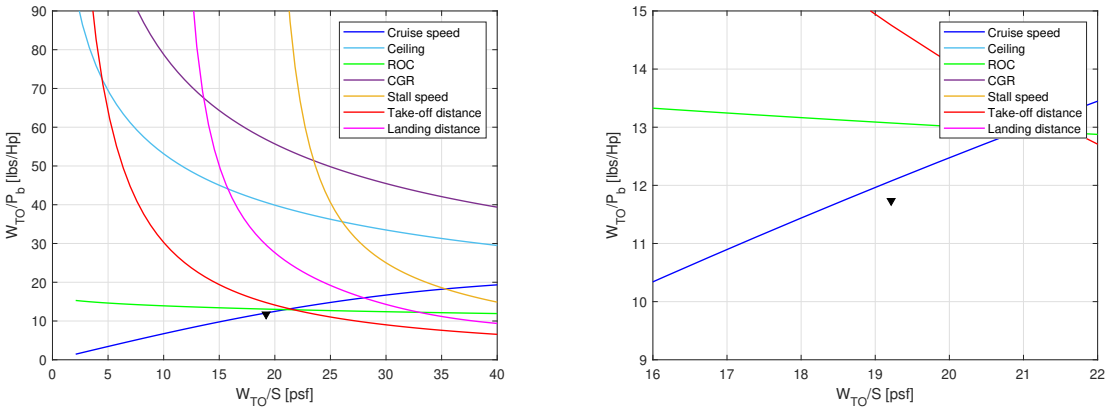

(a) Design point

(b) Zoom on the design point

Figure 26: SMP (Configuration B), with 8 motors

Design point is:

- ***W/S* = 19.2** psf (920 N/m^2) and
- ***W/P* = 11.7** lbf/Hp (0.07 N/W)

3.5 Optimizer and preliminary weight breakdown

Since the airplane had to be equipped with an hybrid-electric powertrain, classical weight estimation methods couldn't be applied effectively (i.e. fuel fraction method). Much research is being recently carried out in order to develop methods able to provide sufficiently accurate weight breakdowns in the case of HE or FE propulsion. The Team decided to exploit the method proposed in [9]. This work is based on the solution of an optimality problem, where the goal is to minimize a merit function J (Team chose as function to be minimized both maximum take-off weight and production cost merit function), while satisfying a series of constraints concerning mission and performance.

$$J = \frac{W_{PGS}}{W_{PGS_{REF}}} + \frac{W_{fuel}}{W_{fuel_{REF}}} + \frac{W_{EM}}{W_{EM_{REF}}} + \frac{W_{battery}}{W_{battery_{REF}}}$$

$W_{PGS_{REF}}$, $W_{fuel_{REF}}$, $W_{EM_{REF}}$, $W_{battery_{REF}}$ represent some reference values whose task is to scale the weights, which are actually the parameters to be optimized. The production cost-function was estimated with method proposed in [10]. Eventually results highlighted how minimizing the weight-merit function is equal to minimizing the cost-merit function. Fundamental inputs to the aforementioned algorithm were the power loading and wing loading previously determined and sizing mission data. Flight mechanics is imposed with a set of constraints.

Considered constraints are reported below.

- $\beta_{lower}\, W_{TO_{reg}} \leq W_{TO} \leq \beta_{upper}\, W_{TO_{reg}}$ where $W_{TO_{reg}}$ is in accordance with regression in Figure 15 and β_{lower} and β_{upper} are bound imposed in Figure 15.
- $\theta_{lower}\, P_{SMP} \leq P_{available} \leq \theta_{upper}\, P_{SMP}$ where P_{SMP} is Power present in 26 and θ_{lower} and θ_{upper} are bound imposed by Team.
- Battery power and energy limits: battery SOC must not exceed bounds imposed by RFP. Power and energy delivered from battery pack can not exceed maximum imposed by batteries technology.
- TO distance must be less than TO distance limit imposed by RFP.
- Throttle must be between 0% and 100% so σ must between 0 and 1.
- At the end of the mission, the remaining fuel is 10 % of the initial value, imposed by Team.
- Power recharge (from PGS to battery) must be greater than 0.

Results of preliminary sizing process are shown in Table 8.

Component	**Weight** [lbs]	**Mass** [kg]
PGS	395.3	179.3
Fuel	165.0	74.9
EM	100.7	45.7
Battery	563.3	255.5
Empty	1720.2	780.3
Payload	870.8	395
MTOW (MTOM)	3815	1730.7

Table 8: Optimizer outputs

4 Initial Sizing And Lofting

4.1 Geometry Sizing

Given the initial MTOM estimation, the regression formula for twin engine GA airplanes presented in [11] yielded an initial **fuselage length** estimation of 8.38 m. However, this length only served as an initial guess for the first sketches. Later, it was increased to a final value of 9.58 m. The actual **wing size** was simply determined as $\frac{W}{W/S}$: resulting surface was $S = 18.45$ m^2. This value was taken as a fixed reference for all the following calculations. For **empennage** initial sizing, a tail arm estimation was needed. This was initially considered to be 4.5m, that is equal to 53% of the computed fuselage length. The horizontal and tail areas were estimated using the following tail volume coefficients, corresponding to typical values for twin engine GA aircraft, as suggested by Raymer:

- $c_{HT} = 0.80$
- $c_{VT} = 0.07$

These coefficients yielded initial an horizontal tail surface of 4.49 m^2 and a vertical tail surface of 3.99 m^2. These values were later adjusted to account for stability and control requirements.

4.2 Cabin Design

RFP requires the airplane to be able to accommodate passengers up to the 99% male adult. Proper margins were added to this constraint, in order to offer better comfort. A structural depth of 3.8 cm was considered, plus a cabin floor thickness of 2.9 cm. Table 9 shows a summary of **cabin section** lofting.

	Height [cm]	Width [cm]
Sitting 99% adult	144	55.1
Margin	10	7
Structural Depth	3.8	3.8
Floor Depth	3	-
Internal Dimension	154	117.2
External Dimension	164.6	124.8

Table 9

Regarding the cockpit, as shown in Figure 27, the Team made sure to allow a pilot downwards visibility of 15°, plus upwards visibility angle of 35° which is more than the minimum requirements of 14 CFR 23.773, *Pilot Compartment View*. Moreover, the wing positioning and windows will allow for proper lateral field of view (FOV).

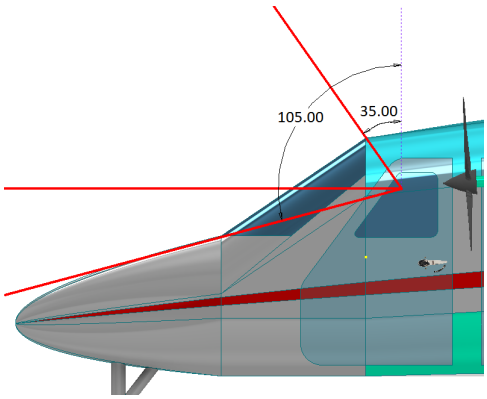

Figure 27: Visibility angles

Regarding **access doors**, the configuration chosen was the one with two doors on the left side, which is common in many GA aircraft. This allows to save weight with respect to a 3-doors configuration. Passengers' door was appropriately designed to be 85 cm wide to allow for easy cargo loading and unloading. As previously said, the aircraft can be used for different applications: aerotaxi, flight school, cargo and medical. Cabin was design in order to accommodate the peculiarities of these four uses with little to no customization required: for flight school the two piloting stations are both operative, for aerotaxi one of the two (the left one) is transformed into a passenger seat by detaching the control wheel and pedals, which can be easily done by a ground operator. For cargo uses, passenger seats are removed and nets installed to separate cargo from pilot; for medical uses, passenger seats are removed and a medical stretcher support and a rotating seat for the doctor are installed.

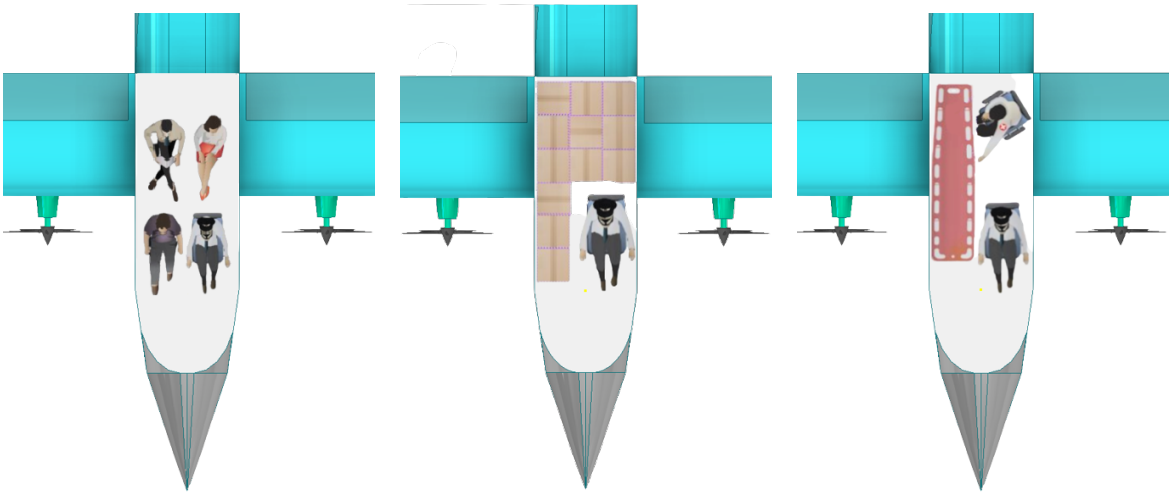

(a) Aerotaxi/flight school configuration

(b) Cargo configuration

(c) Medical configuration

Figure 28: Cabin layouts

5 Aerodynamics

5.1 Aero-propulsive interaction

Given the strong importance of aero-propulsive interaction on overall design process and final aircraft performance, this topic was investigated at first, prior to wing and propulsion design.

As stated by [6], the goal of the DEP system is basically to increase wing's cruise efficiency. Most GA wings are larger than they need to be for cruise 'optimized' configuration. DEP is intended to provide typical takeoff and landing performance with a smaller wing. The challenge is to design an airfoil/flap/DEP system that meets all of the mission requirements that the larger GA wing meets. As a consequence, distributed propulsion needs higher aspect ratio wings to minimize the increase in induced drag. This fact can be clearly seen in the design outcome of X-57 Maxwell versus original Tecnam P2006T. Moreover, given the surface area, higher AR means higher wingspan, which is needed to accommodate the number (possibly high) of motors. Another aspect to be taken into account is the blown lift 'feasibility' over all flight phases. As noted in [7], the aircraft must have the capability to perform a stabilized approach to landing, while the high-lift system is activated. This in turns has an impact on propellers and flaps design. Effects of blown lift and DEP sizing are treated in more detail in Section 5.4

5.2 Airfoil and wing design

Airfoil selection

Initially, main concern was about STOL performance. Therefore some high lift airfoils have been considered at first: WORTMANN FX 72-MS-150B, WORTMANN FX 74-Cl5-140 MOD (smoothed), Selig S1223, Eppler 420 and Eppler E423 were compared. Such airfoils are ideal for low speed flight but present strong disadvantages at higher speeds (i.e. high absolute value of pitching moment coefficient and low lift-to-drag ratio at designed cruise C_L). In fact, other characteristics are desirable beyond C_L performance. Ideal airfoil should present the following properties:

- High maximum lift coefficient C_{Lmax}
- High stall angle of attack α_{stall}
- High lift curve slope $C_{L/\alpha}$
- High (more negative) zero-lift angle of attack α_0
- Smooth stalling behaviour
- Low (absolute value) pitching moment coefficient C_m
- Low minimum drag coefficient $C_{D_{min}}$

- Low drag coefficient $C_{D_{min}}$
- High lift-to-drag ratio $\left(\frac{C_L}{C_D}\right)_{max}$

The following set of airfoil have been compared then: NACA 1412, NACA 2412, NACA 4412, NACA 63-212, NASA/LANGLEY MS(1)-0313, NASA/LANGLEY MS(1)-0317. Analysis have been carried out using XFOIL and XFLR5. Airfoils characteristics have been evaluated at different Reynolds numbers and configurations, corresponding to cruise, take off, landing and clean stall conditions.

Airfoil	$C_{D_{min}}$	C_m	$C_{L_{max}}$	$C_{L_{max}}$, $\delta = 20°$	$C_{L_{max}}$, $\delta = 40°$	E_{max}	$\%t/c$	Stall
NACA 2412	0.005	-0.053	1.685	1.97	2.06	115	0.12	Smooth
NACA 4412	0.005	-0.104	1.76	1.98	2.04	155	0.12	Smooth
MS 313	0.005	-0.086	1.90	2.11	2.19	105	0.13	Moderate
MS 317	0.005	-0.088	1.96	2.17	2.25	98	0.17	Smooth
S 1223	0.010	-0.285	2.4	2.45	2.4	147	0.12	Sharp
E 423	0.008	-0.245	2.1	2.25	2.25	194	0.12	Moderate

Table 10: Airfoil comparison

Simulations have been performed at Mach= 0 (incompressible field) for Re= $2.80x10^6$ and Re= $4.40x10^6$. These Reynolds numbers are representatives of MAC airfoil at low speed and high speed flight conditions.

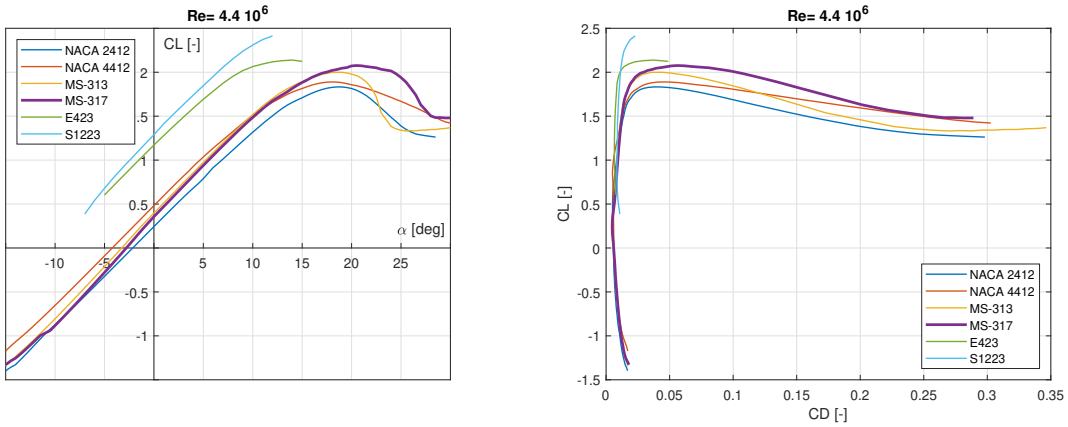

(a) Airfoil C_L-α curve

(b) Airfoil polar curve

Figure 29: Airfoils curves

The airfoil that best fit the requirements has turned out to be NASA/LANGLEY MS(1)-0317. It presents good characteristics at high speed operation, in terms of lift-to-drag ratio, pitching moment coefficient and minimum drag, keeping however good performance at low speed flight i.e. high stall AOA, high $C_{L_{MAX}}$ and smooth stall behavior. Moreover, its higher thickness ($\frac{t}{c} = 17\%$) has a positive impact on structural stiffness of high AR wings.

Wing design

As soon as the weight has been fixed, surface and wingspan were defined to be $S = 18.45$ m^2 and $b = 13.70$ m^2. Different wing planforms have been evaluated, starting from a conventional rectangular shape to tapered and semi-tapered solutions. To define the final optimized shape, a code based on Prandtl's lifting line theory was implemented. The optimum was set as the elliptic lift distribution, while the constraint to be satisfied was the total amount of C_L to be equal to required C_L at equilibrium. Leading edge sweep angle was set to zero in order to facilitate the installation of motors along the span and to prevent interference between motors blown effects. Dihedral angle was set to zero. Manufacturing semplicity has been considered too. Parameters to be optimized were untapered semispan portion (x), wing incidence (i_w), geometric twist angle (α_t) and taper ratio (λ). The outcomes of optimization process are shown in table 11.

x	i_w	α_t	λ
0.54	0.68°	-1.9°	0.42

Table 11: Optimization parameters

In view of the results obtained, the Teams decided to set $i_w = 0°$ for simplicity, in order to let the wing operate in the vicinity of maximum lift-to-drag ratio's AOA during cruise phase. In fact, output value did not lead to any particular advantage. Wingtips are twisted $-1.9°$ in order to decrease local AOA and let this portion of the wing stall at higher angle of attack. Taper ratio was increased at $\lambda = 0.6$ to prevent wing tip stall and enforce wing root portion to stall first. This expedient helps to ease stall awareness and prevention. Stall progression over the wing is shown in Figure 30b. The plot depicts C_L distribution along wing semi-span for different AOA. Stall arises at 19° AOA involving, at most, 29% of semi-span. The span of rectangular planform is wide enough to let flaps to be installed and to be blown effectively.

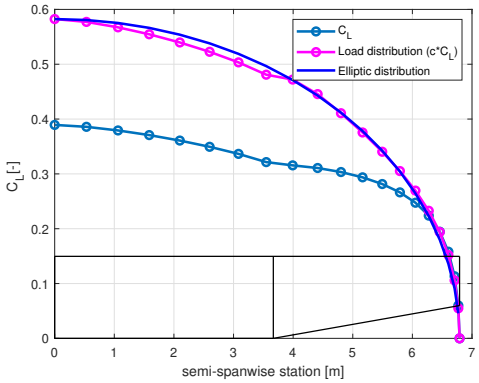

(a) C_L and Load distribution

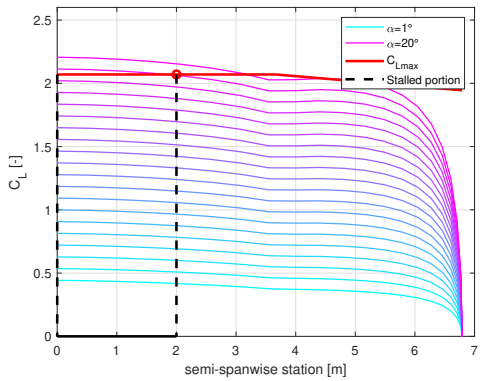

(b) Stall behavior

Figure 30: Wing characteristics

5.3 Drag polar curves

Analysis of aerodynamic properties of the entire aircraft have been conducted with XFLR5. Clean, flaps 20° and flaps 40° configurations have been considered. Eventually the software didn't reach convergence for flapped wing, hence, estimations with empirical formulas proposed by Raymer have been done.

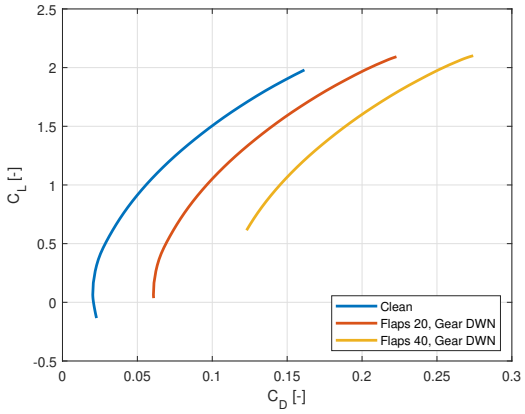

(a) Aircraft estimated drag polars

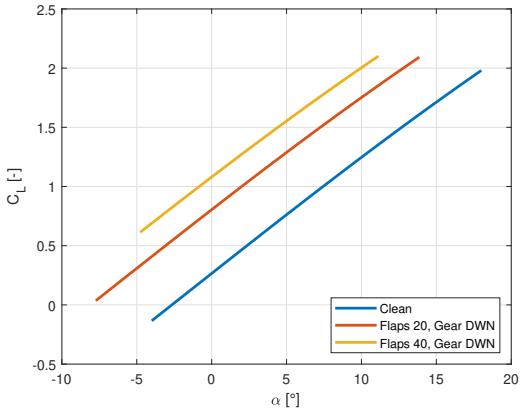

(b) Aircraft lift curves

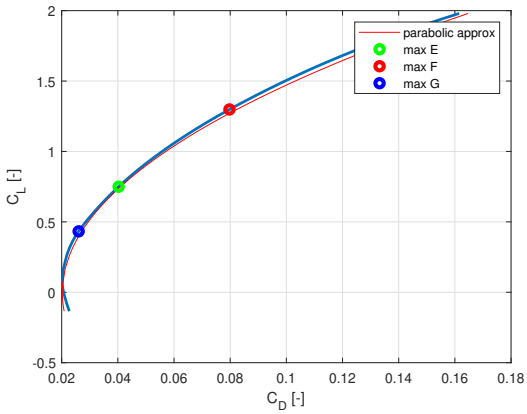

(c) Clean polar with parabolic approximation

Figure 31

Plots and aerodynamic characteristics are referred to **unblown aircraft**. In Figure 31a can be noted that plain flap does not provide large increase of maximum C_L, in fact, for high flap setting, its main effect is to increase drag. Lift curves maintain approximately the same slope. In Figure 31c clean polar is shown along with its parabolic approximation and characteristic points (maximum lift-to-drag ratio, max F and max G). Parabolic polar parameters are $\boldsymbol{C_{D_0} = 0.0202}$ and $\boldsymbol{K = 0.0368}$

5.4 Blown lift effects - DEP sizing

As previously cited in section 3.4 a MATLAB program has been implemented in order to predict effect of DEP on aircraft overall aerodynamic. Input for the program are N, D_P, i_P, x_c, Δy and ΔY . Output of the program are the increase in lift coefficient ΔC_L, zero-lift drag coefficient ΔC_{D0} and induced drag coefficient ΔC_{Di} for each flight phase and aircraft configuration. Following a trial and error approach, the Team was able to estimate an initial sizing for DEP, capable of ensuring desired characteristics. Final DEP geometrical layout is: **N**=8, $\boldsymbol{D_P}$**=1.18 m**, $i_P = 3°$ and $\boldsymbol{\Delta Y}$**=0.9**. Distance between axis of the propellers is 1.52 m, while distance of propeller disk from LE is 42 cm. Effect of DEP system is shown in Figures 32, superimposed to drag polar of unblown aircraft.

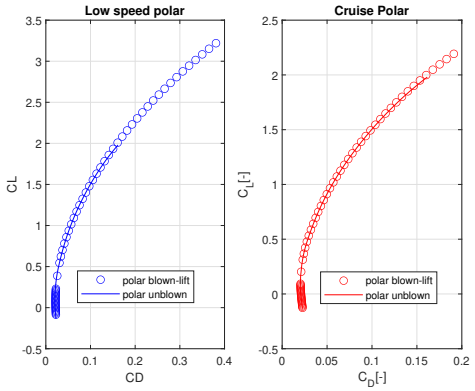

(a) Clean configuration

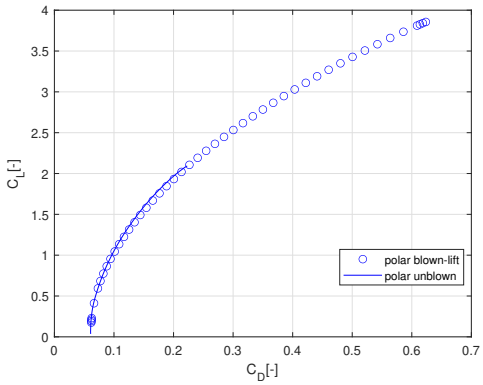

(b) Take-off configuration

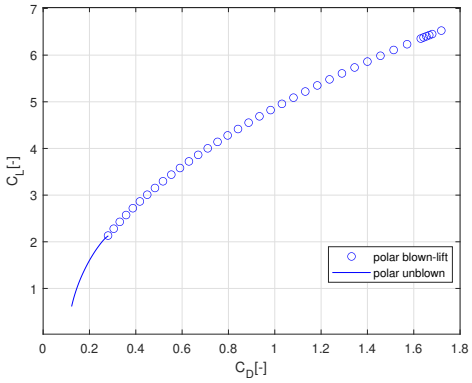

(c) Landing configuration

Figure 32: Estimated blown drag polars

Solid lines represent unblown aircraft drag polars, dots represent blown polar data estimated with Patterson model. At low speed flight conditions and high power settings, increase in C_L due to blown lift is huge. The increase is even greater with deflected flaps, since the propeller jet is deflected downwards.

5.5 Flaps design

Blown lift technology requires a proper flap deflection to be defined in order to balance lift increase, drag increase and thrust increase. Simple plain flap was chosen as it represents the best trade off between complexity, weight and lift enhancement. In order to achieve desired C_L increment, flapped surface was determined using formulas suggested by Raymer:

$$\Delta C_{L_{MAX}} = 0.9(\Delta C_{l_{MAX}})_{airfoil} \frac{S_{flapped}}{S_{ref}} cos\Lambda_{H.L.}$$

$$\Delta \alpha_{ZL} = (\Delta \alpha_{ZL})_{airfoil} \frac{S_{flapped}}{S_{ref}} cos\Lambda_{H.L.}$$

After that, flap chord and flap deflection were selected. Raymer and Gudmundsson suggest that typical flap chord should be of the order of 20%-30% of wing chord. To define $\frac{c_f}{c}$ and flap deflection angle, sensitivity studies have been conducted using XFLR5 data. Figures 33 show properties of airfoils with respect to flap deflection and hinge position over chord.

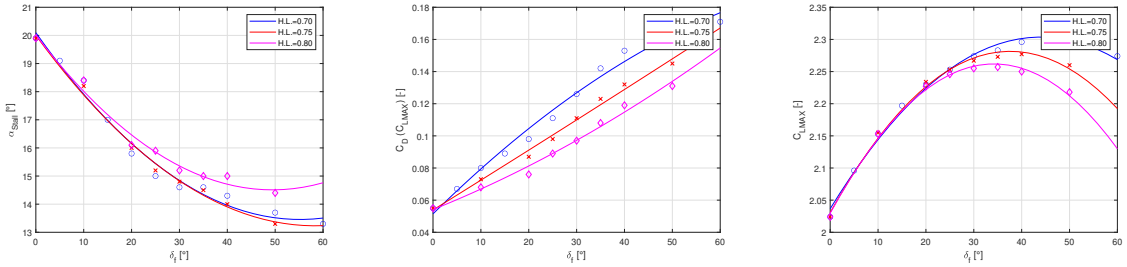

(a) AOA vs flap deflection **(b)** C_D vs flap deflection **(c)** C_L vs flap deflection

Figure 33: Airfoil performance with flaps

Final design led to a flap span of $b_f/b = 0.52$ and a $c_f/c = 0.30$ (hinge line chord with respect to wing's rectangular section chord), this meets also structural constraints imposed by wing main spar. Regarding flap deflection, a study on flap-DEP interaction has been carried out [7]. As shown in figure below, to perform a stabilized approach at high C_L, a positive C_X must be achieved.This strongly depends on flap deflection.

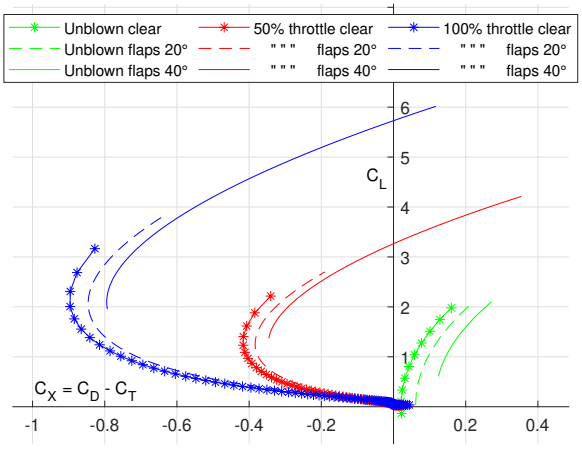

Figure 34: Blown lift vs throttle and flap deflection

As shown in Figure 34, to fly a decelerated path (meaning $C_X > 0$) while generating high C_L, large flap deflections are needed. Maximum flaps deflection therefore has been set to $\delta_f^{MAX} = 40°$

5.6 Ailerons

The aircraft must exhibit a minimum bank angle within a certain specified time in response to aileron deflection. As explained in Subsection 11.1, the Team decided to relie on military aviation standard for Flying and Handling qualities concerning roll control. MIL-F-8785C states a roll control requirement for a class II aircraft, in low speed flight conditions: the aircraft must be able to reach 30° bank angle in 1.8 s. Despite the low landing speed, wing blowing allows an increase in air flow speed on control surface, guaranteeing adequate control authority even at terminal flight phases. The output design parameters needed to met requirement are listed below:

c_a/MAC_{HT} [-]	y_i% [-]	y_o% [-]	δ_a^{MAX} [°]
0.25	60	96	±25

Table 12: Aileron design parameters

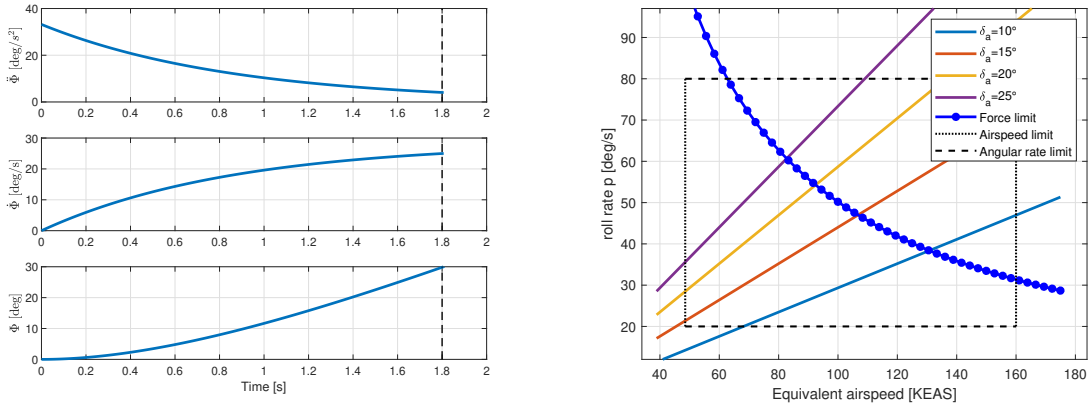

(a) Roll response

(b) Aileron control box

Figure 35

To evaluate the command authority in relation to the maximum force sustainable by the pilot during a roll maneuver, a control box has been implemented. Starting from moments equilibrium at steady state around roll axis, it is possible to obtain, for a given airspeed range, the roll rate values for fixed aileron deflection. An average pilot must be able to exert a control effort without exceeding a maximum limit force of 222 N on command wheel for lateral control. This limit force imply a limit roll rate achievable so as not to over-strain the pilot.
Once the desired airspeed range and a roll rate band have been set, the control box provides a map of the roll command authority.

5.7 Tail design

Based on volumetric coefficients indicated by Raymer and Gudmundsson an initial sizing of tail surfaces has been carried out. The result was checked to be acceptable from the standpoint of static stability, controllability, aircraft dimensions and aesthetics.

Horizontal tail and elevator

Horizontal tail data are shown in Table below.

S_{HT} [m^2]	b_{HT} [m]	λ_{HT} [-]	c_{HT}^{root} [m]	c_{HT}^{tip} [m]	$\mathbf{AR}_{HT}$ [-]
4.45	4.48	0.60	1.244	0.746	4.5
V_{HT} [-]	L_{HT} [m]	i_{HT} [°]	$\Lambda_{quarter}$ [°]	$\bar{y}_{HT}$ [m]	$\mathbf{MAC}_{HT}$ [m]
0.80	4.5	0	9.4	1.03	1.016

Table 13: Horizontal tail geometrical data

The elevator has been sized for take-off rotation requirement and to ensure proper longitudinal control for every CG position inside the actual CG excursion limits. Design parameters are reported in table below.

c_e/MAC_{HT} [-]	b_e/b_{HT} [-]	δ_e^{MAX} [°]
0.35	0.90	±30

Table 14: Elevator data

A parameter of great importance for airplane's flying qualities is elevator gradient with respect to equivalent airspeed. This parameter is related to the 'instinctivity' of longitudinal control. The fact that curves are positive, monotonically decreasing, asymptotically flattening with respect to EAS means that to a positive (or negative) change in speed, correspond an elevator's deflection of the same sign (positive downward, negative upward), with a significant command displacement at lower speed than at higher speed. Regarding stick force control, airworthiness requires not to exceed a maximum value of applicable force (333 N for temporary application and 44.6 N for prolonged application) while ensuring a minimum force gradient at trim condition. The expression of stick force as function of the square of speed plus a constant term, as suggested in [12], leads at these results:

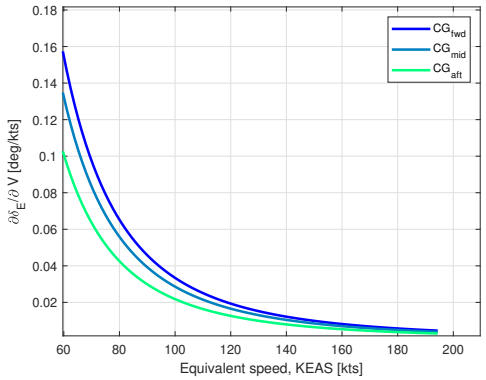

Figure 36: Elevator deflection gradient

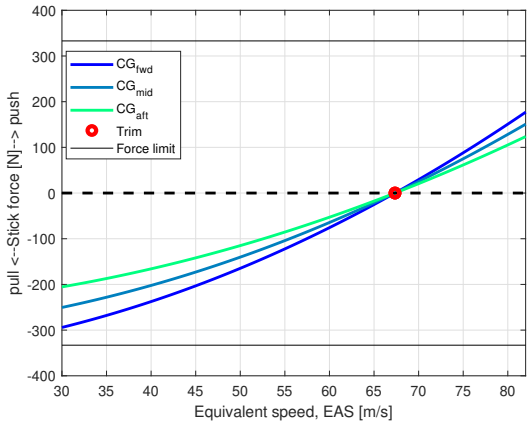

Figure 37: Stick force vs airspeed

C_{H_α}	-0.0238 rad^{-1}
$C_{H_{\delta_e}}$	-0.4131 rad^{-1}
$C_{H_{\delta_t}}$	-0.0985 rad^{-1}
G_e	7 rad/m
$\frac{dF}{dV}^{fwd}$	10.898 Ns/m
$\frac{dF}{dV}^{mid}$	9.277 Ns/m
$\frac{dF}{dV}^{aft}$	7.610 Ns/m

Table 15: Elevator parameters

Force gradient at trim is positive and greater than a minimum value in order to allow the pilot to perceive small changes in airspeed by means of pitch control force changes. A minimum value suggested by Pamadi is $8.7 Ns/m$ achieved for most of admissible CG excursion. The requirements have been met by means of a control tab with 35% of elevator chord, 55% of span length and a gearing ratio of reversible mechanical flight control set to $G_e = 7 rad/m$. Trim solutions are reported below, underlining the effective control achievement for all CG's positions and across the entire speed range without run into controllability stall.

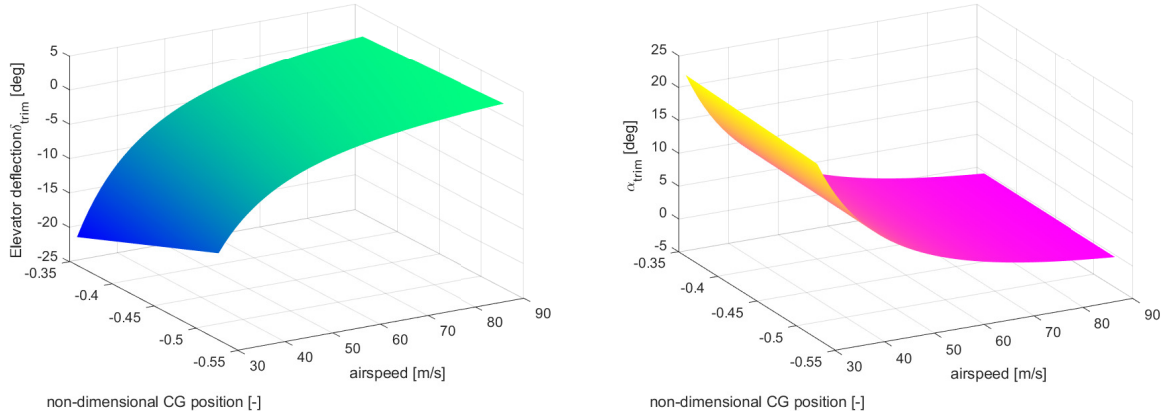

(a) δ_e vs airspeed vs ξ_{CG}

(b) α vs airspeed vs ξ_{CG}

Figure 38: Trim solutions

Vertical tail and Rudder

Initial volumetric coefficient assumed for vertical tail led to an oversized surface. A reduction of coefficient value was necessary. Since motors' positioning could not be modified due to wing blowing constraint, a compromise was found sweeping back the surface, this helps to increase tail arm. Moreover, a dorsal fin was added to increase tail effectiveness. Vertical tail data are shown in Table below.

S_{VT} [m^2]	b_{VT} [m]	λ_{VT} [-]	c_{VT}^{root} [m]	c_{VT}^{tip} [m]	AR_{VT} [-]
2.46	2.00	0.29	2.00	0.58	1.62
V_{VT} [-]	L_{VT} [m]	i_{VT} [°]	$\Lambda_{quarter}$ [°]	$\bar{y}_{VT}$ [m]	MAC_{VT} [m]
0.054	5.246	-	35.8	0.816	1.42

Table 16: Vertical tail geometrical data

Rudder has been sized taking into account **spin recovery** capability. 1/3 of rudder area should be unblanketed by horizontal tail. This was ensured by positioning vertical fin and rudder outside of horizontal tail wake.

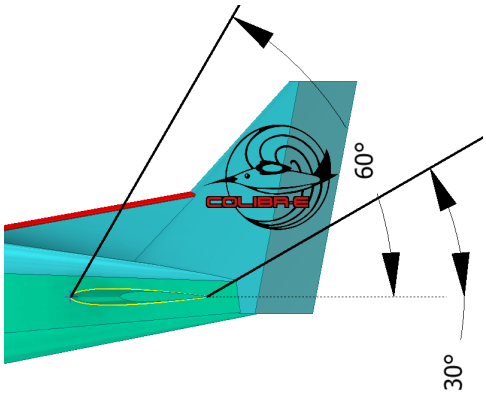

Figure 39: HT VT relative position

c_r/MAC_{VT} [-]	b_r/b_{VT} [-]	δ_r^{MAX} [°]
0.35	1.00	±30

Table 17: Rudder data

Given the low take-off speed, as shown in Figure 40, rudder is not able to counteract effectively a yawing moment deriving by outer motors loss.

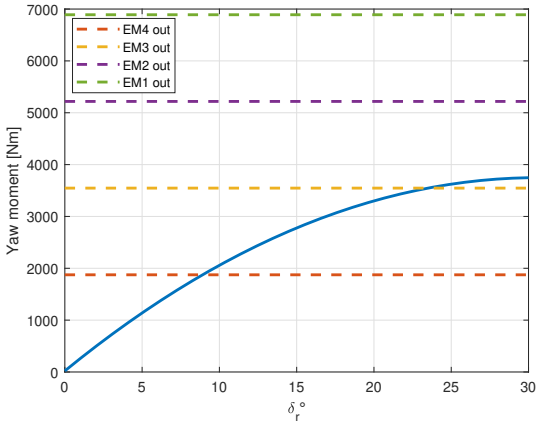

Figure 40: Vertical tail effectiveness

To overcome this problem, it was decided to equip the control unit with an autonomous power control system, which, in the event of a critical motor loss, is able to switch off the symmetrical motor and redistribute the power gap to remaining motors, ensuring controllability during take off run. Referring to the worst thrust condition as the outermost motors loss (EM1,EM2, EM7 EM8, see Figure 49) the control strategy provides, in addition to the symmetrical tip motor shutdown, a power redistribution to recover the yaw moment with the maximum rudder deflection.

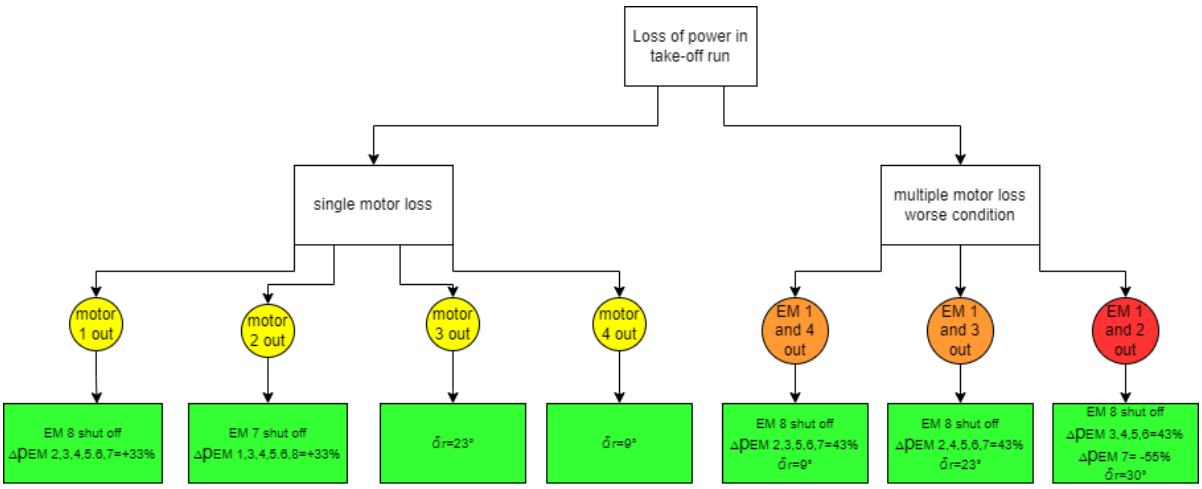

Figure 41: Asymmetric thrust control scheme

The diagram shows the failure modes of motors placed on the left wing. The same reasoning applies to the motors located on the right wing.

5.8 Drag build up

A precise drag assessment has been carried out, based on component buildup method [11] [13]. At first, this method estimates the parasite drag contribution of each component of the aircraft. For each contribution, the following quantities are needed:

- Flat-plate skin friction drag coefficient, C_{f_c}
- "Form factor" FF, estimating the pressure drag due to separation
- Interference factor Q_c, accounting for interference effects
- Component wetted area

Secondly, a miscellaneous component $C_{D_{misc}}$ is added, in order to account for features such us flaps and landing gear. Thirdly, a leakages and protuberances $C_{D_{L\&P}}$ term is added.

The total drag coefficient for a given configuration is found by summing up all the above components, using the following formula:

$$C_{D_0} = \frac{\sum_c (C_{f_c} FF_c Q_c S_{wet_c})}{S_{ref}} + C_{D_{misc}} + C_{D_{L\&P}}$$

Estimated components values and final aircraft parasite drag coefficients are reported in table 18. The takeoff and landing configurations were also considered. Drag coefficients turned out to be very close to initial assumed values.

Component	C_{D0}
Wing	0.0076
Fuselage	0.0060
Nacelles	0.0022
Horizontal tail	0.0016
Vertical tail	0.0006
Miscellaneous	0.0029
Landing gear	0.0160
Flaps 20°	0.0244
Flaps 40°	0.0733
Configuration	C_{D0}
Clean	0.0209
Takeoff	0.0614
Landing	0.1103

Table 18: Zero-lift Drag Summary

5.9 Aerodynamic data

Estimation of all aerodynamic coefficients and derivatives, have been carried out using XFLR5 and Tornado, which are based on VLM. Two surface model of the aircraft have been implemented and analyzed. Recap of final estimated aerodynamic properties is reported in Tables 19, 20 and 21. All stability and control derivatives are referred to CG.

Configuration	C_{D0} [-]	C_{Dmin} [-]	$\left(\frac{L}{D}\right)_{MAX}$ [-]	C_{L_α} [rad^{-1}]	$C_{L_{MAX}}^{unblown}$ [-]	$C_{L_{MAX}}^{blown}$ [-]	α_{max} [°]
Clean	0.0207	0.0202	18.6	5.50	1.98	3.22	18°
Take-off	0.0612	0.0607	10.8	5.50	2.09	3.85	14°
Landing	0.1101	0.1096	8.0	5.50	2.13	6.00	11°

Table 19: Aircraft aerodynamic properties

$C_{L\alpha}$	5.501 rad^{-1}	$C_{\mathcal{M}\alpha}$	-3.777 rad^{-1}	$C_{Y\beta}$	-0.275 rad^{-1}
C_{Lq}	15.795 rad^{-1}	$C_{\mathcal{M}q}$	-28.722 rad^{-1}	$C_{\mathcal{N}\beta}$	0.108 rad^{-1}

Table 20: Main stability derivatives

$C_{L\delta_e}$	0.755 rad^{-1}	$C_{\mathcal{L}\delta_a}$	0.367 rad^{-1}	$C_{\mathcal{L}\delta_r}$	-0.002 rad^{-1}
$C_{\mathcal{M}\delta_e}$	-2.595 rad^{-1}	$C_{\mathcal{N}\delta_a}$	0.007 rad^{-1}	$C_{\mathcal{N}\delta_r}$	-0.089 rad^{-1}

Table 21: Main control derivatives

6 Propulsion and Systems

6.1 PGS

ICE

The optimizer provided an engine rated power of 170 kW (228 BHP). Therefore, initially considered ICE ranged from the Lycoming O-390 to the O-540 (and similar). Only turbocharged versions where considered, in order to compensate for atmospheric density loss, up to an altitude of 15000 ft. After accurate comparisons, selected engine was the **ULPower UL520T**: it's a 6-cylinder, horizontally opposed turbocharged engine, with a displacement of 5254 cm^3 (figure 42).

The engine can deliver up to 220 BHP max power, at 2700 RPM; MCP is 200 BHP, at 2425 RPM. Maximum torque is 585 Nm, at 2300 RPM. The **optimal operating regime** (recommended) in cruise is 2200-2500 RPM. Figure 43 shows the mechanical power and torque coming from the crankshaft, at ISA sea level conditions, as functions of RPM. The blue lines represent the optimal operating range RPM limits. Figure 44 shows the relation of wide open throttle (WOT) power versus altitude. The engine can burn both MOGAS (with a minimum octane rating of 97) and AVGAS (100LL or UL91). **BSFC** is 0.3 l/BHP/h. **TBO** is 1500 hours or 12 years. An **integrated forced cooling system** is adopted, in order to provide a proper cooling of cylinder heads. This system will be available by 2024 on this type of engine, as the company Sales Manager Mrs Evelyne Huyghebaert reports.

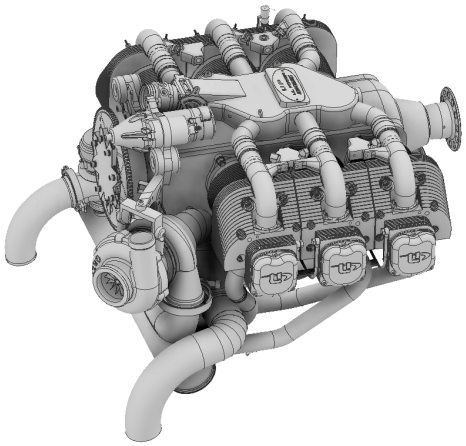

Figure 42: UL520T CAD Model

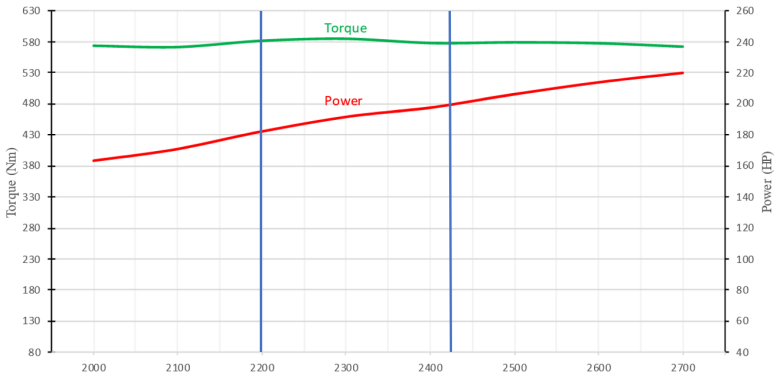

Figure 43: Power/Torque Vs RPM

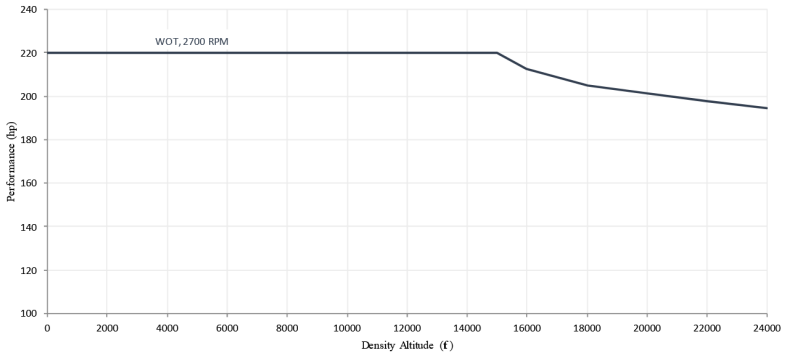

Figure 44: UL520T: Power (Wide Open Throttle) Vs Altitude

Fuel System

The fuel system is composed of two **discrete wing tanks** of 56L (14 US gal) each. No fuel pump is necessary, because fuel the flow to the engine is ensured by gravity feed. This makes the system simpler and allows weight savings.

Generator

Selected generator is the **EMRAX TWIN** (figure 45): it's composed of two axially-stacked (twin) EMRAX268 *axial-flux* generators. It's directly connected to the ICE through a **flexible coupling**, thus it always rotates at the same RPM of the ICE. At 2350 RPM, each generator produces 60 kW. Therefore, two stacked generators will produce 120kW, a very close value to the one provided by the optimizer.

The EMRAX 268 efficiency ranges between 92% to 98% (96% was assumed in calculations). At an RPM range of 2200-2450 RPM, the generator works at it's **maximum efficiency**. Note how this range is very similar to the optimal ICE operating range. Finally, stacking two generators doesn't significantly affect efficiency.

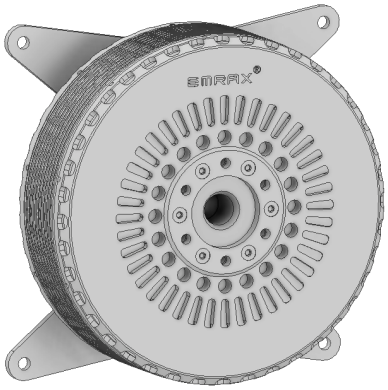

Figure 45: Single EMRAX 268 CAD model

Figure 46 displays EMRAX 268 power and torque curves as functions of crankshaft RPM: optimal regime lies in between the blue lines.

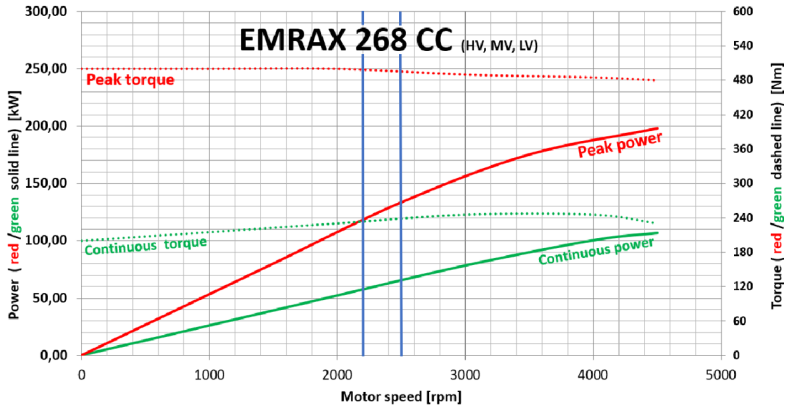

Figure 46: Single EMRAX 268 Power/Torque Vs RPM

Figure 47 shows the efficiency map (optimal regime in between gold lines).

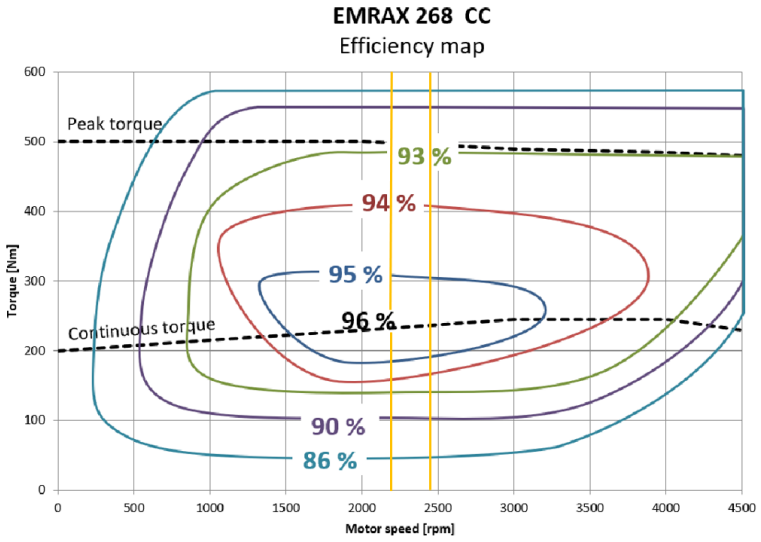

Figure 47

6.2 Electric Motors

The Team decided to employ **Smart Motors**, with integrated motion control systems. This brings many benefits, including easier cooling, simpler power electronics, more reliability and less electromagnetic compatibility issues. Selected electric motors were the **MGM Compro REB30** (figure48). They are brushless direct current (BLDC) motors. With a weight of 8.150 kg, each of them can deliver 30 kW of maximum continuous power, allowing to take advantage of full battery power for a prolonged time. For this reason, the less powerful RET60 motors where discarded. Maximum peak power is 40 kW, depending on supply voltage and RPM: this enables to exploit peak power in case of takeoff or emergency situations (e.g. double motor/propeller loss at takeoff). Maximum torque is 150 Nm, much greater than the maximum required torque at any flight speed/propeller working condition. Limit RPM is 4000, very close to the propellers tip speed limit of 4100 RPM: any higher RPM capability would have been useless. This was another reason to discard the RET60, which is designed to go up to 8000 RPM.

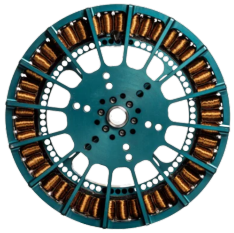

Figure 48: MGM Compro REB30 Motor

6.3 ESC and EPMS

Each motor is strictly connected to its relative electronic speed controller. **MGM Compro HBC 280120** fit perfectly with the chosen EMs: the maximum continuous power is 33 kW. However, product adaptability should allow for a configuration capable of 40 kW of power (EM peak). Each ESC weights 1.180 kg.

EPMS systems are the ”brains” which control the flux of energy and power from storage to the propellers. In order to ensure redundancy, two EMS are needed. One single EMS controls the power flux to the propellers, with a backup one which can replace the first in case of failure. For the purpose of saving weight and cost, a possible alternative would have been to adopt cooperant EPMS (each EPMS controlling half of the motors). It was eventually discarded, because it would have meant to loose 4 motors in case of failure of one EMS: in this case, safety would not be ensured anyhow. In figure 49, a schematic drawing of the adopted propulsion architecture is shown.

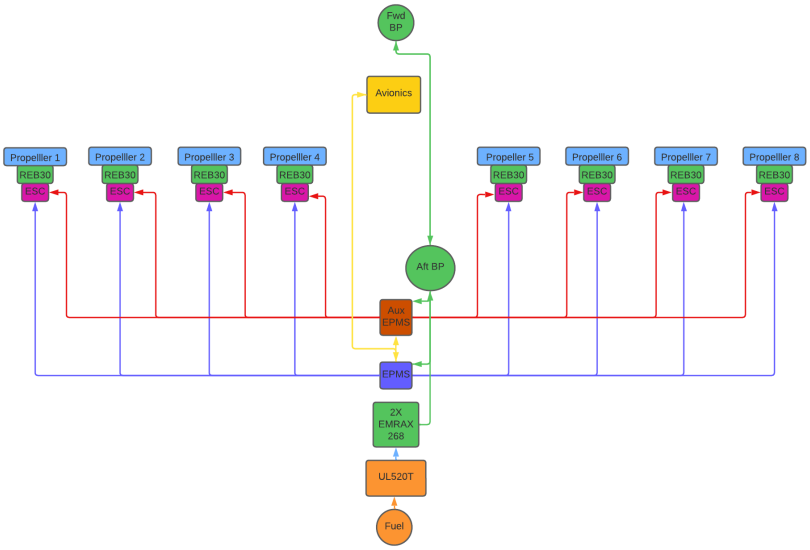

Figure 49: Propulsion System Architecture. Amber: fuel flow. Light blue: mechanical connection. Green: electric power flow. Blue/Red: primary/auxiliary EPMS-motors connection. Yellow: logic connection.

6.4 Propellers

Propeller design was carried out using *JavaProp* software [14]. Sizing constraint was the minimum required static thrust to satisfy TO performance. On the other hand, climb requirements were not as stringent. Moreover, the Team decided to add a minimum cruise efficiency value of 0.80. A summary of requirements is displayed in 22.

Phase	Requirement
TO, 8 EM	minimum static thrust = 1600 N
TO, 6 EM	minimum static thrust = 1900 N
climb, 8 EM	minimum thrust = 412 N
climb, 6 EM	minimum thrust = 550 N
Cruise	minimum η_p = 0.80

Table 22: Propeller Design Requirements

Maximum propellers diameter was limited by DEP implementation to 1.18m. Maximum TO RPM was fixed to 3460, in order to reduce noise pollution. To make FE takeoffs possible, maximum battery power output was considered as a limit in this phase. EM Power limits where eventually considered in any case in which the ICE is turned on. Propeller limitations are summarized in table 23:

Limitation	Value
Maximum diameter [m]	1.18
Maximum TO RPM	3460
Maximum battery power [kW]	27.9
EM MCP [kW]	30
EM Max Power [kW]	40

Table 23: Propeller Design Limitations

Propellers are made of carbon fiber, with a titanium leading edge protection against FOD. The **composite material** allows better TO performance and traction; plus, it brings a series of benefits, such as:

- less weight and vibrations, lower gyroscopic effect
- less repair, longer life
- an increased number of blades
- higher ramp appeal

Figure 50 show the output design. The propellers are of variable-pitch type. Despite being a more costly and heavier solution, it was indeed required. Fixed pitch propellers couldn't allow high TO thrust and sufficient cruise efficiency at the same time.

(a) Blade **(b)** 5-bladed Composite Propeller

Figure 50

Propellers on the two half-wings are counter-rotating (counter-clockwise on right side, seen from behind), allowing a simmetric behaviour.

6.5 Avionics And Electrical System

The airplane will be equipped with an electronically advanced avionics system, making it a *technically advanced airplane* (TAA) as defined by 14 CFR § 61.1.

Garmin G2000 has been chosen as electronic flight instrument system (EFIS). The main interfaces with the pilot are two large 14" touchscreen displays: the primary flight display (PFD) and the multifunction display (MFD). A smaller display lies on the pedestal, with auxiliary functions such has radio controls. A **GPS navigator and autopilot** are integrated in order to allow IFR flight, as per RFP.

6.6 Environmental Control System

The airplane is **not pressurized**, given the typical mission cruise altitude. This allows for a lighter, simpler and cheaper fuselage structural design. Consequently, less on-board power and maintenance will be required. Still, an **oxygen system** with portable oxygen tanks may be integrated, given the RFP requirement of a ceiling of at least 14000 ft. Moreover, for an unpressurized aircraft, 14 CFR § 135.89 prescribes the use of oxygen above 12000 ft (and between 10000 ft and 12000 ft if the flight at those altitudes lasts more than 30 minutes). A possible operative example imposing the use of oxygen is mountain flying. Oxygen tanks can be leaved on ground in any case if the flight altitude will not exceed 10000 ft (at operator discretion). Oxygen system estimated weight is 10 kg, which is not considered for the typical mission analysis. Cabin heating is obtained thanks to heat generated by battery packs. Cooling will be possible thanks to external air.

6.7 Anti-ice system

For flight in icing condition, 14 CFR 23.2165 was consulted. The installation of an anti-ice system has been considered to allow the aircraft to fly in known icing conditions. As stated by 14 CFR 23.2165(b), a means to detect any icing conditions is required. Minimum power loading for anti-ice system [15] is expected to be less than 4 kW/m^2 for temperature of -5 °C and less than 8 kW/m^2 for temperature of -10 °C

6.8 Anti bird-strike systems

In case of flight near wildlife areas the airplane runs into the risk of bird-strike. To reduce the chance of this happening, most airports and airfields already install various systems to scare away flock of birds such as compressed air cannons, sirens and in some cases even falconers. Despite this measures, the chance of a bird impacting the aircraft has to be considered. Having a metal body and eight propellers, reduce the severity of a winged animal impacting the aircraft, anyway the Team still considered necessary to adopt measures to reduce probability of this inconvenience.

The transmit frequencies of the mode sierra transponder already installed on board have been shown to reduce bird presence near the airplane [16]. On top of that a set of strobe lights will be installed to disperse flock of birds with 2 light bulbs installed to grant the availability of at least one strobe light.

Engine emissions and pollution reduction

The main pollutants emitted by every engine are carbon monoxide (CO), carbon dioxide (CO2), hydrocarbons (HC) and nitrogen oxide (NOx). CO2 is the main chemical responsible for greenhouse effect while CO, HC and NOx are highly toxic in case of direct exposure. Reduction of pollutant is of crucial importance, in particular close to populated areas and at low altitudes is extremely important to improve the life quality of citizens and the whole planet.

Thanks to hybrid-electric propulsion and to Team's choice to switch on the ICE only during cruise and transition phases, fuel consumption will be drastically cut down, making sure that all the pollutants emitted will be released at high altitude and will not effect the general population.

Detailed analysis for the selected motor (ULPower UL520T), being recently released, are not currently available. For the following considerations a Lycoming IO-360-A1B6 (with similar performances to UL520T) is taken as a baseline. The Federal Office of Civil Aviation (FOCA) performed a detailed analysis on the emissions of this engine [17]. Data are based on the 40 minutes mission shown in Figure 51

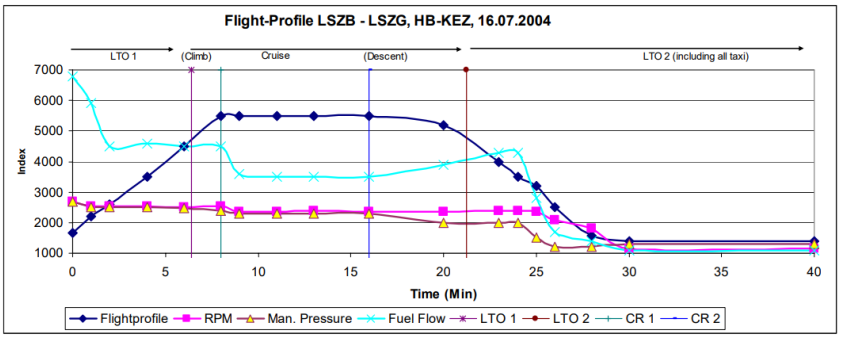

Figure 51: Mission for emission analysis

Results from in-flight measurements are the following:

Phase	$\dot{m}_f$ (kg/s)	CO (g/kg)	HC (g/kg)	NOx (g/kg)
Take-off	0.0136	1278	15.5	1
Climb	0.0106	1288	16.7	1
Cruise	0.0087	1253	8.93	2.55
Approach	0.0062	1342	20.6	1
Taxi	0.0014	1056	43.8	2

Table 24: IO-360-A1B6 emission from [18]

From the Table above it is possible to see that, by performing take-off, climb, approach, landing and taxi in full electric and turning on the engine only during cruise, there is a 50.8% save in NOx, a 84.5% save on HC and a 71.7% save on CO with respect to a standard propulsive system. This represents a homogeneous improvement with respect to today's aircraft and a huge jump towards green aviation!

6.9 Battery Packs and turn-around time

Battery packs have been divided into 5 different BPs of 51 kg each; 3 of them have been placed in the back of the airplane and 2 of them in the front. RFP require to have a turn-around time of 15 minutes between 50 nm missions to allow for loading and unloading of passengers and aircraft servicing. The total amount of energy stored in the batteries is 386 MJ (107,22 kW/h). A 50 nm mission simulation was performed. As a result the airplane arrives at destination with 60% of battery charge. Charging stations differ from one another depending on the amount of kW that they are able to deliver: slow chargers (3-7 kW), rapid chargers (40-50 kW) and ultra-rapid chargers (100-350 kW). To this date a good number of ultra-rapid chargers are available on the market, for example Ionity has produced and made available more than 400 chargers with 350 kW delivery in all Europe [19]. Even being conservative hypothesizing that only 200 kW chargers would be available, the amount of time that it would take to recharge batteries after this kind of mission would be less than 13 minutes. This operation can be easily accomplished while refueling the airplane, making it perfectly reasonable to have a turn around time of less than 15 minutes.

The Team decided to go one step beyond and grant a 15 minutes turn around time regardless of the mission length. To do so, a battery swapping procedure was implemented hence batteries were carefully placed to grant a CG excursion that makes it possible to change them even with no passengers, baggage and fuel on board without having to place an outside support on the airplane.

As it will be thoroughly discussed in 7.6, the landing gear tricycle is designed to solidly keep the airplane firmly on the ground as long as a simple procedure is followed: ”if you need to swap it, the front battery has to be the taken out last and has to be mounted back first”. Note that if this procedure is not followed, the main landing gear will be highly loaded (which has to be avoided if possible), but the airplane will not fall back on its tail.

The amount of electric energy stored in the BPs for emergency reserves and loiter, roughly makes up 25% of the total electric energy on the airplane. The EPMS is programmed to give a ”priority” to the FWD BPs, meaning that the BPs discharge from tail to nose (without dropping below minimum state of charge) and recharges from nose to tail. In normal operations, even after the maximum range mission, the most FWD battery pack will be still charged so that only 4 out of 5 BPs are swappable. The most likely case is to have all FWD BPs charged and the AFT BPs needing to be partially swapped.

Panels and BPs are ergonomically placed so that the batteries can be easily changed without any special equipment but a simple sledge or ramp to slide batteries out. This makes the job of the ground staff easier and faster. A complete battery change can be performed while the airplane is being refueled, making it possible to have a turn around time of 15 minutes on every flight if a charged set of batteries is available at the arrival.

7 Airframe Structure And Weights

7.1 V-n Diagram

The V-n diagram is drawn at MTOM. To construct it, the maneuvering and gust envelope are needed. Since the airplane will be certified in the 'normal' category, in the maneuvering envelope $n_+ = 3.8$ and $n_- = -1.52$. The cruise speed is set to $V_C = 146$ KEAS. As a consequence, the **design dive speed** results being $V_D = 204$ KEAS. The never exceed speed will be therefore $V_{NE} = 217$ KTAS. The maneuvering speed is $V_A = 100$ KEAS. The positive and negative stall speeds are $V_{S+} = 51$ KEAS and $V_{S-} = 69$ KEAS.

Next, the gust envelope is constructed. For this category of aircraft, positive and negative 50 ft/s gusts must be considered at V_C; instead, positive and negative 25 ft/s gusts must be considered at V_D. This information allows to build the gust envelope.

All this data is reported in the V-n diagram in figure 52. Darker green area represents the case of fully deployed flaps, for which stall speed is $V_{S0} = 31$ KEAS and maximum flap extended speed is $V_F = 72$ KEAS. In

both diagrams, the aero-propulsive interaction is accounted for.

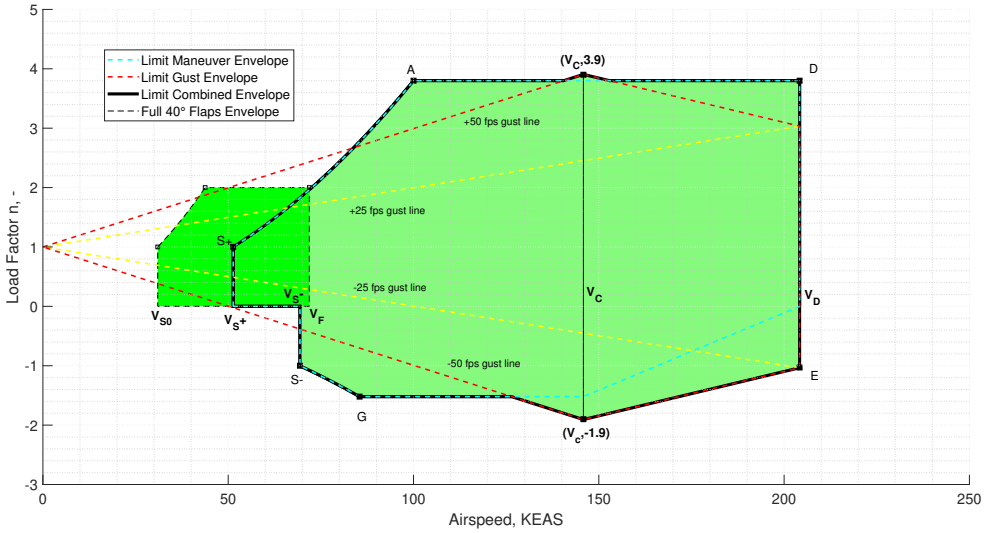

Figure 52: V-n plot

7.2 Materials Selection

The Team decided to go for a **classical aluminum construction**: composite materials could give an estimated 15% structural weight reduction [20], which wouldn't be enough to justify the increase in costs. Moreover, a strong importance was given to the feedback obtained by potential customers, who tended as well to prefer classical manufacturing methods. On top of that, adopting a composite construction would increase maintenance cost and time between inspections, which has to be minimised as much as possible. Adopting a new technology such as an hybrid-electric propulsive system will naturally increase maintenance frequency: in order to have an overall flight hours-to-maintenance hours ratio similar or better than competitors', the use of simple but reliable structural strategies is mandatory. Finally an aluminum airframe will make the airplane safer in case of FOD, which in light of this RFP specifications, has a better chance of happening. This is due to the fact that the airplane has to take-off even from gravel, dirt and grass runways.

Different aluminum alloys were taken into account. After different considerations, two primary structural aluminum alloys where selected:

- **Al-2024-T3** for lifting surfaces and fuselage shell
- **Al-7075-T6** for structures required to carry higher stresses, such as upper wing surfaces, spars, stringers and fuselage frames [21]

Al2024-T3 has a lower maximum stress but it performs greatly under fatigue stress while Al-7075-T6 can sustain greater maximum stresses but it performs worse under fatigue. A summary of the proprieties of the two alloys is reported in table 25, according to [22]. Minimum gage thickness for aluminum sheets was set to a typical value of 0.3 mm [13].

Property	**Al2024-T3**	**Al7075-T6**
Density [kg/m^3]	2770	2800
Young's modulus [Gpa]	72.4	71
Yield tensile strength [Mpa]	324	476
Ultimate tensile strength [Mpa]	441	524
Yield compressive strength [MPa]	269	469
Ultimate shear strength [Mpa]	269	317

Table 25: Main Airframe Materials

7.3 Preliminary Structural Design

In order to carry out a preliminary **structural analysis**, the Team decided to make use of a software called *NeoCASS*. NeoCASS (Next generation Conceptual Aero Structural Sizing) is a free suite of Matlab modules, initially developed at Politecnico di Milano. It allows to tackle all aspects of aero-structural analysis of a design layout at the conceptual stage. Software architecture is shown in figure 53 . As shown, there are two main modules: Guess and Smartcad.

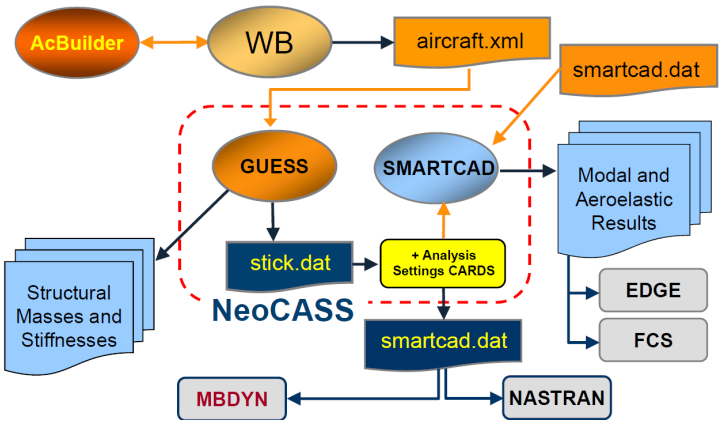

Figure 53: NeoCASS Architecture

Guess (Generic Unknowns Estimator in Structural Sizing) computes the total amount of load-bearing structure, based on real material properties, aircraft layout and load conditions.

The typical step by step sequence of operations is the following:

1. Input of aircraft geometric description, weight and balance (WB) and technological properties through XML file (done through 'AcBuilder' module)
2. input of sizing mode (automatic or user-defined), via 'Trim Cards'
3. Initial structural sizing and generation of a stick model

Loads are determined on rigid aircraft using VLM-based aerodynamics. Then, each component is sized section by section. Adopted structural layouts are:

1. Multi-web structure for lifting surfaces and carrythrough component
2. Stiffened framed/unframed shell for the fuselage
3. A typical wingbox section

Once the aero-structural model is built by Guess, Smartcad (Simplified Models for Aeroelasticity in Conceptual Aircraft Design) can be run in order to:

1. Perform a structural analysis
2. Perform an aeroelastic analysis
3. Produce various outputs (e.g. vibration modes, flutter boundaries, corrected inertia properties).

Initially, the Team inserted the geometrical description of the airplane into AcBuilder module (including the two discrete wing tanks). Then, the WeightsBalance (WB) module was run, in order to integrate the previously estimated mass properties (Structural, concentrated and distributed) into the model description. Finally, the Technology module was used to add the technological properties and materials selected:

- For lifting surfaces, the semi-monocoque concept was implemented, adopting L-shaped spar caps and Z-shaped stiffeners (figure 54a)
- For the fuselage, the Z-stiffened shell concept was used, with frames optimized for best buckling 54b

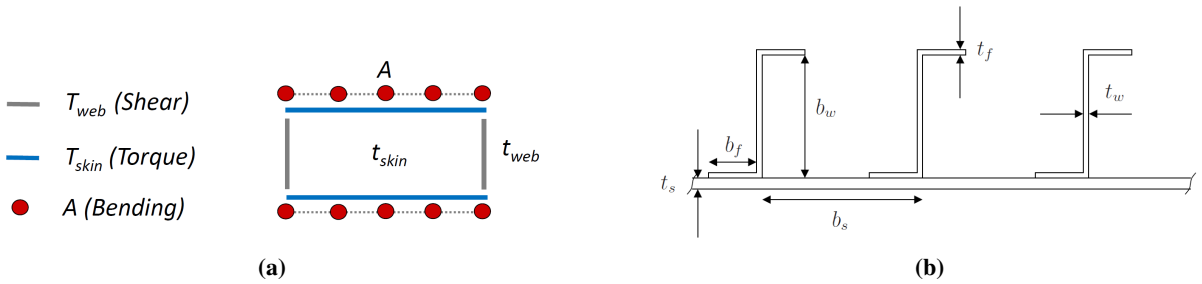

(a) **(b)**

Figure 54

At a later time, a built-in function called 'WBTableViewer' has been employed to refine the mass properties inserted and to add particular features of the airplane (namely, the 8 under-the-wing propellers and the battery packs). The following step was the selection of the sizing mode. Needless to say, selected sizing mode was the automatic one, corresponding to FAR23/CS23. In this way, the structural model was sized in order to withstand a series of 30 maneuver/loading conditions, summarized in table 26.

Maneuver IDs	Description	14 CFR Reference
1-4	Maximum Load Factor at V_C, V_D	Sec. 23.333
5-10	Sudden Aft Movement of Pitch Control at V_A, V_C, V_D	Sec. 23.423b
11-22	Sideslip Maneuvers at V_S, V_A	Sec. 23.441a
23-26	Aileron Abrupt Deflection at V_A	Sec. 23.349, 23.455
27-29	Gusts at V_B, V_C, V_D	Sec. 23.443
30	Taildown landing at V_{ref}	Sec. 23.75

Table 26: Sizing Maneuvers

7.4 Refined Mass Breakdown

The refined (final) mass breakdown is reported in table 27 and in Figure55. It was developed by comparison between statistical regressions by Torenbeek, Raymer and Nicolai. Raymer formulas seemed to yield a better matching with respect to the preliminary estimated empty weight. Thus, they were finally chosen for all the non-structural components (structural components values are NeoCASS outputs). Finally, some weights were estimated using Torenbeek formulas or by looking at typical values for similar items (propellers, EPMS, etc...). Resulting MTOM served as input to all the following performance analyses. Note that oxygen system (in brackets) is not considered in the standard weight statement. It will be an optional, to be used just if needed (not in standard missions).

Component	**Mass** [kg]	**Weight** [lbf]
Wing	210.2	463.4
HT	22.9	50.5
VT	15.3	33.7
Fuselage	150.7	332.2
Main LG	62.8	138.4
Nose LG	19.1	42.1
PGS	162	357.1
Air induction, propulsion installation	20.4	44.9
Fuel system	15.6	34.4
BP	255.5	563.3
EM, ESC	74.6	164.4
Propellers, spinners	19.6	43.2
FCS	41.8	18.9
Electrical system	68.3	150.6
Avionics	40	88.2
Air conditioning, anti-icing	43.2	95.2
(Oxygen system)	(10)	(22.0)
Furnishings	72.5	159.8
Structure Total	481	1060.4
Powerplant Total	547.7	1207.5
Fixed Equipment Total	265.8	585.9
Useful Load	465.6	1026.4
MTOM (MTOW)	1760.1	3880.2

Table 27: Refined Mass Breakdown

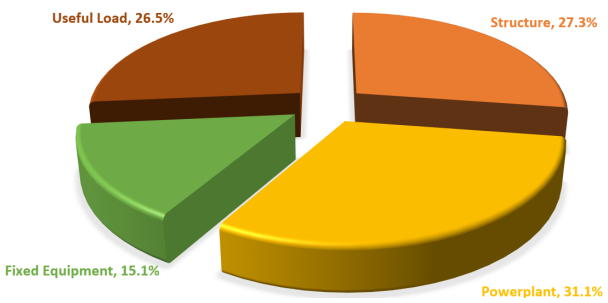

Figure 55: Mass Breakdown Pie Chart

Figure 56 shows the mass distribution along the fuselage axis.

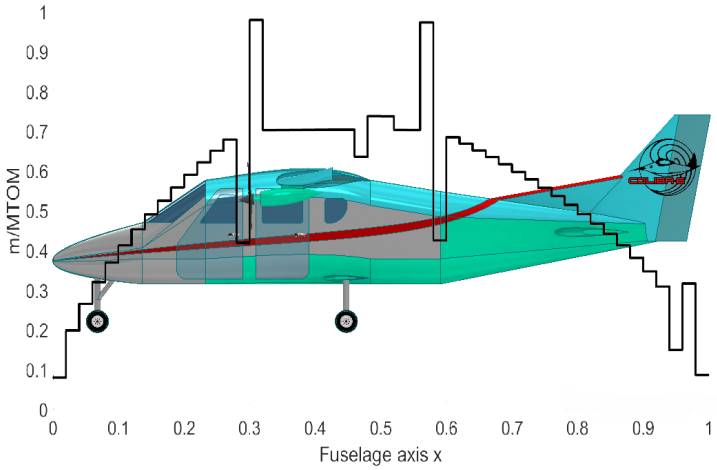

Figure 56: Longitudinal Mass Distribution

7.4.1 Load Envelopes And Sizing Maneuvers

Guess generated model and relative computed masses correspond to a structure withstanding all the 30 maneuvers above. As a remark, load envelopes, encompassing all the loads to be carried, can be plotted. Figures 57 and 58 show load envelopes at wing root and at fuselage/wing intersection, for fuselage and wing, respectively.

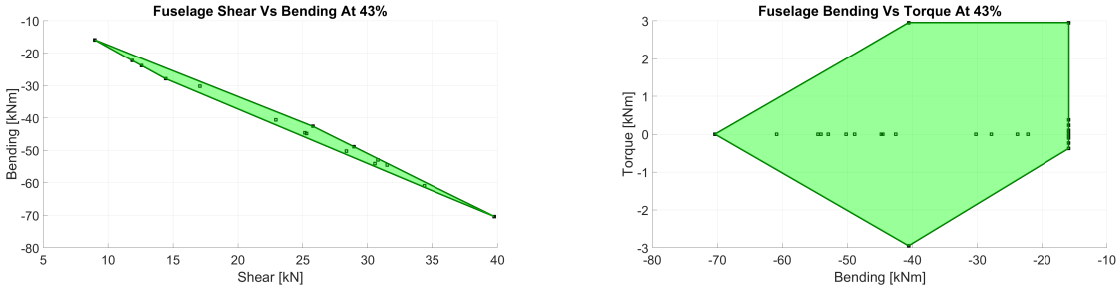

(a) **(b)**

Figure 57: Load Envelopes: Fuselage

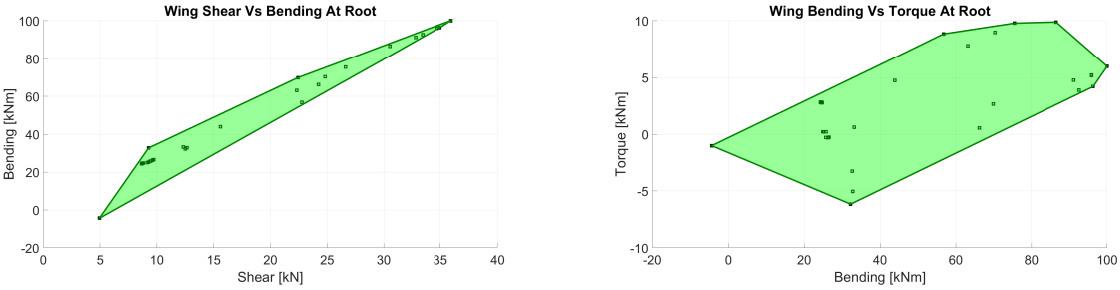

(a) **(b)**

Figure 58: Load Envelopes: Wing

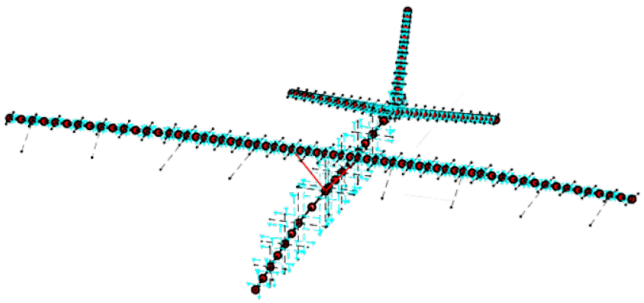

Figure 59: Stick Model

component	sizing maneuver
wing, fuselage	Gust @ V_c, 0 m
HT	sideslip maneuver at max rudder deflection @ V_A, 0 m
VT	sudden aft movement of pitch control @ V_C, 0 m

Table 28: Sizing Maneuvers

7.4.2 Aeroelastic Analysis

Flutter diagram is shown in figure 60. The upper part of the diagram represents the imaginary part of each eigenvalue (frequency). The lower part shows the parameter g of each eigenvaue, defined as $g = 2\frac{Re(s)}{|Im/(s)|}$.

As can be seen, no coalescence of frequencies is found and all the g parameters remain negative up to 150 m/s, well beyond flight envelope boundaries. Therefore, no flutter is expected to happen.

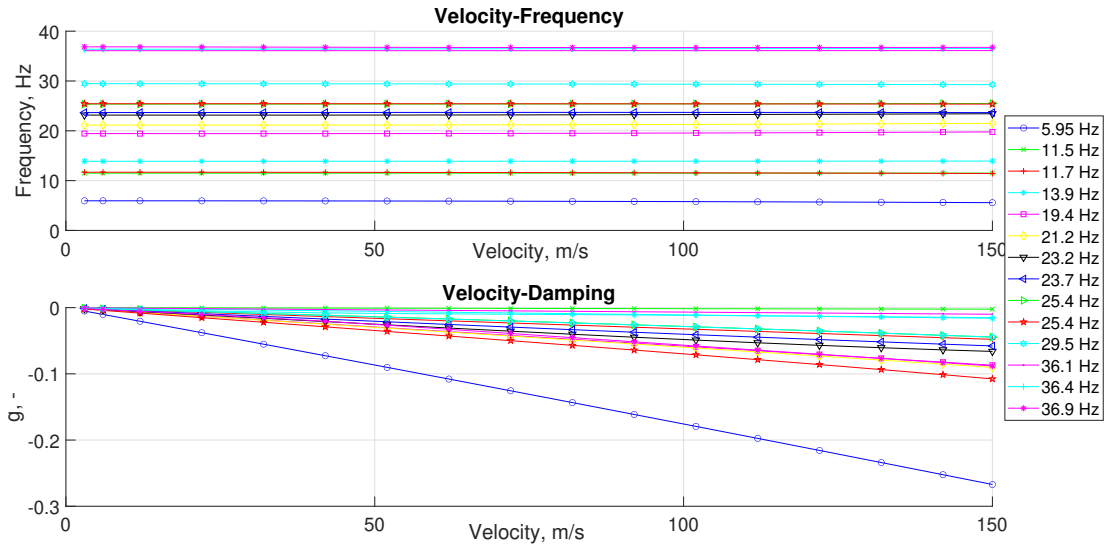

Figure 60: Flutter Diagram

7.5 PGS/BP compartment

In order to increase the maintainability of the aircraft the Team decided to implement a compartment accessible from the right side of the airplane. Thanks to this access panel, maintenance staff will be able to easily reach both the ICE and the generator in order to monitor the health of the components and repair/replace them in case of damage avoiding unnecessary shop visits and reducing maintenance time.
In Figure 61 and 62 a split view of the airplane is shown with also a detailed right view to highlight the compartment doors to access PGS and BPs.

Figure 61: Airplane split view

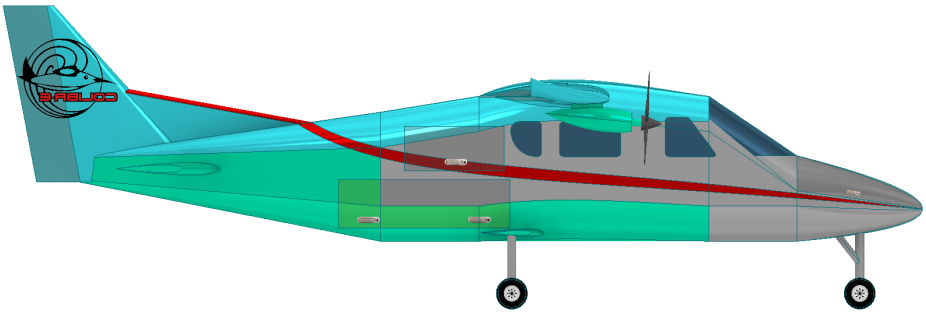

Figure 62: Airplane right view

7.6 Landing Gear

Tricycle placement and retraction system

To place MLG and NLG accordingly to safety standards, the procedure presented by Gudmundsson in the chapter ”Anatomy of the landing gear” was followed [13] as shown in Figure 63 and Figure 64. Knowing the position of the CG and its excursion, the max FWD, max AFT and highest position can be evaluated. By drawing the tail strike line at a 15 degrees angle and intersecting it with its perpendicular passing through the highest most AFT CG position, the MLG contact point is found.

In order to correctly position the NLG some considerations about the maneuverability of the airplane had to be made: if the NLG carries more than 20% of aircraft weight when the CG is at the FWD limit, the high friction between the tire and ground will make it hard to turn, due to the high force required by the pilot on the controls. On the other hand, if the NLG carries less than 10% when the CG is at the aft limit, the tire will begin to skid on the ground due to lack of ground friction.

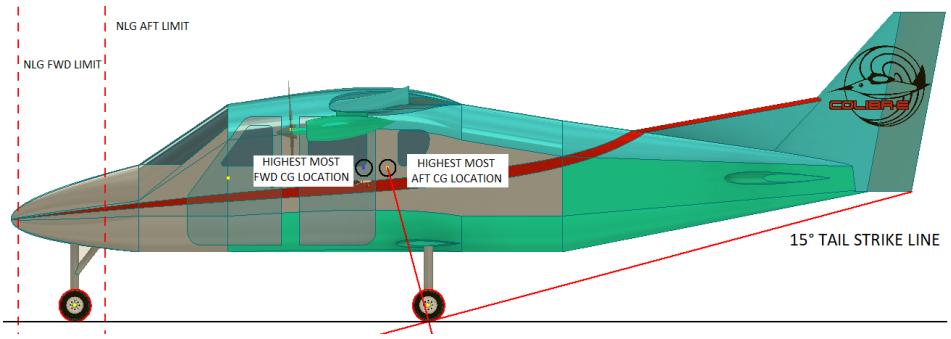

Figure 63: Landing gear longitudinal placement

As soon as that NLG and MLG are correctly placed in the longitudinal direction, a correct distance between the two tires of the MLG has to be selected in order to avoid overturning during ground maneuvers. Two parallel lines are traced: the first one passing through NLG and MLG and the second one through the FWD CG limit. Then, a perpendicular line representing the ground is drawn. The angle between the latter and the one representing the distance between ground and highest CG position (Hcg) has to be lower than 63 degrees for ground operating airplanes.

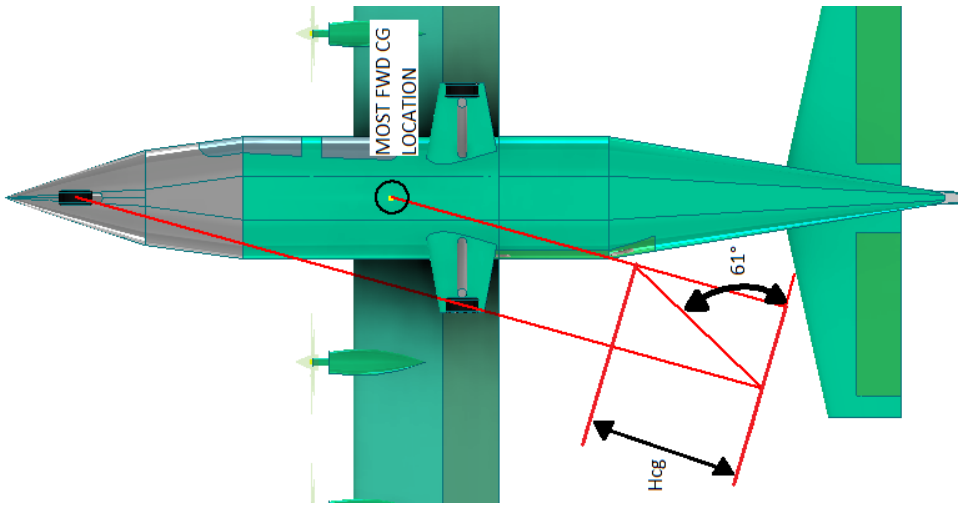

Figure 64: Landing gear span-wise placement

As can be seen from the picture above, to grant ground stability of the airplane the MLG has to be placed ”outside of the fuselage”. At the same time, a retractable landing gear was needed to reduce drag.

This led to a Tecnam P2006T like solution, with two fins on the side of the fuselage to allow for gear strut positioning and gear retraction. In light of all previous choices taken in order to increase maintainability of the airplane, the Team decided to implement a retractable landing gear system, which will greatly improve cruise efficiency without increasing the maintenance hour-to-flight hour ratio in a significant way.

Nose landing gear will retract backwards and main landing gear inwards. The two mechanisms are schematized in Figure 65.

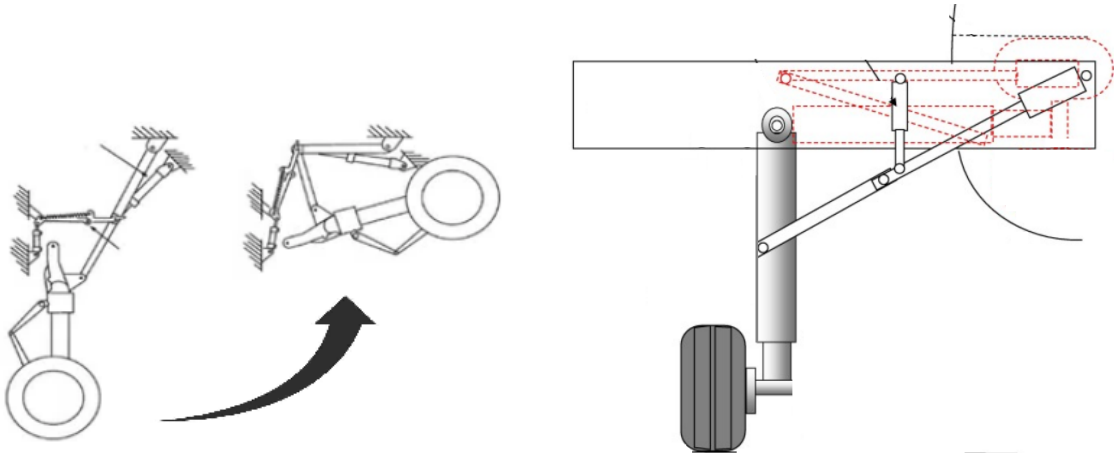

(a) Nose landing gear **(b)** Main landing gear

Figure 65: Landing gear retraction system

Tire selection

As previously established, the airplane under project needs to take-off and land on unprepared or semi-prepared runways. The tire has to be able to absorb shocks and not fail under rough conditions. As stated by Gudmundsson [13] and Roskam [23] a Type III tire 6 inches wide and with a diameter of 14 inches is the best choice for this kind of application.

The inflation pressure of the tire is also an important parameter. In order to provide a greater cushioning on impact the inflation pressure of the tire has to be < 40 psi. If this wasn't the case, an uneven and unimproved runway could cause an explosion of the tire with repercussions on safety. Based on MTOW and stall speed in landing configuration it is possible to know the kinetic energy that has to be dissipated by the breaks: this amounts to 225280 Joules.

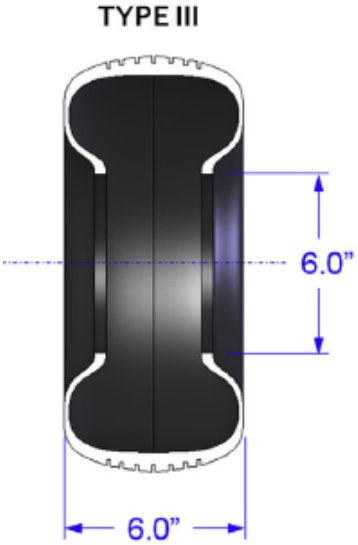

Figure 66: Type III tire

7.7 Complete mass scheme and CG excursion

All components were precisely placed, in order to grant both ground stability and control/stability during flight, even if the airplane takes-off with only 4 of 5 BPs on board. This condition was considered in order to make it possible to dispatch the airplane after a BP fail without ballast, to reach a location where a new BP is available. Thanks to the BPs being all of the same type, the FWD and AFT packs can be interchanged, making it possible to select the missing pack before T-O. The dispatching condition under this circumstance is the following:

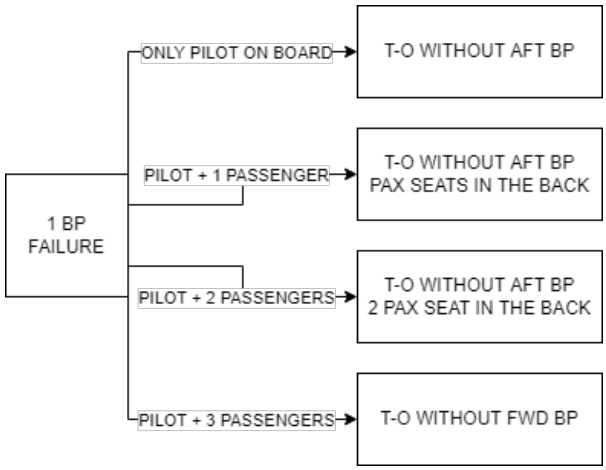

Figure 67: Dispatch condition

In the next picture and tables the complete mass positioning scheme and CG excursion are reported. Note that 'Operational limits' are referred to conditions in which the airplane is in flight mode, while the 'Ground limits' refer to maintenance/handling conditions. OMH is the 1 pilot, no pax, full bag, 1 FWD BP absent condition; GMH is the max fuel, no BP, no pilot, no pax, no bag condition; G/OMFWD is the 1 pilot, full pax, full fuel, no bag condition; OMAFT is the 1 pilot, full pax, full bag 1 FWD BP absent condition; GMAFT is the no fuel, no pax, no bag, one FWD BP absent, all AFT BP absent.

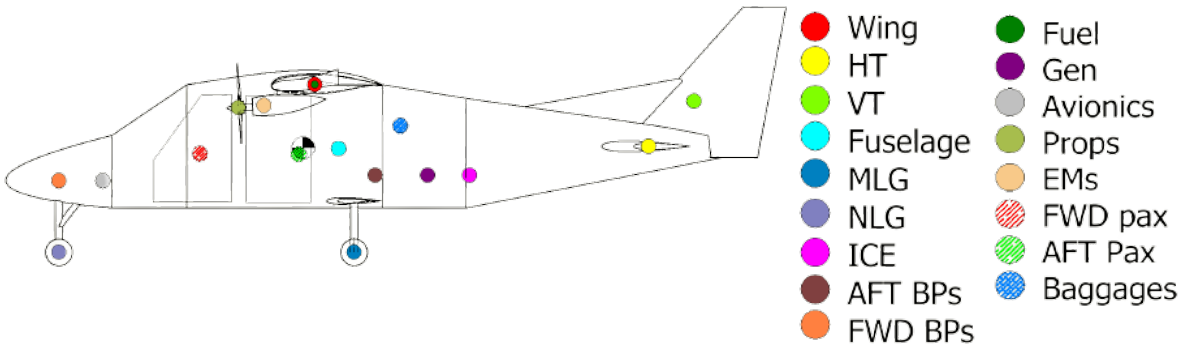

Figure 68: Complete mass scheme

Component	**X position** (wrt nose)	**Z position** (wrt bottom of fuselage)
Wing	4136.04 [mm] (13.56 [ft])	1646.00 [mm] (5.40 [ft])
HT	8599.50 [mm] (28.21 [ft])	822.99 [mm] (2.70 [ft])
VT	9206.18 [mm] (30.20 [ft])	1425.00 [mm] (4.67 [ft])
Fuselage	4436.79 [mm] (14,55 [ft])	799.88 [mm] (2.62 [ft])
MLG	4659.27 [mm] (15.28[ft])	-592.40 [mm] (-1.94 [ft])
NLG	712.00 [mm] (0.56 [ft])	-592.40 [mm] (-1.94 [ft])
ICE	6204.29 [mm] (20.35 [ft])	436.57 [mm] (1.43 [ft])
AFT BPs	4942.79 [mm] (16.21 [ft])	436.57 [mm] (1.43 [ft])
FWD BPs	712.79 [mm] (2.33 [ft])	362.21 [mm] (1.18 [ft])
Fuel	4136.04 [mm] (13.56 [ft])	1646.00 [mm] (5.40 [ft])
GEN	5643.79 [mm] (18.51 [ft])	436.57 [mm] (1.43 [ft])
Avionics	1302.79 [mm] (4.27 [ft])	362.21 [mm] (1.18 [ft])
Props	3113.53 [mm] (10.21 [ft])	1338.42 [mm] (4.39 [ft])
EMs	3455.45 [mm] (11.33 [ft])	1368.07 [mm] (4.48 [ft])
FWD Pax	2600.48 [mm] (8.53 [ft])	726.00 [mm] (2.38 [ft])
AFT Pax	3923.65 [mm] (12.87 [ft])	726.00 [mm] (2.38 [ft])
Baggages	5278.79 [mm] (17.31 [ft])	1097.72 [mm] (3.60 [ft])

Table 29: Complete mass positions

Condition	**CG X position** (wrt nose)	**CG Z position** (wrt bottom of fuselage)
Full load	3981.63 [mm] (13.06 [ft])	809.76 [mm] (2.65 [ft])
Empty	4147.33 [mm] (13.60 [ft])	824.25 [mm] (2.70 [ft])
Operational Max height	—	845.11 [mm] (2.77 [ft])
Ground Max height condition	—	945.66 [mm] (3.10 [ft])
Ground/Operational FWD limit	3936.52 [mm] (12.91 [ft])	—
Operational AFT limit	4091.50 [mm] (13.42 [ft])	—
Ground AFT limit	4201.02 [mm] (13.78 [ft])	—

Table 30: Complete CG positions

8 Stability And Control

Longitudinal static stability

As stated by 14 CFR 23.2145, aircraft must have static longitudinal, lateral, and directional stability in normal operations. Longitudinal static stability is achieved ensuring that the center of gravity lies in front of neutral point, for every CG position. Aircraft CG travel is defined by maximum excursions of the center of gravity: x axis is considered positive pointing forward (towards the aircraft nose) and origin is the wing leading edge. Maximum positions are reported below.

x_{CG}^{AFT} [m]	x_{CG}^{MID} [m]	x_{CG}^{FWD} [m]
-0.527	-0.428	-0.359

Table 31: CG limit positions

The study of static stability has been conducted using Crocco's diagram. This tool allows to retrieve information about stability, controllability and trim equilibrium. The value of pitching moment at LE is reported as function of lift coefficient at trim, generating two bundles of parallel lines parameterized with α (isoclinic lines) and δ_e (stick lines).

As reported in [24], it is possible to prove that by plotting C_L on y-axis and $-C_{M_{LE}}$ on x-axis, the abscissas corresponding to $C_L = 1$ represent the non-dimensional positions with respect to the MAC, along the roll axis of the aircraft. Every line starting from the origin and marking a specific non-dimensional position of CG on $C_L = 1$ represent the trim solution in terms of C_L and $C_{M_{LE}}$ for that particular CG position (baricentric line), underlining α and δ_e required to achieve a specific vertical equilibrium condition (C_L).

The baricentric line passing through the intersection between isoclinic line for α_{max} and stick line for $\delta_{e_{max}up} < 0$ mark a position on roll axis for the most forward admissible CG position to not be exceeded in order to not run into a controllability stall before reaching aerodynamic stall. Again, is possible to prove that the stick line for $\delta_e = \delta_{e0}$ mark the neutral point position at $\xi_N = 0.6133$, behind the LE, which is consistent with the value retrieved by two surfaces formulation.

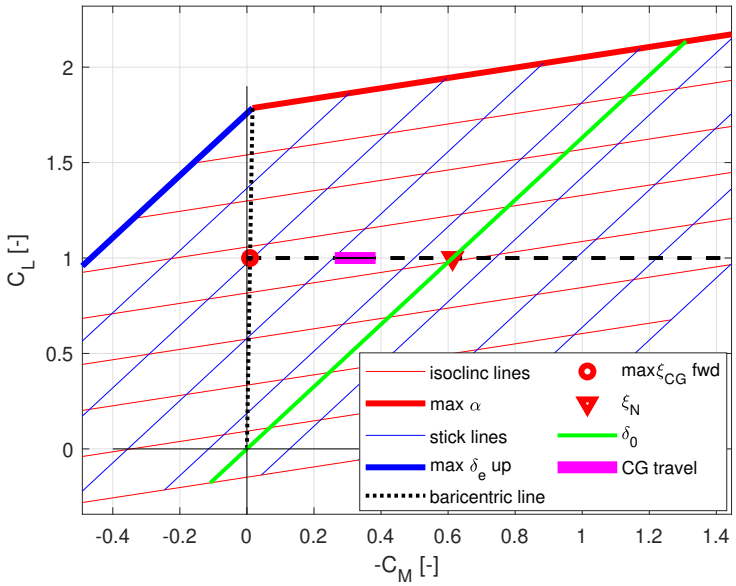

Figure 69: Crocco's diagram, clean configuration

The actual CG travel lays into allowed limitations, ensuring a static margin SM$\geqslant$ 22.87% as percentage of MAC, a value slightly higher than theoretical $5 \div 15\%$ but which still represents an excellent compromise between stability and controllability.

Also the 'force control' approach has been considered, searching for a stick free static stability limitation. The outcome, that strongly depends on C_{H_α} and C_{H_δ} (estimated from DATCOM [25]), is $\xi_{N_{free}} = 0.6007$ behind LE, laying ahead ξ_N as expected. Static margin and CG limitations are shown in figures below.

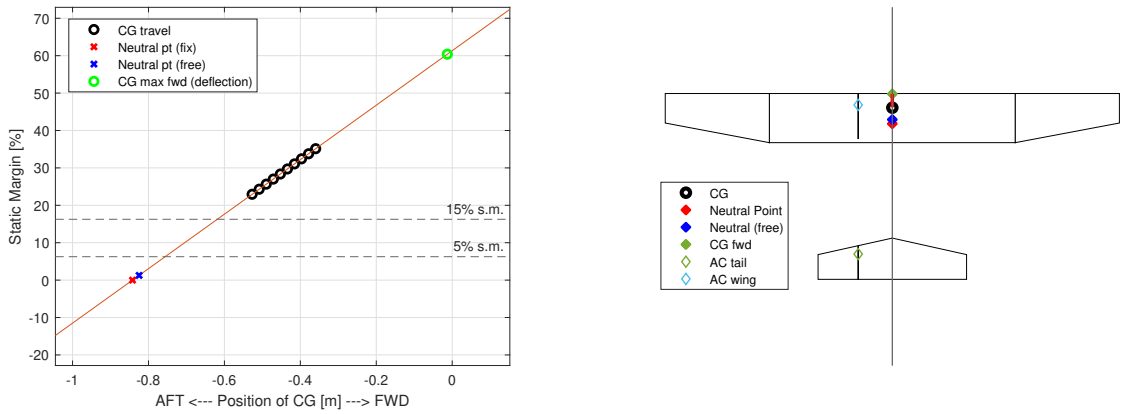

(a) Static margin

(b) CG position and limitations

Figure 70: Longitudinal CG position

Lateral-directional static stability

Lateral-directional static stability is ensured by the sign of yawing moment and roll moment derivatives with respect to sideslip angle. In particular, $C_{\mathcal{L}_{G_\beta}} < 0$ and $C_{\mathcal{N}_{G_\beta}} > 0$. This is our case.

Dynamic response

Dynamic stability characteristics requirements are specified in 14 CFR 23.2145(a)(2) and 14 CFR 23.2145(b). Analysis of decoupled longitudinal and lateral-directional dynamics have been performed.

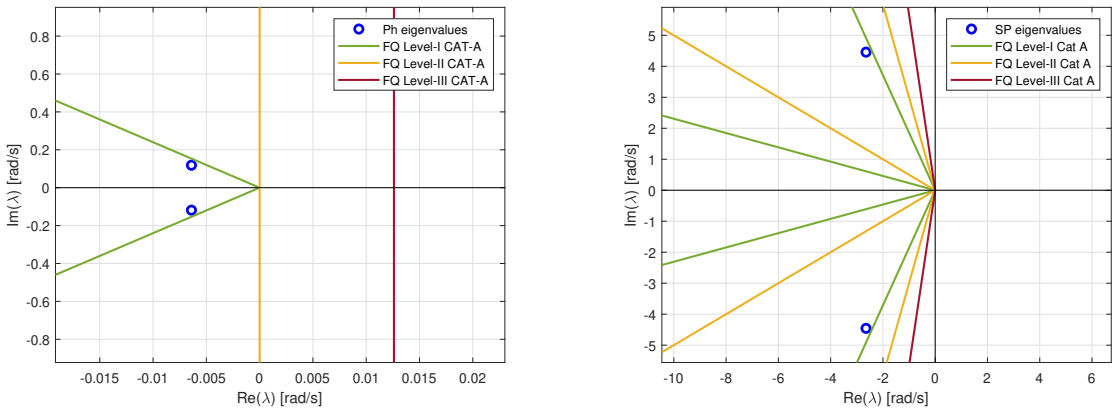

(a) Phugoid mode **(b)** Short period mode

Figure 71: Longitudinal eigenvalues

Aircraft belongs to FQ Level 1 for category A regarding both short period mode and phugoid mode. Concerning Lateral-directional dynamic modes meet Level 1 FQ as well.

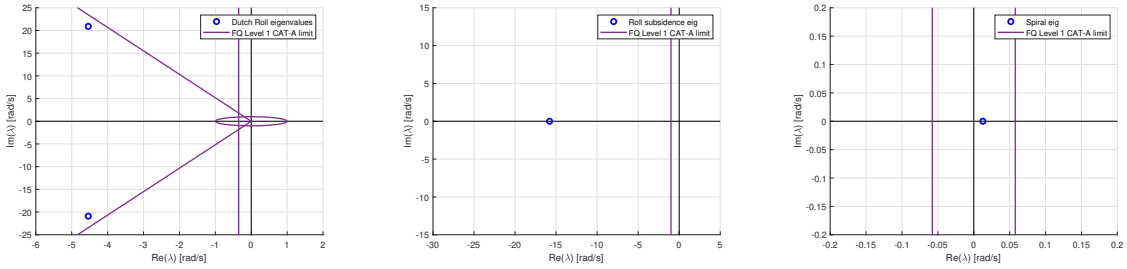

(a) Dutch Roll **(b)** Roll subsidence **(c)** Spiral

Figure 72: Lateral-directional eigenvalues

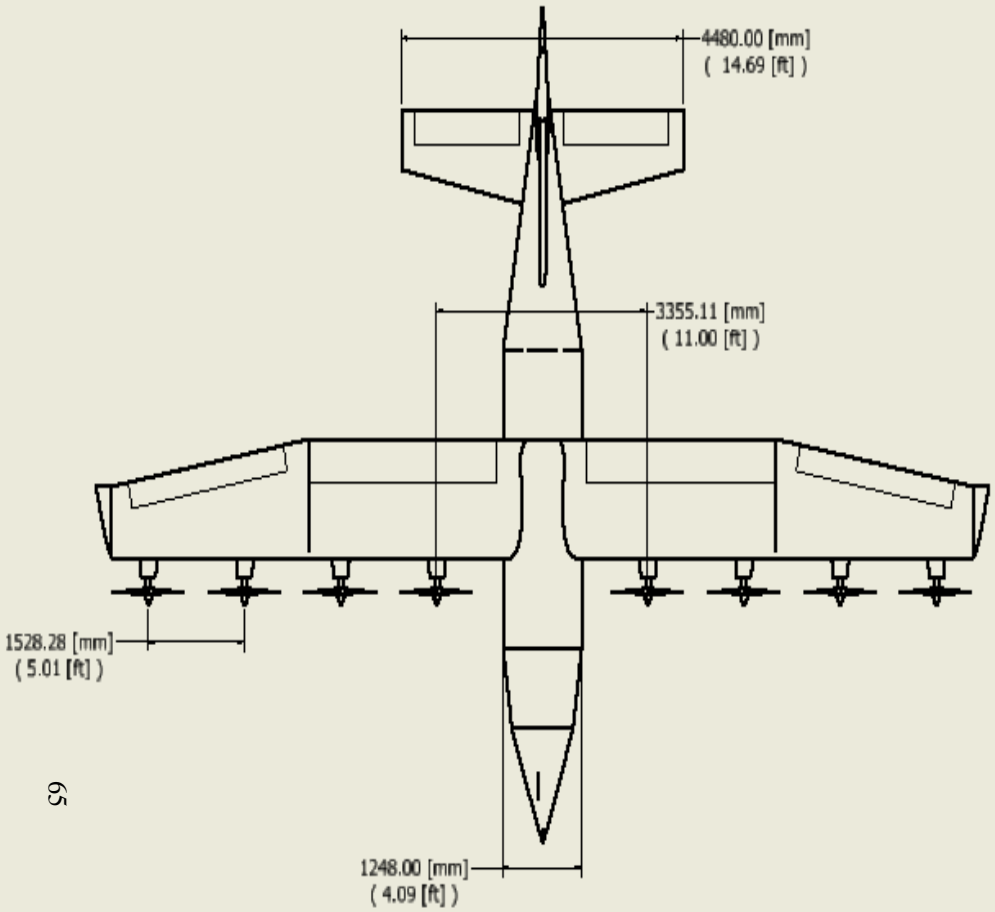
4480.00 [mm]
(14.69 [ft])
3355.11 [mm]
(11.00 [ft])
1528.28 [mm]
(5.01 [ft])
1248.00 [mm]
(4.09 [ft])

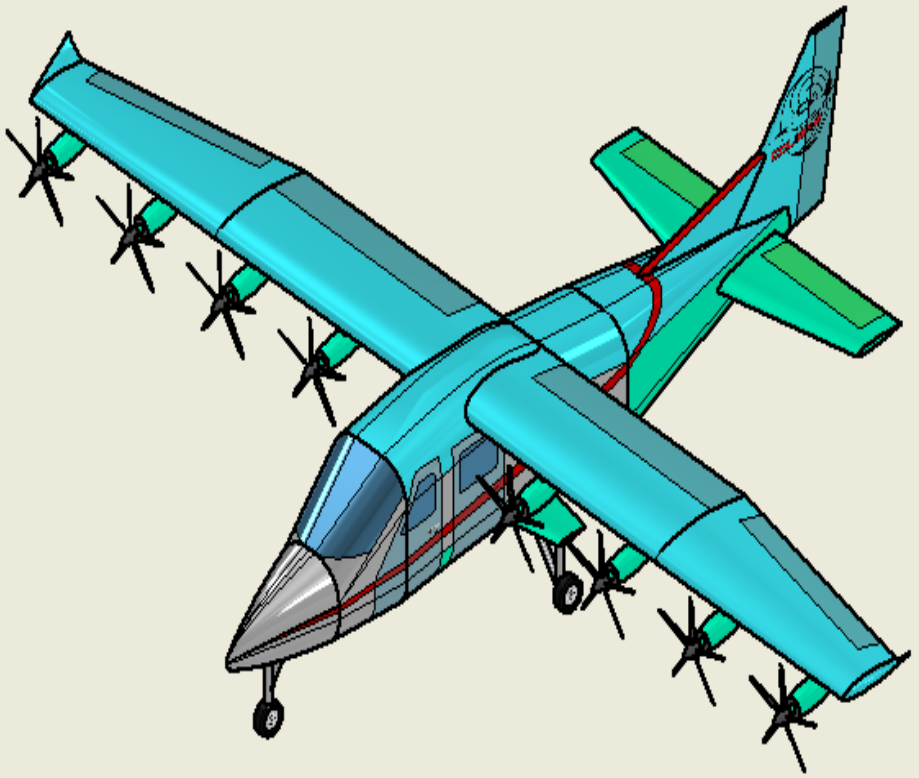

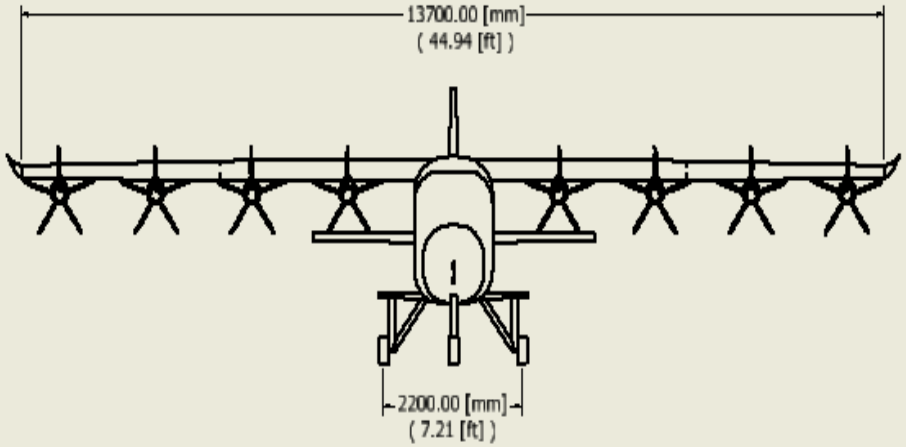
13700.00 [mm]
(44.94 [ft])
2200.00 [mm]
(7.21 [ft])

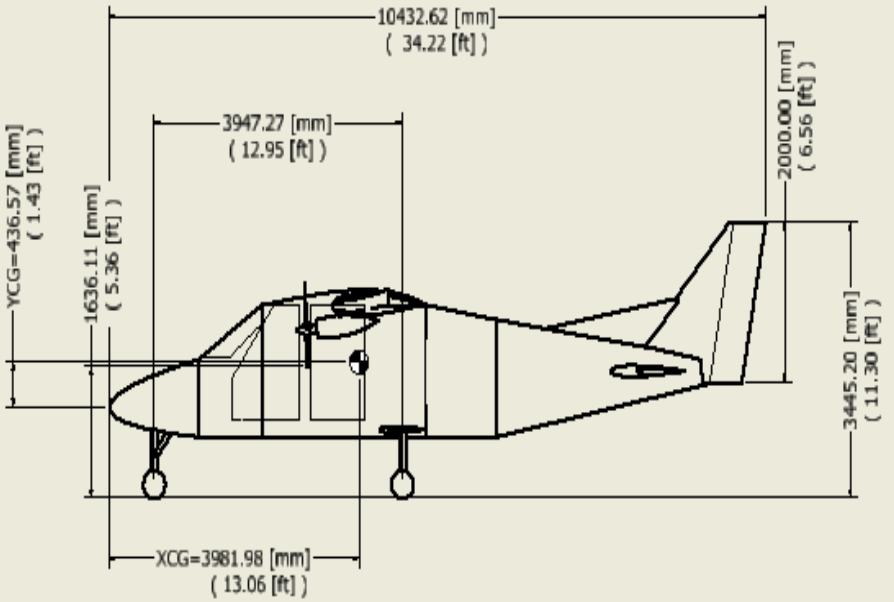
10432.62 [mm]
(34.22 [ft])
3947.27 [mm]
(12.95 [ft])
2000.00 [mm]
(6.56 [ft])
YCG=436.57 [mm]
(1.43 [ft])
1636.11 [mm]
(5.36 [ft])
3445.20 [mm]
(11.30 [ft])
XCG=3981.98 [mm]
(13.06 [ft])

Scale 1/40

9 Performance Analysis

Performance analysis is conducted considering the aircraft at MTOW, assuming standard ISA conditions and load factor equal to 1. Given the aircraft characteristic speeds, it is possible to approximate CAS with EAS, neglecting compressibility effects. Characteristic equivalent airspeeds (EAS) are reported below.

V_{S0}	31 kts	V_X	52 kts
V_{S1}	39 kts	V_Y	66 kts
V_{STALL}^{Clean}	42 kts	$V_{max\mathcal{E}}$	68 kts
V_{NE}	189 kts	$V_{max\mathcal{R}}$	89 kts

Table 32

9.1 Take-off

Nominal take-off is performed at MTOW, flaps 20° configuration and maximum power. In normal operations, PGS is not working during take-off, therefore EM brake power is limited by battery power flow limitation. In this condition each EM absorbs 27.9 kW and produces 1250 N of static thrust. If extra thrust is needed for special performance, PGS can be turned on, rising brake power of each EM to 40 kW, which is EM's peak power operating limit. In this condition, static thrust of each EM rises to 1500 N. Take-off distance is shown in Figure 73a.

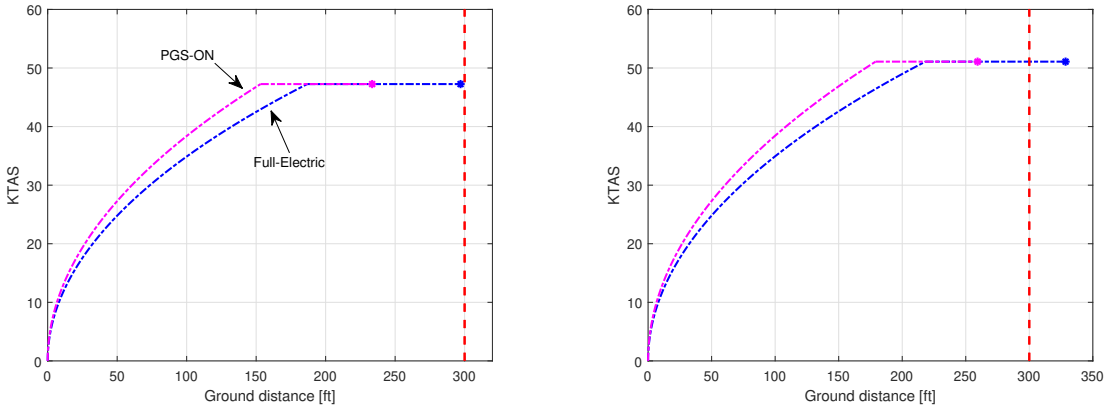

(a) TO distance at sea level

(b) TO distance at 5000 ft

Figure 73

First curve represents ground distance covered during acceleration from null speed to climb speed V_2. Horizontal line represents distance covered during initial climb phase until the 50' obstacle is cleared.

The latter phase is performed at constant speed. Field length is evaluated at ISA+18°F both at sea level and 5000 ft. Full electric configuration performs take-off in a field length of $\mathcal{S}_{TO}$ **= 297 ft**, while PGS assisted take-off ensure a $\mathcal{S}_{TO}$ **= 233 ft** field length at sea level. At an altitude of 5000 ft, take-off lengths increase, therefore only with PGS working is possible to satisfy field length constraint. Balanced field length was computed as shown in Figure 74in order to prove whether, in case of worst thrust condition as defined in Subsection 5.7, it is possible to conclude take-off or not inside limit imposed by AIAA RFP.

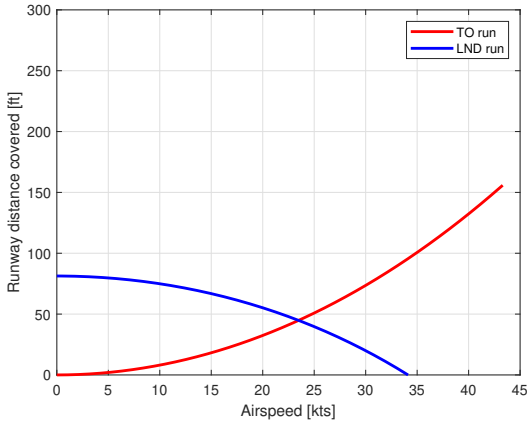

Figure 74: Balanced field

9.2 Climb

As Figure 75 shows, required initial rate of climb is widely satisfied both in FE and MCP power settings. Initial rate of climb at sea level ISA+18F results to be 2300 fpm with both electric and fossil fuel propulsion operating, while it results to be 2100 fpm in FE setting. Climb path angle is plotted as well.

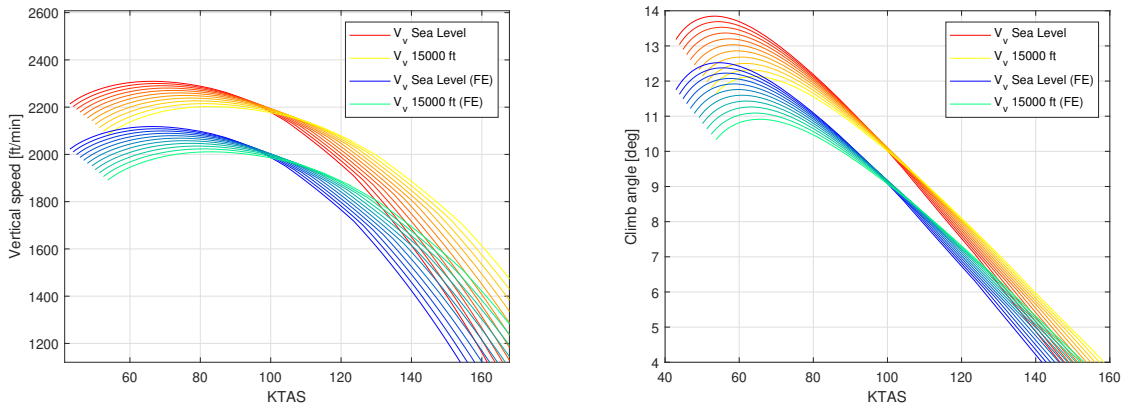

(a) **(b)**

Figure 75

9.3 Cruise

Conventional airplane lose a significant amount of weight during cruise. Instead, electric and hybrid-electric airplanes weight does not change with range, or changes very slightly. In the case of ***Colibr-e Sapphire***, weight change keeps below 5% of MTOM, in any condition. Consequently, Breguet formulation for integral cruise performance can't be adopted. Instead, the procedure proposed in [13] was followed: it requires to compute the theoretical amount of stored energy, with full tanks. This value was found to be 1.11×10^6 Wh.

At this point, propulsive efficiency losses have to be considered, for both the fuel and batteries chains. Table 33 shows a summary of computed values: values on the right account also for cruise propeller efficiency.

Source	Efficiency	Total Efficiency
Fuel	0.27	0.23
Batteries	0.89	0.77

Table 33: Propulsive Efficiencies

Accounting for efficiencies losses, the available amount of energy reduces to 3.13×10^5 Wh. From this energy, 3.22×10^4 Wh (11%) have to be subtracted, to account for climb to cruise altitude, descent plus terminal and taxi phases. Therefore, the actual available energy for cruise is $E_{av} = 2.81 \times 10^5$ Wh.

It is assumed that the airplane flies at a constant cruise altitude and at a constant mass of 1720 kg (MTOM minus half of maximum fuel mass). Power required P_r can be computed as function of a given cruise speed V_{cr} and of its relative lift coefficient, knowing the drag polar. At this point, endurance can be computed as $\mathcal{E} = \frac{E_{av}}{P_r}$. Range follows from endurance: $\mathcal{R} = V_{cr} \times \mathcal{E}$. Figure 76 shows endurance and range for varying cruise speed. **Maximum endurance** $\mathcal{E}_M$ = 6 h 30' whereas **maximum range** $\mathcal{R}_M$ = 583 nm. Optimal points are highlited, as well as points corresponding to the design cruise speed of 160 knots.

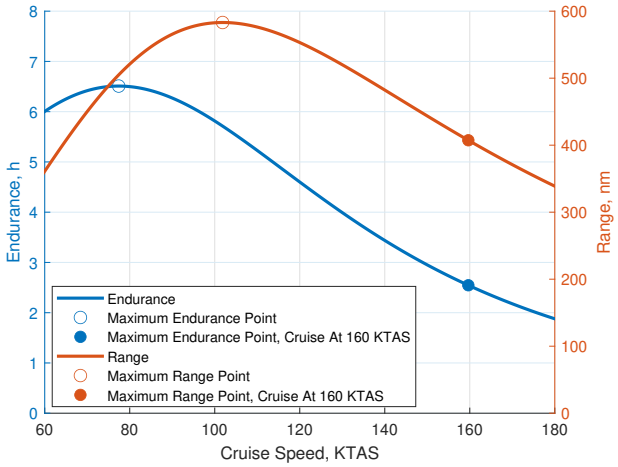

Figure 76: Integral Cruise Performance

Figure 77 shows the **payload-range chart**. With three quarters full tanks, maximum payload weight is set to 320 kg, which is 20 kg more than RFP payload assumptions. At maximum payload weight, maximum range is 453 nm (point B). Trading the 20 kg of extra payload for fuel allows to reach the maximum allowable fuel weight of 80 kg. In this case, range is 570 nm (C). Finally, lowering the number of passengers on board increases the range, up to a **ferry range** of 687 nm (D).

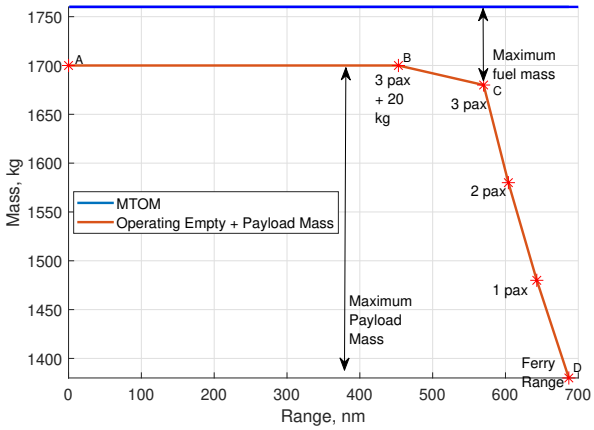

Figure 77: Payload-Range Chart

9.4 Landing

Standard approach angle is 3°, nevertheless to meet the requirement about field length, a much steeper angle must be achieved during final descent. To perform a landing from 50' obstacle in just 300 ft, final descent angle is expected to be of 15°. Steep approach angles don't lead necessarily to an unstable approach. IATA (International Air Transport Association) [26] states that prerequisite for a stable approach is: rate of descent commensurate with the approach angle and approach speed. Unstable approach occurs whenever approach does not meet the stable approach criteria defined by the operator in its SOPs (Standard Operating Procedures). Specifically about sink rate, the document states that an approach is stable when: "Sink rate is no greater than 1,000 feet/minute; if an approach requires a sink rate greater than 1,000 feet/minute a special briefing should be conducted". Since is V_{APP} = 40 kts (TAS), the steep descent entails that vertical speed during descent is V_V = 10 kts (5 m/s) which leads to a sink rate of 984 ft/min. Simulation of a landing at MTOW , sea level ISA+18°F condition led to the following results: an approach distance of $\mathcal{S}_{APP}$ **= 154** ft, a flare distance of $\mathcal{S}_{FL}$ **= 65** ft and a braking distance of $\mathcal{S}_{BR}$ **= 75** ft. The latter is achieved thanks to low kinetic energy at touch-down coupled with a braking action on wheels. Total landing distance results to be $\mathcal{S}_{LND}$ **= 294** ft.

9.5 Flight envelope

Unlike internal combustion engines, EMs don't lose power with altitude. This fact has an impact on flight envelope since theoretically there is not an absolute ceiling. The only limitation is propeller efficiency which decreases with increasing airspeed, anyway this happens at high altitudes. In this case, altitude is limited by practical and operative considerations. For an unpressurized aircraft, 14 CFR § 135.89 prescribes the use of oxygen above 12000 ft (and between 10000 ft and 12000 ft if the flight at those altitudes lasts more than 30 minutes). Flight envelopes have been considered up to 15000 ft (14000 ft is the lower limit imposed by the RFP).

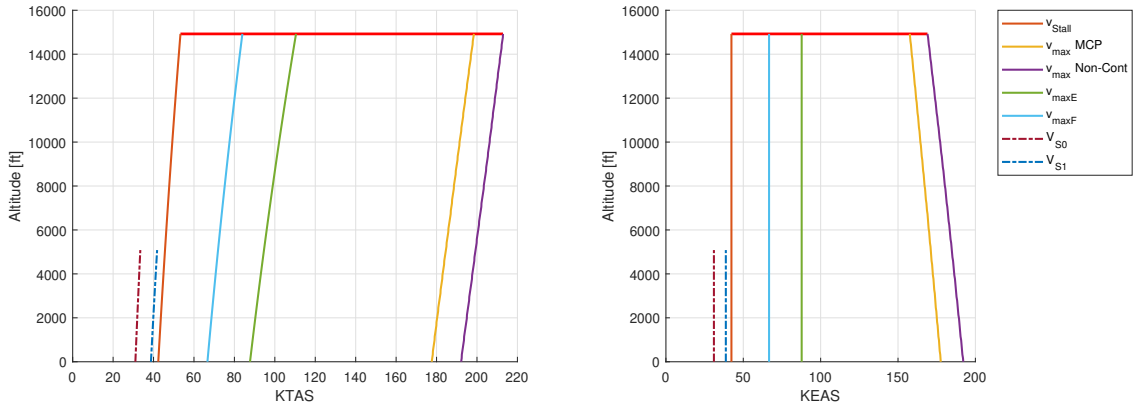

Figure 78: Flight envelope

9.6 Turning Performance

Turning performance was assessed at sea level condition, evaluating Penaud diagram for different load factors up to the maximum admissible for structural sizing.

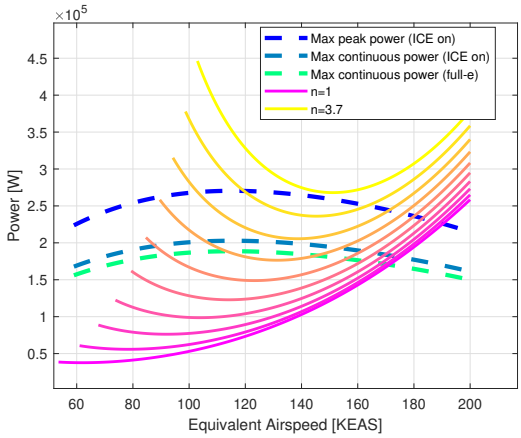

Figure 79: Penaud diagram for different load factors

From this, it is possible to derive an optimal V-n envelope that implies top performance in terms of radius, track inversion time and maximum bank angle achievable for a steady level turning flight.

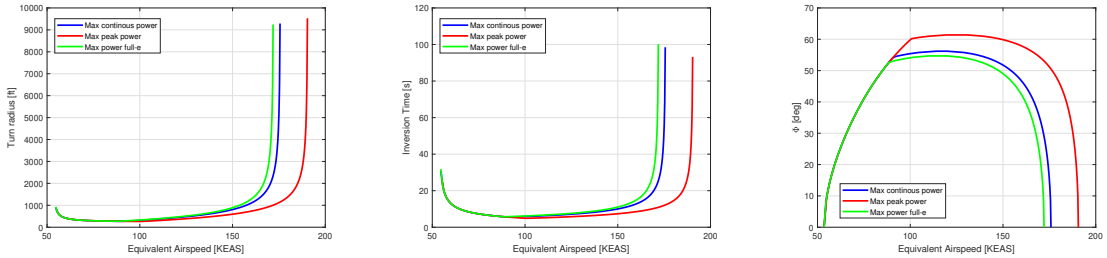

(a) Turn radius **(b)** Inversion time **(c)** Max.bank angle

Figure 80: Steady level turning flight top performance

In the following graph is reported the turn performance map, showing how rapidly the aircraft can maneuver at specific airspeed. The cross plot of ”iso-n” curves and ”iso-Radius” curves returns the value of turning rate achievable at a specific airspeed, for a given turn radius and a given load factor (or bank angle). Also in this case, each of three power setting considered defines a set of turn rate values that can be reached for a steady level turning flight.

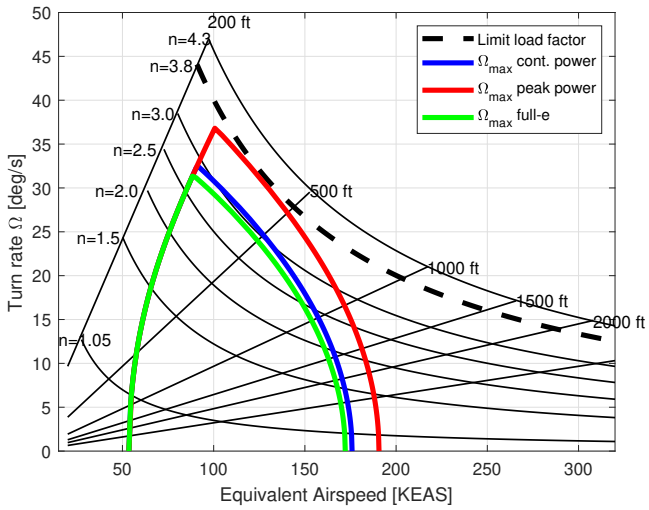

Figure 81: Turn performance map

9.7 Mission Simulations

Mission Profile A - IFR Cruise Mission (Sizing Mission)

Sizing mission profile is flown at a cruise speed of **160 KTAS** and cruise altitude of 9000 ft. The PGS is turned on during cruise only, as suggested by RFP. 14 CFR § 91.167 imposes fuel reserves for flight in IFR conditions. These must be equal to the fuel required to fly for 45' at sea level and at normal cruise speed, after the intended mission. This requirement has been translated by the Team into a 45' loiter, to be guaranteed with electric power only. **Diversion distance** to an alternate airport has been set to 26 nm, considering the average distance from possible alternate airports, both in Europe and in the USA [27]. Also, a minimum final tank level of 5% was enforced, as a safety margin. A sketch of the sizing mission profile is reported in figure 82.

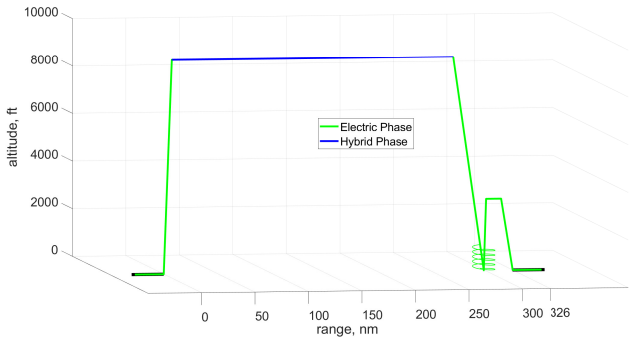

Figure 82: Sizing Mission Profile

Figure 83 shows relevant time histories for the sizing mission. BPs SOC at the end of the mission will be 65.1%, not considering a possible loiter and diversion. Total fuel burned is 96.7 L (26,5 US gal).

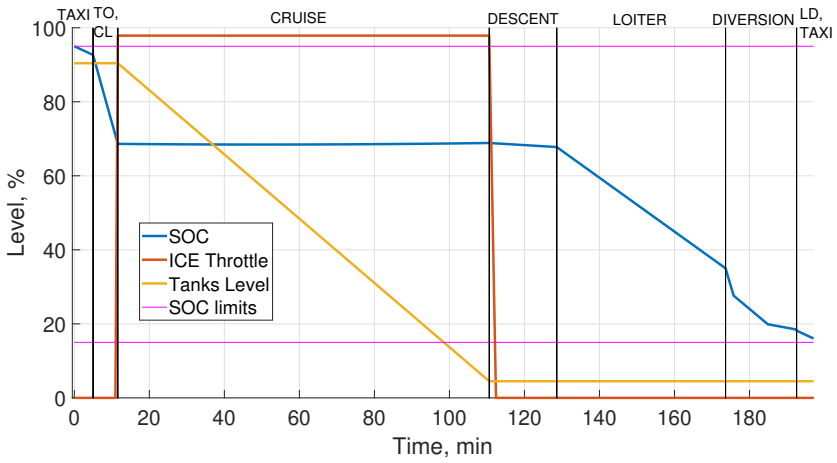

Figure 83: Sizing Mission Time Histories

Figure 84 shows examples of a 150 nm mission (half of design range) and of a 50 nm mission. For the 150 nm mission, final SOC and total fuel burned are 64.3% and 40.4 L (10.7 US gal), respectively. For the 50 nm mission these values become 65.7% and 5.4 L (1.4 US gal). This means that the 15' **turnaround time** will be granted by swapping 2 BP and/or by recharging them.

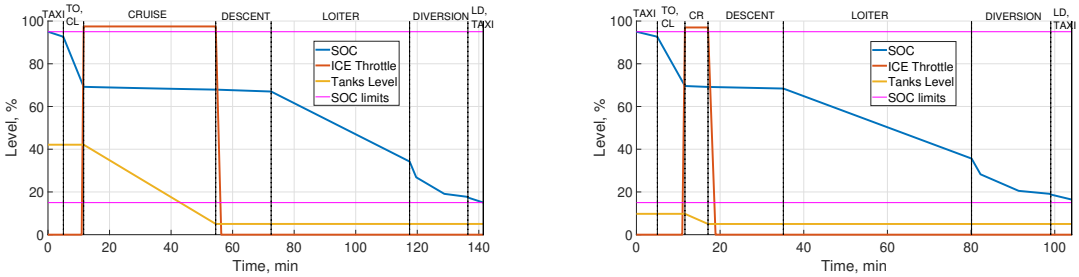

(a) 150 nm IFR Mission Time Histories

(b) 50 nm IFR Mission Time Histories

Figure 84

Mission Profile B - Simple Cruise Mission

A possible simple cruise mission was simulated, without the diversion and with loiter time reduced to 20 minutes. Cruise speed and altitude are fixed to 160 KTAS and 9000 ft, as for the IFR mission. Related plots are shown in figure 86.

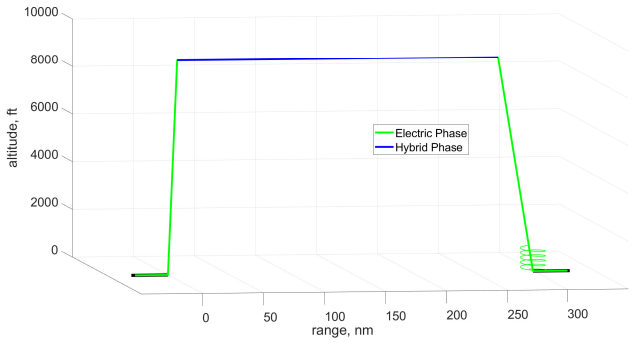

Figure 85: Simple Cruise Profile

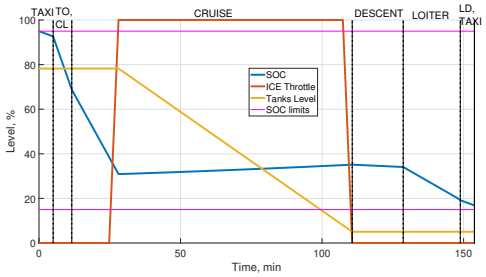

(a) 300 nm Simple Cruise Mission Time Histories

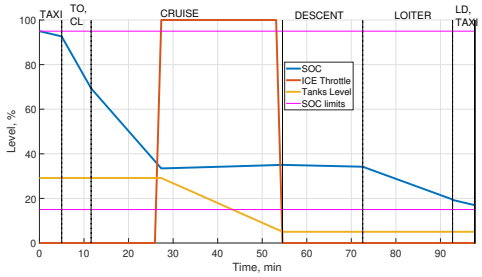

(b) 150 nm Simple Cruise Mission Time Histories

Figure 86

In the case of a simple 50 nm cruise mission, the PGS can be kept off, allowing a zero-emissions flight (Figure 87 a)). Instead, Figure 87 b) shows an example in which the PGS is also used during descent, in order to reach the final destination with at least 60 % SOC. In turn, this will allow a 15' **turnaround time**, also in cases when battery swapping/recharge is not available at arrival.

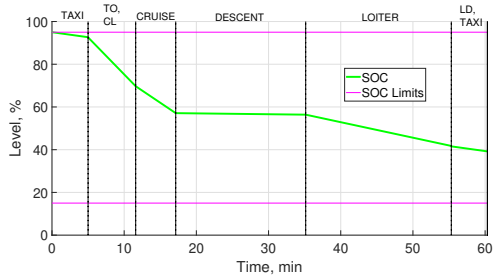

(a) 50 nm Simple Cruise Mission Time Histories, PGS OFF

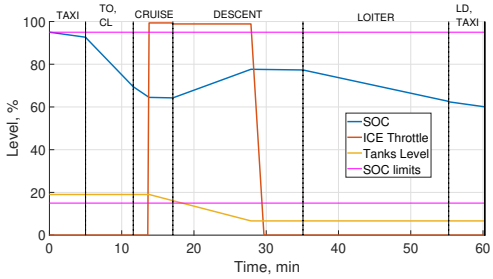

(b) 50 nm Simple Cruise Mission Time Histories, PGS ON

Figure 87

Full Eletric Version

A possible full-electric (FE) version of the airplane can be envisioned. In this version, the PGS and the relative fuel system are removed. This allows to substitute them with additional BPs, positioned in place of the PGS. In this way, energy stored in BP is increased by 70% (from 256 kg to 433 kg), without significantly affecting weight and balance properties. Maximum PE IFR range results to be 96 nm.

Figure 88 presents the SOC time histories for 50 and 96 nm FE IFR range missions.

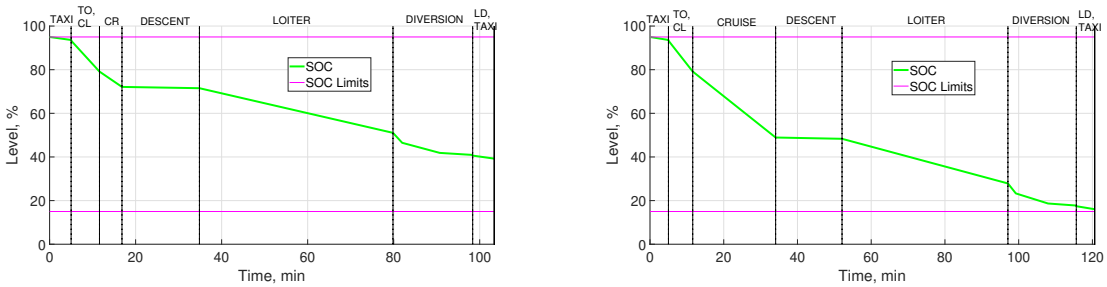

(a) 50 nm IFR PE Mission Time Histories

(b) 96 nm IFR PE Mission Time Histories

Figure 88

9.7.1 Remarks On Mission Profiles

Mission profile A can represent the typical aerotaxi/commercial transport IFR mission, as well as IFR cargo missions. Mission profile B could simulate a standard VFR mission, as well as a training mission or a potential medical mission. Moreover, given the significant endurance performance, a possible use as a SAR aircraft can be expected.

10 Cost Analysis

10.1 Aircraft Development and Procurement Cost

The Development and Procurement Costs of Aircraft (DAPCA) model was developed in 1967 to predict the cost related to procurement and development of new military aircraft. Over the years this method was updated and corrected giving birth to the DAPCA-IV and the Cost Estimation Relationships (CERs). This model, developed by Eastlake & Blackwell, has been furtherly modified by Gudmundsson in order to be better applied to the estimation of general aviation costs. Nevertheless, this model, developed in 2014, is not able to predict the cost related to the peculiarities of the hybrid-electric system. In the year 2019 a modification of the Gudmundsson model was developed by D. Felix Finger [10] integrating various correction factors for design choices to the original method taking into account various aspects related to the development and procuring process as well as the operating cost for a hybrid-electric general aviation aircraft.

The Team also contacted D. Felix Finger and, after a meeting, different parameters (such as the EMs, BP, materials, fees cost and the ratio between flight and maintenance hours) were discussed and adapted to the specific case under exam to get a perfect model suitable to the specific airplane under project. Finally all cost were translated in 2031 to account for inflation acquiring Consumer Price Index (CPI).

Based on the market analysis, the average number of aircraft produced in one year for the competitors is 225 1, in order to be as conservative as possible the Team choose to take a production rate of 8 airplane per month, meaning 96 airplane per year (less than half of the original one). This leads to a prediction of 480 planes built in 5 years.

The certification and construction cost is greatly influenced on the labour cost. The average wage for an engineer in the aeronautical field can range between 37 $/hr and 59 $/hr [28] and the average wage of a technician in a typical aircraft plant can go between 12 $/hr and 20 $/hr depending on the statistics. However, the employer has to cover a bigger cost than the amount of money received by the worker, this cost is defined as the rate of labour and includes the non-wage labour cost which consists in taxes and benefits. According to the United States Department of Labour and the Eurostat, this accounts for an increment of the 30% for the US [29] and 25% for the EU [30]. Taking this into account, a rate of labour of 75 $/hr was taken for engineers, 42 $/hr for the tooling technicians

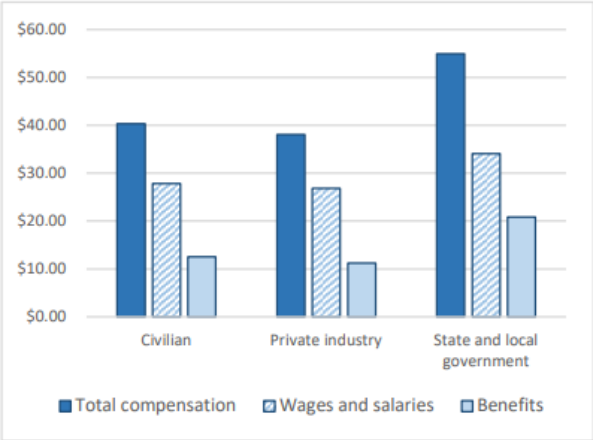

Figure 89: Non-wage cost in the US

and 36 $/hr for the manufacturing department employees.

	Man-hours	Rate, $/hr	Total Cost	Cost Per Unit	
Engineering	38.517	$ 75	$ 16.189.274	$ 33.727	
Development support	→		$ 542.650	$ 1.130	
Flight test operations	→		$ 122.176	$ 254	
Tooling	35.589	$ 42	$ 5.550.899	$ 11.564	
Certification cost	→		**$ 22.404.999**		
Manufactoring labor	345.000	$ 36	$ 46.123.156	$ 96.089	
Quality control	→		$ 8.630.621	$ 17.980	
Materials/equipment	→		$ 8.823.364	$ 18.382	
Units produced in 5 years	→				480
Quantity Discount Factor	→				0,8573
				Without QDF	**With QDF**
Battery pack(s)	→			$ 25.915	$ 22.217
ICE + GEN	→			$ 58.468	$ 50.125
Engine(s)	→			$ 33.240	$ 28.497
Propeller(s)	→			$ 32.668	$ 28.006
Avionics	→			$ 84.283	$ 72.256
TOTAL COST TO PRODUCE	→			$ 413.700	**$ 380.226**
Manufactorer's liability insurance	→				$ 57.034
MINIMUM SELLING PRICE	→				**$ 437.260**
Profit	→				15%
ACTUAL SELLING PRICE	→				**$ 502.849**

Figure 90: Development and Procurement Cost

For flight test operation three prototypes have been considered (two not flying and one flying).

To estimate the cost of the BPs, a price of 150 $/kWh based on [10] after a discussion with D. Felix Finger and Siemens.

To calculate the price of ICE, generator and electric motors the Team reached ULPower, Emrax and MGM Compro to discuss prices of the components and cost increments needed to install said components on the aircraft. The price of the composite 5 blade propeller was estimated from different manufacturers such as E-Props, Sensenich and Whirlwind.Please note how the necessity of a variable pitch propeller translates to an increment in the procurement cost, the increment in price increases with the diameters of the propeller, ***Colibr-e Sapphire*** has small propellers so total propeller prices increases by just 8800 $ with respect to fixed pitch ones. Avionics consists in flight instruments, ESC and EPMS.

As it can be seen, the production cost of each aircraft has to be increased taking into account the manufacturer's liability insurance and the profit percentage (each taken as 15%).

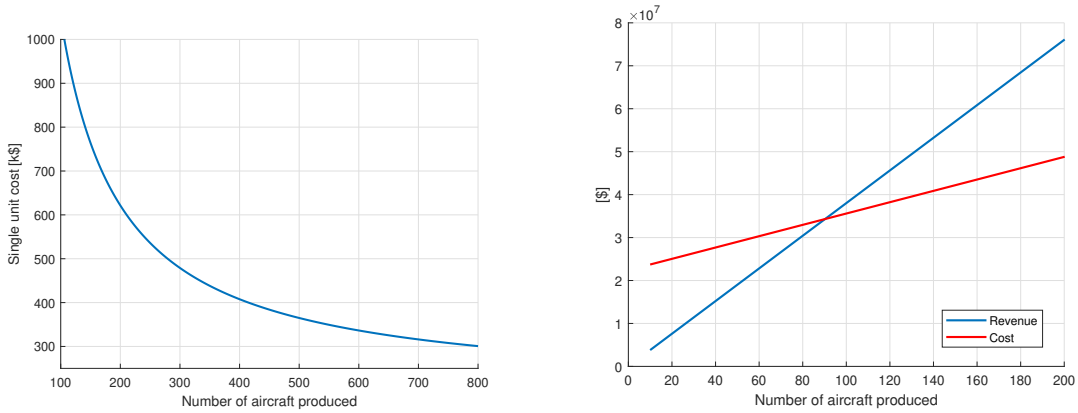

(a) Cost versus Number produced

(b) Break even analysis

Figure 91: Cost development over time

Figure 91 shows how the price to produce each aircraft decreases with the number of aircraft produced in the 5 year period time. Given the production rate and knowing the selling price of each aircraft, production and development costs, it is possible to estimate a break even number of 90 airplanes.

10.2 Operating Costs

The aircraft operating cost is of crucial interest for the operators and customers. Those costs can be subdivided in Variable Direct Operating Costs (VDOC) which is the cost of operating the airplane, Fixed Direct Operating Cost (FDOC) which is the cost to own the aircraft and Indirect Operating Cost that are linked to capital cost and service provision cost.

Variable Direct Operating Costs

VDOC includes fuel cost, electric energy cost, crew wage, maintenance cost, landing fees, ground handling fees and navigation charges.

As previously mentioned in the market analysis, the three selected fuels are AVGAS, MOGAS and JET A-1. The price per flight hours for this three is respectively 47.05 $/hr, 50.28 $/hr and 46.65 $/hr. By choosing to run the aircraft on Jet A-1 some money could have been saved, but the fuel availability would have been reduced by a lot, since it is not available in most airfield. Because of that, AVGAS was selected.

When it comes to recharging batteries on ground, the price is composed by that of the energy entering the batteries, plus the one dissipated due to inefficiencies. As stated [31], the charging efficiency for electric cars ranges from 82% to 92%, a value of 85% can be taken. Note that this value is greater than the charging efficiency on air because energy has to go from the charging plug directly into batteries without passing through ICE and generator.

Fees consist of three different aspects: landing fees, ground handling fees and navigation fees. The aircraft under consideration will not only be able to depart from airports, instead, as a matter of fact, the vast majority of flights will start and finish in airfields, where fees are much lower. In order to be conservative the Team decided to reduce the fees cost by just 25% with respect to the one related to the airports.

VDOC		
	Annual (630 hr)	Per hour
Avgas	$ 29.641,50	$ 47,05
Electricity	$ 13.078,80	$ 20,76
Fees	$ 19.523,89	$ 30,99
Maintenance	$ 7.560,00	$ 12,00
TOTAL	**$ 69.804,19**	**$ 110,80**
Pilot	→	$ 90,00
TOTAL with pilot	→	**$ 200,80**

Figure 92: Variable Direct Operating Costs

All previous choices made by the Team, such as (but not limited to): not to use composite materials, to forsee the possibility of frequent swap of the batteries, to have easy access to engine and generator, and to use electric motors with higher reliability, led to an airplane which is easy to maintain despite having a cutting-edge propulsive system technology. In detail, for a FAR23 certified aircraft, the ratio between maintenance hours and flight hours is $F_{mf} = 0.30 - 0.35$. After the previous consideration this ratio can be reduced to $F_{mf} = 0.2$. Furtherly reducing this parameters would be unreasonable as stated by various aircraft owners and D. Felix Finger himself, because, considering all the events that an aircraft is subjected to (which are not predictable by just a numerical formula), at least 10-12 minute of maintenance every flight hour would be required.

Fixed Direct Operating Cost

FDOC take into account the repricing of the batteries and the airplane itself, the insurance cost, the storage cost and annual inspections.

To estimate the aircraft depreciation a life expectancy of the airplane and the number of flight hours per year have to be taken into account. A general aviation airplane has generally 20 years of life, so this number has been taken. Moreover, looking at statistics published by the Aircraft Owners and Pilots Association (AOPA) relative to the years 2015, 2016 and 2017 [32] relative for both flight schools and aerotaxi operations a number of 630 flight hours per year has been considered.

FDOC		
	Annual (630 hr)	Per hour
Aircraft depreciation	$ 19.438,27	$ 30,85
Battery depreciation	$ 1.576,70	$ 2,50
Insurance	$ 6.331,50	$ 10,05
Storage	$ 2.249,98	$ 3,57
Inspection	$ 500,00	$ 0,79
TOTAL	**$ 30.096,42**	**$ 47,77**

Figure 93: Fixed Direct Operating Costs

For the battery depreciation the number of charge-discharge cycle before end of life has to be considered,

after all the consideration made in the chapter dedicate to this topic, a value of 2000 cycles was taken.

The typical insurance for an aircraft depends on many factor such as the pilot experience, pilot age, use of the aircraft, type of aircraft etc... There is not a single model to be applied in order to evaluate this cost, but it is plausible to assume that the insurance for an hybrid-electric aircraft will have little to no difference from that of a standard FAR23 aircraft, so the model proposed by Gudmundsson was used.

For the storage cost a value of 3000 $ per year was considered, once again this amount is related to the aircraft storage in airports' hangars, it is to be expected that the price for storing the airplane in an airfield would be lower, moreover the storage condition of ***Colibr-e Sapphire*** are not so strict because of the absence of composite materials. So in the end this value was reduced by 25%.

Annual inspections are required in order to own an airplane, the cost can be considered 500 $ as suggested by Gudmundsson [13].

Indirect Operating Cost

If the airplane is operated in a commercial environment, another cost has to be considered: the IOC. This consists of Selling, General & Administration (SG&A) costs and Capital Expenditures (CAPEX).
The Capital Expenditures is the payment reported on the balance sheet made by a company to purchase goods. Assuming a linear depreciation, the average CAPEX can be calculated as:

$$0.5 * WAAC * P_{ac}$$

The Selling, General & Administrative expenses have the biggest impact on a company income as they represent the biggest non-productive cost. This expenses are calculated as the operating costs multiplied by a surcharge factor:

$$F_{SGA} * C_{operations}$$

Note that these costs can vary from company to company depending on the annual budget, expenses and deals with various suppliers and sellers, so it can't be predicted with accuracy in this report.

10.2.1 Results

What emerges from the market analysis is that the airplane will cost 380226 $ to be produced and will be sold (considering the liability insurance and the 15% profit) at a price of 502849 $, making it more than 20% cheaper than the competitors' airplane with similar performances and more than three times cheaper than competitor's helicopters. Moreover the agility of the airplane comes into play, making it an extremely appealing airplane to purchase from an operator, with it being used both for aerotaxi and flight school without any difference needed in

design. If the customer then wants to purchase the airplane in a cargo or medical configuration all the manufacture has to do is to disassemble three of the 4 seats substituting it with rails and nets for the cargo and with a medical stretcher mount and a rotating seat for the medical one. Thanks to this aspect the airplane cost, the assembly plant configuration and the delivery time will have little to no difference regardless of the airplane configuration needed by the customer.

Talking about the operating cost, thanks to the lower cost of electricity with respect to fuel, the choices made by the Team to allow for the airplane to be easy to maintain, the fact that the airplane operates mostly from airfields, the implement of future technologies such as Li-S batteries and the affordable selling price of the aircraft, the airplane under project will be able to have in 2031 a Direct Operating Cost 20% lower than the operating cost that the competitors have today. It is noticeable how, due to lower and lower availability of components, increasing gas prices, increasing taxation due to pollution and inflation the operating cost of competitors will only increase and this difference is only expected to grow. Comparing ***Colibr-e Sapphire*** with helicopters and medical airplanes, the reduction in operating cost becomes huge with a crushing 1380% difference.

	Annual (630 hr)	Per hour
TOTAL VDOC (without pilot)	$ 69.804,19	$ 110,80
TOTAL FDOC	$ 30.096,46	$ 47,77
TOTAL DIRECT OPERATING COST	**$ 99.900,65**	**$ 158,57**

Figure 94: Total Direct Operating Costs

10.3 Business Case

Aerotaxi Operator

Let's imagine a scenario in which an operator chose to integrate the ***Colibr-e Sapphire*** in its fleet. In the vast majority of cases the airplane is not purchased from scratch but rather leased. The average dry lease is a 7 year contract with a typical monthly rate of 1% of the airplane price, for newer aircraft adopting new technologies this rate lowers to 0.7%.

The lease payment must be spread across the flight hours and has to be added to the hourly DOC. The number of flight hours in a year was taken as 630 [32].

Given a profit of 30%, the flight can be sold at 408.57 $ an

FDOC		
	Per year	Per hour
	$71.495,97	$113,49
VDOC		
	Per year	Per hour
	$126.504,00	$200,80
TOTAL with profit	30% guadagni	
	Price per year	Price per hour
	$257.399,96	$408,57
PER PERSON		
	Price per year	Price per hour
	$85.799,99	$136,19
REVENUE PER YEAR	$257.399,96	
COST PER YEAR	$197.999,97	
PROFIT PER YEAR	**$59.399,99**	

Figure 95: Aerotaxi business case

hour (this price includes the crew cost). This means that at

the end of the year, the operator will close with a net profit of 59399.99$ and after the lease contract conclusion, the company would have fully repaid the lease and gained 416123.54 $ per airplane.

Moreover, it's important to note how the price of the flight is extremely competitive with the current aerotaxi market. The price of one hour of flight on the ***Colibr-e Sapphire*** including the pilot cost and the profit margin for the operator, is still lower than the hourly cost to just operate most helicopters (not including pilot, leasing and profit). If we then consider E-VTOLs, the prices reach 3.6 $ per kilometer to 11$ per mile amounting to roughly 790 $ to 1300 $ an hour [33], which is more than one time and half to almost three times as much as it would cost to fly on the airplane under project.

Talking about other airplane used for aerotaxi purposes the typical price is 1500 $ up to 3500 $ [34] [35] per hour for a light jet, which is more than three times to eight and a half times more than the price to fly on the ***Colibr-e Sapphire***. If we consider that the cruise speed of these aircraft can be higher than 150 knots, the price to use the airplane in question would still be incredibly convenient even if the cruise speed of the competitors is more than double.

Cargo Operator

The second business case presented is the one of a cargo operator using the airplane under project in cargo configuration as a utility aircraft for shipping goods with a dry lease. The useful payload can be rounded up to 300 kg, however it is possible that the airplane gets loaded with large but light weighted cargo filling up the usable volume before reaching the maximum useful payload weight. In this case the volumetric weight must be taken into account: for each package the volumetric weight has to be estimated as the volume of the package (in cubic meters) times 167, if the volumetric weight exceeds the actual weight of the product, the volumetric weight becomes the chargeable weight [36]. For the purpose of this analysis, an average condition in which half of the cargo is charged with the actual weight and the other half with the volumetric one is considered, leading to a useful weight of 261.63 kg. The typical price to ship a package via air is 5 $/kg but can even jump to 8 $/kg and more [36]. The Team decided to use 5 $/kg for the purpose of this analysis.

FDOC		
	Per year	Per hour
	$76.590,48	$106,38
VDOC		
	Per year	Per hour
	$152.013,60	$211,13
PROFIT PER FLIGHT	5 $/kg	
	Price per flight	
	$1.308,15	
REVENUE PER YEAR	$627.912,00	
COST PER YEAR	$228.604,08	
PROFIT PER YEAR	**$399.307,92**	

Figure 96: Cargo business case

Considering the airplane flying on a regular basis 4 days a week, 3 hours a day (two routes of 1.5 hours each) and loading cargo before most of the take-offs, an amount of 480 useful flights has been considered perfectly reasonable. Considering the direct operating cost, the lease cost and the wage of the pilot, the operator will close its balance at the end of the year with a net profit of 399'307.92 $ which means that after the 7 year contract with the lessor, the operator will gain 2.7 million dollars of profit.

Private and Commercial Pilot Licence

Let's now consider the case of a flight school that chooses to operate with ***Colibr-e Sapphire***, after integrating it in its fleet with a dry lease. In order to get a PPL, the FAA gives a minimum standard of 40 hours, 8 of which have to be more than 90 minutes long, while for the CPL, 250 hours are necessary, 60 of which have to be more than 90 minutes long.

For the missions below 90 minutes, given the hourly autonomy of the aircraft, it is possible to operate it with three students on board plus the instructor optimizing the fees and spreading the DOC and cost of the instructor among all students on board, while for the missions longer than 90 minutes just one student has to be onboard. On average it takes 2 months to get a PPL. Depending on the flight school dimensions and how many students gets a licence each month, the plane will fly an increasing amount of hours, so that the bigger is the school the smaller will be the price. The DOC also includes the lease cost, cost of the instructor and a 10% margin.

PPL	32 hr of <90 min flight 8 hr of >90 min flight								
Students per month	hours per year	VDOC (32 hr) per pilot	FDOC (32 hr) per pilot	VDOC (8 hr) per pilot	FDOC (8 hr) per pilot	MEAN HOURLY RATE	10 % PROFIT	**PRICE PER FLIGHT HOUR**	**FIGHT COST TO GET A PPL LICENCE**
1 (private PPL)	240	$ 186,79	$ 121,33	$ 166,13	$ 121,33	$ 303,98		$ 334,38	$ 13.375,12
3 (medium school)	720	$ 50,78	$ 14,04	$ 166,13	$ 42,11	$ 93,50		$ 102,85	$ 4.114,00
6 (big school)	1440	$ 50,78	$ 7,43	$ 166,13	$ 22,31	$ 80,25		**$ 88,28**	**$ 3.531,00**

CPL	190 hr of <90 min flight 60 hr of >90 min flight								
Students per month	hours per year	VDOC (190 hr) per pilot	FDOC (190 hr) per pilot	VDOC (60 hr) per pilot	FDOC (60 hr) per pilot	MEAN HOURLY RATE	10 % PROFIT	**PRICE PER FLIGHT HOUR**	**FIGHT COST TO GET A CPL LICENCE**
1 (private CPL)	240	$ 186,79	$ 121,33	$ 166,13	$ 121,33	$ 303,16		$ 333,48	$ 83.369,00
3 (medium school)	720	$ 50,78	$ 14,04	$ 166,13	$ 42,11	$ 99,24		$ 109,16	$ 27.291,00
6 (big school)	1440	$ 50,78	$ 7,43	$ 166,13	$ 22,31	$ 89,46		**$ 98,41**	**$ 24.601,50**

Figure 97: Private and Commercial Pilot Licence

If we consider the standard cost to get a PPL and CPL, these are respectively 10'000 $ and 100'000 $ [37]. 70% of this price consists in the cost related to the airplane operations plus the cost of the instructor [38]. This means that getting a licence with ***Colibr-e Sapphire*** in a large flight school can make a pilot save up to 3500 $ for a PPL and 45'000 $ for a CPL (price may vary depending on profit percentage for the flight school).

Leasing Analysis

Up to now the business cases presented, considered the hypothesis of a dry lease of 7 years with a monthly rate of 0.7% being made to get the airplane. Needless to say that if a large company with a big enough investment fund decides to purchase the airplane from scratch, the hourly cost will be lower. Formally speaking "a lease is a contract outlining the terms under which one party agrees to rent an asset in this case, property owned by another party. It guarantees the lessee, also known as the tenant, use of the property and guarantees the lessor (the property owner or landlord) regular payments for a specified period in exchange. Both the lessee and the lessor face consequences if they fail to uphold the terms of the contract" [39]. In the case of a dry lease the lessor provides the aircraft to the lessee without crew, ground staff, maintenance ecc... this type of lease is typically used by banks or leasing companies (lessor) providing airplanes to air operator (lessee), but the lessor may also be a major airline providing airplanes to a regional airline. A wet lease is an arrangement in which the lessor provides the lessee the aircraft complete with crew, maintenance, ground staff and insurance. This type of lease is typically used by major airline (lessor) providing the asset to a smaller operator (lessee). On the figure below an hourly cost comparison between a dry and wet leased and a purchased airplane in different scenarios is reported.

DRY LEASE			
	200 h/y	600 h/y	1200 h/y
1% monthly rate	$551,62	$259,41	$186,36
0,7% monthly rate	$462,90	$229,84	$171,57
0,5% monthly rate	$403,76	$210,12	$161,71
BUY	$255,90	$160,84	$137,07
WET LEASE			
	200 h/y	600 h/y	1200 h/y
20% profit from lessor	$503,10	$248,75	$185,15
BUY	$255,90	$160,84	$137,07

Figure 98: Lease VS Buy

10.4 Life Cycle Cost

Life cycle cost is the cost of researching and developing, purchasing, operating and disposing of an aircraft fleet. In figure 99 the life cycle of the typical aerotaxi aircraft flying 630 hours a year for a 20 years life time is reported.

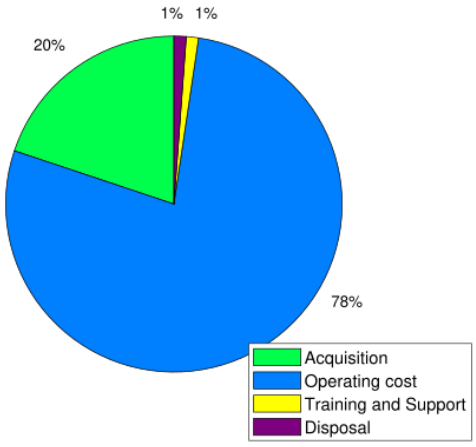

Figure 99: Aircraft Life Cycle

11 Certification and Safety

11.1 Certification

The aircraft is required to to be certified under FAR 23 standards. This regulation recently changed to include new propulsive technologies (mainly electric propulsion).

Previous versions of this certification standard focused strongly on the distinction between single-engine and twin-engine, the most recent version partially gave up this distinction and some standards, where a certain amount of engines were required to work, focus now on the percentage of available thrust. This clarification perfectly suits the ***Colibr-e Sapphire*** and makes an airplane with an 8 engines DEP certifiable under this standard.

Unfortunately, in some sub parts the distinction between single and twin-engine is still present (for example climb requirements), in this case the aircraft was considered a twin-engine and the number of available engine translated into a corresponding percentage of thrust in the relative wing.

FAR 23 also does not include a detailed performance standard subpart, instead the FAA suggests a compliance with military standard.

11.2 Future Applications

Many start-up companies are developing small electric STOLs in order to innovate urban and regional mobility. As an example, Electra Aero [40] aims to link cities and districts with a quiet and less polluting aircraft and is pushing this concept to the limit by considering ultra short runways built inside cities and buildings' rooftops. With this specific application, safety and certification are main concerns. Extremely high level of reliability has to be granted: operating in complex environmental, such as flying near buildings and high density populated areas, means that new risk analysis have to be performed to insure safety.

As of today, airplane urban transport is not possible due to certification restrictions and limitations. ***Colibr-e Sapphire***, thanks to it's remarkable STOL performances, small noise pollution and very low emissions, represents frontline with new technologies applications to accomplish urban and interurban missions, making it possible in the future to enter this market.

11.3 Safety

Different safety risks affecting aircraft and occupants have been considered, ranging from structural damage to electronic and mechanical component fail to weather conditions and improper maneuvers. Hazards and corresponding risks, along the relative probability and severity are schematized in the next page with relative hard and soft barriers undertaken in order to respect safety standards.

Possible failure of one or more barriers (escalator factors) have been considered and escalator barriers have been chosen to mitigate risk and severity. In accordance with 2022 ICAO safety matrix in Figure 100, the compliance of every considered hazard is within acceptable limits.

Note: In case of both EPMS failure 1A compliance is accepted as the probability and severity can not be furtherly lowered without implementing a third EPMS as a backup for the backup, this solution was not considered as it would represent a big cost, a bigger complexity and the risk is already extremely improbable.

Also in the case of mid-air collision a 1A compliance is accepted as the risk of this happening, after implementing a TCAS and with the correct pilot training is as low as reasonably possible and can not be furtherly lowered.

Risk probability	Risk severity				
	Catastrophic A	Hazardous B	Major C	Minor D	Negligible E
Frequent 5	5A	5B	5C	5D	5E
Occasional 4	4A	4B	4C	4D	4E
Remote 3	3A	3B	3C	3D	3E
Improbable 2	2A	2B	2C	2D	2E
Extremely improbable 1	1A	1B	1C	1D	1E

Figure 100: ICAO Safety Matrix

Hazard	Risk description	Probability	Severity	Compliance before barriers	Risk Mitigation	Escaletor factors	Escaletor barriers	Probability	Severity	Compliance
Critical technical failures	One engine out	Remote	Minor	3D	EPMS management 8 motors	EPMS not operating	EPMS redoundancy	Remote	Negligible	3E
	50% power loss due to BMS loss of redoundancy	Extr. improbable	Hazardous	1B	EPMS management 8 motors Pilot training	EPMS not operating Pilot performances not adeguate	EPMS redoundancy Pilots periodical checks according regulations	Extr. Improbable	Major	1C
	Total power loss	Extr. Improbable	Catastrophic	1A	BP system isolation PGU system isolation Component redoundancy Pilot training	Absense of maintenance check Pilot performances not adeguate	Approved maintenance procedures Pilots periodical checks according regulations	Extr. Improbable	Hazardous	1B
	ICE/generator fail	Improbable	Major	2C	Power from BP	BP not working	Multiple BPs	Improbable	Minor	2D
	one BMS fail	Improbable	Hazardous	2B	Backup EPMS	Backup EPMS not working	Pilot training	Improbable	Minor	2D
	Two BMS fail	Extr. Improbable	Catastrophic	1A	Pilot training	Pilot performances not adeguate	Pilot periodical checks according regulations	Extr. Improbable	Catastrophic	1A
	Battery pack fail	Remote	Hazardous	3B	Li-S batteries installed Power from remaining BP Power from PGU	PGU not working	Remaining BPs sufficient for propulsion	Improbable	Minor	2D
	Battery fire	Remote	Catastrophic	3A	Isolated BP cases Li-S batteries installed Automatic fire warning/extinguisher	Automatic fire system not working	Pilot monitorning and activation available	Extr. Improbable	Hazardous	1B
	Landing gear fail	Improbable	Hazardous	2B	Emergency gravity deployment	Landing gear doors stucked	Mechanical unlock actuator	Improbable	Minor	2D
Operations near wild life aeras	Bird-strike	Remote	Hazardous	3B	Trasponder S Strobe lights 8 engines Pilot training	One trasponder inoperative Strobe lights inoperative Pilot performances not adeguate	Dual trasponders installed Multiple strobe lights installed Pilot periodical checks according regulations	Improbable	Minor	2D
Loss of control	Stall	Improbable	Catastrophic	2A	Pilot Training Stall warning Aircraft design to regain stability	Stall warning not working Pilot performances not adeguate	AOA emergency indicator Pilot periodical checks according regulations	Extr. improbable	Minor	1D
	Spin	Improbable	Catastrophic	2A	Pilot Training Stall warning Aircraft design to regain stability	Stall warning not working Pilot performances not adeguate	AOA emergency Pilot periodical checks according regulations	Extr. improbable	Minor	1D
	Crash landing	improbable	Catastrophic	2A	Aircraft structural design EGPWS Pilot training	EGPWS not working Pilot performances not adeguate Pilot performances not adeguate	En-route charts and minima Pilot periodical checks according regulations	Extr. Iprobable	Hazardous	1B
Cold weather operations	Ice formation	Remote	Hazardous	3B	Anti ice systems De-ice systems	Anti ice/De-ice system inoperative	Dispatch conditions: avoid ice conditions	Improbable	Minor	2D
Operations in controlled/uncontrolled aerspace	Mid-air collision	Improbable	Catastrophic	2A	TCAS Pilot training	One TCAS system inoperative Pilot performances not adeguate	Dual TCAS systems installed Pilot periodical checks according regulations	Extr. Improbable	Catastrophic	1A
FOD	Aircraft damage due to strike/ingestion	Remote	Majour	3C	Aircraft structural design Runway inspections	Runway inspection not performed	Pilot check	Extr. Improbable	Minor	1D

12 Conclusions

Aviation world is rapidly evolving. Next generation aircraft have to cope with the need to reduce noise, greenhouse and toxic gasses emissions and new design missions to allow for an innovation in air mobility.

Colibr-e Sapphire represents one of the best solutions in aviation. Thanks to it's innovative propulsion system and the ability to perform a full electric take-off and landing, total emissions can be cut down up to 80% and low altitude emissions will be completely erased.

Simple solutions when it comes to the structure of the airplane and the assumption of technologies already close the end of their developing phase (such as Li-S batteries) are adopted. These technologies grants the airplane to be launched by 2031, moreover increases reliability, makes the airplane easy to be maintained and affordable to be purchased.

Low selling price and operating cost makes it extremely competitive from a marketing prospective. Purchasing and maintaining ***Colibr-e Sapphire*** is more than 20% cheaper than competitors' airplanes and three times cheaper than similar helicopters/VTOLs.

Thanks to its remarkable STOL performances, the airplane will be able to take-off and land from any airport and airfield opening a new air transport concept: using airplanes to interlink small and big cities taking passengers to their destination in an easy, safe and quick way.

As a consequence of an accurate design, ***Colibr-e Sapphire*** will not only be able to be used as an aerotaxi but can be used by flight schools as a trainer, for cargo use and as a medical airplane with little to no customization needed.

This is what makes ***Colibr-e Sapphire*** the ultimate Agile Hybrid-Electric STOL Aircraft.

Special Thanks

Special thanks goes to PhD D.Felix Finger for sharing his knowledge about hybrid-electric configurations and cost analysis; Professor Sergio Ricci for his help on the use of NeoCASS tool; Cpt Vincenzino Romani for his overall aircraft and aviation world knowledge; Evielyne Huyghebaert and Alberto Comincioli for engine consultations; Boris Guič for electric motor consultations.

Bibliography

Books

[2] J. Roskam. *Airplane Design*. Airplane Design pt. 5. DARcorporation, 1985. ISBN: 9781884885501. URL: https://books.google.it/books?id=mMU47Ld7yQkC.

[11] Daniel Raymer. *Aircraft design: a conceptual approach*. American Institute of Aeronautics and Astronautics, Inc., 2012.

[12] D McLean. *Performance, Stability, Dynamics, and Control of Airplanes, BN Pamadi, American Institute of Aeronautics and Astronautics, 1801 Alexnader Bell Drive, Reston, VA 20191, USA. 1998. 766pp. Illustrated. 94.94 (Non-Members).* Vol. 103. 1021. Cambridge University Press, 1999, pp. 174–175.

[13] Snorri Gudmundsson. *General aviation aircraft design: Applied Methods and Procedures*. Butterworth-Heinemann, 2013.

[20] Leland M Nicolai and Grant E Carichner. *Fundamentals of aircraft and airship design, Volume 1–Aircraft Design*. American Institute of Aeronautics and Astronautics, 2010.

[21] Adrian P Mouritz. *Introduction to aerospace materials*. Elsevier, 2012.

[23] Jan Roskam. *Airplane Design: Preliminary configuration design and integration of the propulsion system*. DARcorporation, 1985.

Articles, Technical Reports

[5] David Sziroczak et al. "Conceptual design of small aircraft with hybrid-electric propulsion systems". In: *Energy* 204 (2020), p. 117937. ISSN: 0360-5442. DOI: https://doi.org/10.1016/j.energy.2020.117937. URL: https://www.sciencedirect.com/science/article/pii/S0360544220310446.

[6] Jeffrey K. Viken et al. "Design of the Cruise and Flap Airfoil for the X-57 Maxwell Distributed Electric Propulsion Aircraft". In: (). DOI: 10.2514/6.2017-3922. eprint: https://arc.aiaa.org/doi/pdf/10.2514/6.2017-3922. URL: https://arc.aiaa.org/doi/abs/10.2514/6.2017-3922.

[7] Christopher Courtin et al. "Feasibility Study of Short Takeoff and Landing Urban Air Mobility Vehicles using Geometric Programming". In: (). DOI: 10.2514/6.2018-4151. eprint: https://arc.aiaa.org/doi/pdf/10.2514/6.2018-4151. URL: https://arc.aiaa.org/doi/abs/10.2514/6.2018-4151.

[8] ANDREA MATRONE. "Performance-based preliminary sizing of aircraft with distributed propulsion". In: (2019).

[9] Carlo ED Riboldi. “An optimal approach to the preliminary design of small hybrid-electric aircraft”. In: *Aerospace Science and Technology* 81 (2018), pp. 14–31.

[10] D Felix Finger et al. “Cost estimation methods for hybrid-electric general aviation aircraft”. In: (2019), pp. 265–277.

[15] Richard Hann et al. “Experimental Heat Loads for Electrothermal Anti-Icing and De-Icing on UAVs”. In: *Aerospace* 8.3 (2021). ISSN: 2226-4310. DOI: 10.3390/aerospace8030083. URL: https://www.mdpi.com/2226-4310/8/3/83.

[22] US FAA. “MIL-HDBK-5J. Metallic Materials and Elements for Aerospace Vehicle Structures”. In: (2003).

[24] Marco Borri and Lorenzo Trainelli. “Basic airplane equilibrium and stability revisited”. In: 23 (2007), p. 25.

[27] I Geiß and A Strohmayer. “Operational Energy and Power Reserves for Hybrid-Electric and Electric Aircraft”. In: (2021).

Websites

[1] *Aviation and shipping emissions in focus*. URL: https://www.eea.europa.eu/articles/aviation-and-shipping-emissions-in-focus/.

[4] *SAFT Three battery technologies that could poewr the future*. URL: https://www.saftbatteries.com/media-resources/our-stories/three-battery-technologies-could-power-future.

[14] *JavaProp - Design and Analysis of Propellers*. URL: https://www.mh-aerotools.de/airfoils/javaprop.htm.

[17] *FOCA DATA BASE FOR AIRCRAFT PISTON ENGINE EMISSION FACTORS (Appendix 2: In-flight Measurements)*. URL: https://www.hjelmco.com/upl/files/2428.pdf/.

[18] *FOCA aircraft piston engine emission database*. URL: https://www.bazl.admin.ch/bazl/en/home/specialists/regulations-and-guidelines/environment/pollutant-emissions/aircraft-engine-emissions/report--appendices--database-and-data-sheets.html/.

[19] *How long does it take to charge an electric car? Charging speeds explained*. URL: https://www.rac.co.uk/drive/electric-cars/charging/electric-car-charging-speeds/.

[26] *Unstable Approaches: Risk Mitigation Policies, Procedures and Best Practice, Third Edition*. URL: https://canso.fra1.digitaloceanspaces.com/uploads/2020/08/Unstable-Approaches-3rd-Edition.pdf.

[28] *U.S. BUREAU OF LABOR STATISTICS aerospace engineers wage*. URL: https://www.bls.gov/oes/current/oes172011.htm/.

[29] *U.S. BUREAU OF LABOR STATISTICS Employer Costs for Employee Compensation*. URL: https://www.bls.gov/news.release/pdf/ecec.pdf/.

[30] *EUROSTAT Hourly labour costs*. URL: https://ec.europa.eu/eurostat/statistics-explained/index.php?title=Hourly_labour_costs/.

[31] *APISAT Electric Car Charging Test*. URL: https://www.adac.de/rund-ums-fahrzeug/tests/elektromobilitaet/stromverbrauch-elektroautos-adac-test/?redirectId=quer.Elektroautos%20Ecotest/.

[32] *AOPA State of general aviation*. URL: https://download.aopa.org/hr/Report_on_General_Aviation_Trends.pdf/.

[33] *How Much Will It Cost to Fly on eVTOL Air Taxis?* URL: https://www.flyingmag.com/evtol-air-taxi-passenger-prices/.

[34] *Aerotaxi: un volo tutto tuo*. URL: https://www.missionline.it/aerotaxi-un-volo-tutto-tuo/.

[35] *AIR TAXI COST in the Washington DC area*. URL: https://skywayairtaxi.com/air-taxi-cost-pricing/.

[36] *Air Freight Air Cargo Shipping: Air Freight Charges, Rates, Costs Quotes*. URL: https://www.freightos.com/freight-resources/air-freight-rates-cost-prices/.

[37] *How Much Does It Cost To Get a Pilot's License?* URL: https://www.indeed.com/career-advice/career-development/how-much-does-it-cost-to-get-a-pilot's-license/.

[38] *Private Pilot's License (PPL) Cost + Ways to Save*. URL: https://airplaneacademy.com/how-much-does-it-cost-to-get-a-private-pilots-license/.

[39] *What Is a Lease?* URL: https://www.investopedia.com/terms/l/lease.asp/.

[40] *Electra.Aero*. URL: https://www.electra.aero/.